University of Nottingham
UK | CHINA | MALAYSIA

Centre for Additive Manufacturing
University of Nottingham

ADDITIVE MANUFACTURING OF MITRAL ANNULOPLASTY DEVICES

Charlotte Blake, BSc (Hons)

Supervisors: Professor Ruth Goodridge, Professor Donal McNally, Professor Ricky Wildman

Thesis submitted to the University of Nottingham
for the degree of Doctor of Philosophy, June 2021

JUNE 2021

Abstract

Mitral valve annuloplasty is a common surgical procedure performed on thousands of patients each year across the world. A less invasive and more successful method of resolving mitral valve regurgitation, repair surgeries now outnumber replacement of the mitral valve in its entirety. As a result, a range of supportive annuloplasty ring devices for maintaining the surgical repair are now available for lifelong implantation. However, these devices underserve some populations leading to replacement surgeries, and rely on assumptions made on the natural, healthy anatomy of the mitral valve.

Additive manufacturing (AM) has, for the last few decades, become increasingly adopted into the medical industry. With applications ranging from educational aids to surgical instruments and long-term implantable devices, this field is rapidly expanding and encompassing a greater breadth of medical specialities. In particular, the manufacturing of patient-specific products with reasonable cost and high fidelity is a key area of development for medical applications of additive manufacturing methods. Significant research has already been undertaken in the fields of orthopaedics, regenerative medicine, and pharmaceuticals, producing long-term implantable metal devices, complex polymer scaffolds, and novel drug delivery methods.

Personalized annuloplasty rings could lead to greater surgery success rates enabling greater repair longevity, reduced reoperation rates, and reduced risk of future valve replacement. This project aimed to investigate the suitability of the AM technique, selective laser melting (SLM), to create annuloplasty rings tailored to each patient.

To achieve this goal, this research focussed first on comparing the existing design assumptions applied to commercial annuloplasty devices against human anatomy using cadaveric dissection and measurement. These studies concluded that whilst the assumed 3:4 ratio applied in annuloplasty design was a good average across a population, the ratio was inconsistent between subjects and could lead to difficulties in sizing devices appropriately for an individual patient.

Following this, methods of design and manufacturing were investigated, comparing various tools available in commercial medical-CAD software, Materialise Mimics®. The commonly applied “thresholding” method of isolating structures from patient scan data was found to be insufficient for isolation of soft tissue structures such as the mitral valve annulus from the surrounding cardiac tissue due to the similarity in densities reducing contrast on the scan. A

method of single-point design using insertion points of the valve leaflets throughout the scan was shown to be sufficient to reproduce a mitral annular structure, which was then manufactured in the Ti6Al4V alloy, which has been shown to be biocompatible in some orthopaedic applications, using SLM.

Post-processing techniques appropriate for the specific application of this device into the cardiovascular system were also investigated. The novel electrolyte jet machining process was employed to moderate surface unevenness caused by inherent properties of the powder bed SLM process, such as stepping or loose powder particles. This process was tested with a range of parameter sets producing varying topographies and therefore applied to different needs of the annuloplasty device. Firstly, the process was applied for reduction of coagulation on the surface of Ti6Al4V alloy samples, and then for amplification of fibroblastic cell growth. The primary parameter sets were found to produce a small reduction in platelet adhesion when compared against as-built SLM surfaces, however failed to reduce the platelet activity to that found on conventionally manufactured Ti6Al4V samples. The secondary parameter sets did not produce any improvement in fibroblastic proliferation in short term studies, however SLM samples were found to be significantly more favourable to fibroblast growth than conventionally manufactured surfaces of the same material grade.

Finally, future avenues for work are discussed, including next steps for each of the three areas investigated in this thesis and a view to the future of novel annuloplasty devices as a whole. Recommendations for other applications of electrolyte jet machining are provided, including the potential for anti-biofouling surface processing given the lack of cell survivability found in these studies. Further design recommendations are considered, from computational modelling of the valve through to structured surgical prediction integrated with design of the annuloplasty device.

“HAVE SOME FIRE. BE UNSTOPPABLE.
BE A FORCE OF NATURE."

– CHRISTINA YANG

Table of Contents

Table of Figures

Table of abbreviations

AM	*Additive manufacturing*
ADP	*Adenosine diphosphate*
CAD	*Computer aided design*
CNC	*Computer numerical control*
CT	*Computed tomography*
DED	*Directed energy deposition*
EJM	*Electrolyte jet machining*
FDM	*Fused deposition modelling*
FITC	*Fluorescein isothiocyanate*
FSL	*Function-spacer-lipid*
LARS	*Ligament Augmentation and Reconstruction System*
LVAD	*Left ventricular assist device*
MRI	*Magnetic resonance imaging*
PBF	*Powder bed fusion*
PEEK	*Polyether ether ketone*
PerCP	*Peridinin-chlorophyll-Protein*
PET	*Polyethylene terephthalate*
PTFE	*Polytetrafluoroethylene*
SEM	*Scanning electron microscopy*
SLA	*Stereolithography*
SLM	*Selective Laser Melting*
TOE	*Trans-oesophageal echocardiogram (also TEE in US style)*
TPU	*Thermoplastic polyurethane*
TTE	*Trans-thoracic echocardiogram*
VEGF	*Vascular endothelial growth factor*
XPS	*X-ray photoelectron spectroscopy*

List of Publications, Presentations and Awards

"Additive manufacturing for personalised mitral annuloplasty devices" Charlotte Blake, Donal McNally, Chirattikan Srisook, Jonathon Mitchell-Smith, Rudolf Billeter-Clark, James Dixon, Ruth Goodridge. **Oral Presentation, Additive Manufacturing Meets Medicine, Lübeck, Germany, September 2019**

"*Predicting the healthy valve: relationships between the dimensions of the human mitral annulus"* Charlotte Blake, Chirattikan Srisook, Rudolf Billeter-Clark, Donal McNally, Ricky Wildman, Ruth Goodridge. **Poster presentation, The 14th international symposium on Biomechanics in Vascular Biology and Cardiovascular Disease, London, UK, April 2019**

"Implants on demand: bespoke mitral valve repair with additive manufacturing" Charlotte Blake, Donal McNally, Ruth Goodridge, Ricky Wildman, James Dixon. **Poster presentation, STEM for Britain finalist, London, UK, March 2019**

"Altering topology of additively manufactured metal surfaces using electrochemical jet machining to limit platelet activity" Charlotte Blake, Donal McNally, Ruth Goodridge, Ricky Wildman, Jonathon Mitchell-Smith, Adam Clare. **Poster presentation, The Third Annual Biomaterials Discovery Workshop, Nottingham, UK, January 2019**

"Quantification of platelets on additively manufactured surfaces using energy-dispersive X-ray spectroscopy" Charlotte Blake, Ruth Goodridge, Donal McNally, Ricky Wildman. **Poster presentation, Engineering Research Showcase, University of Nottingham, May 2018**

Dean Moore Scholarship, in recognition of the progress made in research and contribution to the postgraduate community. **Award, University of Nottingham, April 2018**

"Can additive manufacturing improve cardiac surgery through production of patient-specific implants?" Charlotte Blake, Ruth Goodridge, Donal McNally, Ricky Wildman. **Poster presentation, Engineering Research Showcase, University of Nottingham, May 2017**

Works currently in progress

"Human mitral valve anatomy and the impact on restoration of valve dimensions in annuloplasty" Charlotte Blake, Chirattikan Srisook, Donal McNally, Rudolf Billeter-Clark, Ruth Goodridge. **Journal Paper, intended for "*Heart*", pending submission.**

"Control of platelet response to additively manufactured titanium parts using electrolyte jet machining" Charlotte Blake, Jonathon Mitchell-Smith, Donal McNally, Adam Clare, Ruth Goodridge, Ricky Wildman. **Journal Paper, in preparation.**

Acknowledgements

Throughout the formation of this work, I was lucky to be guided, encouraged, and inspired by an incredible group of people both in research and in life. Firstly, I would like to thank David Richens for the inspiration of this work and clinical guidance at the outset of the project. The team at NUH welcomed me kindly into their clinical settings and provided wisdom and surgical knowledge that put me in such a privileged position as an Engineering researcher. Thank you for trusting me with your vision for the future of cardiac surgery.

I would like to thank the support and guidance given to me by supervisors and academic partners: Ruth, Donal, Ricky, James, Rudi, Mark H and Mark E, Denise, and so many others who helped me when I needed it most. You dedicated time and effort into my development, encouraged my imagination, led with kindness and creativity, and taught me how to be a better researcher. Your willingness to collaborate and endorse work from so many fields pushed this work in a way that would not have been possible without the compassion and flexibility that you brought to my supervision.

My academic colleagues proved a daily source of encouragement, be it academic or emotional. To the (not a) lunch club: few people understand one another in the way I felt understood by you all. Sitting silently together in the staff room of the AMB when stressed was a solace that not many others could provide, and shouting each other down to enforce productivity probably helped a bit too. I sincerely wish you all the best, wherever it takes us all. Adam, Andrew, Emma, Fiona, Han, Liz, Lewis, Matthew, Jing, and Vicente; you are all great researchers and even greater friends.

To the *Gluton 3f Kittons* and Terry, who inspired my scientific goals from the start. I might not have stuck with Physiology, but you kept my thirst for knowledge alive and pushed me on to expand into research across disciplines. My continued scientific endeavours come in large part back to the joy you all brought to them and continue to bring to this day. Rebee, Mark, Lucia, Daniella and Nyree – I promise to read your theses or sit through OSCEs as needed.

Finally, to my family and long-time friends, thank you for putting up with me and helping me all the way to the end. By carrot or by stick, you pushed me through the finish line. My amazing parents even read this thesis cover to cover at least three times over in spite of the content being far outside their fields (Dad, I'm sorry it was so long). My best friends and partner sat through late nights and early mornings supporting ideas and complications alike. So to my Mum and Dad, Tompy, Hatty, Joe, and Marc: thank you for being by my side for so many years. Your friendship and love extend far beyond the pages of this thesis but your contribution to it in maintaining me throughout the work is greater than you could possibly know. You are always in my corner and I will forever be in yours.

To everyone who walked alongside me to this point: thank you, I hope I live up to what you dreamed for me.

1 Introduction

1.1 Cardiovascular disease

According to the British Heart Foundation, cardiovascular disease is responsible for around 28% of all deaths in the UK, with healthcare costs estimated to be around £9 billion per year. Further, the cost to the UK economy through disability, early death and other related costs is nearly £20 billion annually (BHF, 2019).

This demand is only increasing over time: whilst mortality has fallen steadily over time, the demand on healthcare has risen as admissions and interventions increased (Bhatnagar *et al.*, 2016).

Cardiovascular disease includes all possible diseases of the heart and the circulatory system. This includes coronary artery disease and heart attacks, arrhythmias, pericardial disease, and valvular diseases.

1.1.1 Cardiovascular devices

Implantable cardiovascular devices are employed in a range of diseases related to a reduction in function of the circulatory system. Some devices are temporary measures, intended for short-term support of heart activity, whilst others have an expectation of lasting the remainder of a patient's life.

Short term devices are often used to support the heart during waiting periods or emergency situations. Left ventricular assist devices (LVADs) have historically been used as a "bridge" for patients waiting for heart transplant, to prevent worsening of the heart condition and support the output of the heart in the meantime (Birks *et al.*, 2006). More recent developments however have allowed LVADs to become a long-term device used for patients who cannot receive a heart transplant and will remain on the LVAD for the remainder of their life (Pagani *et al.*, 2009).

Longer-term cardiovascular implants include implantable cardioverter defibrillators and pacemakers, replacement valves, and stents (Zhang *et al.*, 2018). These devices are designed to support the working of the heart for the remainder of life, in situations where one specific function has failed. As such, these devices carry a high risk compared to those used for shorter periods of time (Zhang *et al.*, 2018). With the addition of these supportive measures, the heart itself is still able to function and does not require full replacement or support, and as such these smaller interventions can still provide a significant increase in quality or quantity of life.

Novel developments in cardiovascular devices are continually being produced. A large field of work surrounds provision of minimally invasive techniques to provide these devices, avoiding full sternotomy and the added risk of complications associated with the more invasive techniques (Grabow and Schmitz, 2018).

New materials have allowed investigation into resorbable devices, particularly in valvular support or in the case of stents, where removal or resizing of the device could be beneficial, but would currently require a full reoperation (Grabow and Schmitz, 2018). Removal of a stent once the heart is haemodynamically stable, along with the potential inclusion of bioactive substances or drugs to be eluted, could be of great benefit to patients (D'Souza *et al.*, 2008).

Finally, as with many areas of medicine, attentions have turned to personalising cardiovascular surgery and providing a more individualised care than is currently available. This personalisation ranges from medication choice and surgical planning, but also includes the early investigations into development of bespoke cardiovascular devices which respond to individual need rather than a population average (Jain, 2017; Vukicevic, Mosadegh, *et al.*, 2017). This thesis will focus on the development specifically of a mitral valve annuloplasty device, personalised for this very purpose.

1.1.2 Mitral valve disease

Mitral valve disease is the most common cardiac valvular disease consisting of both mitral regurgitation and mitral stenosis. Along with all other cardiovascular diseases, demand for mitral valve surgeries has been increasing. In 2018-19, 3,574 mitral valve repairs or replacements were undertaken within the NHS in England, compared to 2,725 cases in 2008-9, representing a 31% increase in surgical cases over 10 years (NHS Digital, 2019).

The mitral valve is a bileaflet valve separating the left atrium and ventricle. The valve leaflets are held in place by chordae tendineae and papillary muscles, which aid control of the opening and closing of the valve during diastole and systole.

The valve itself is made up of two separate leaflets and the mitral annulus. The posterior leaflet of the valve is roughly divided into three scallops, P1, P2 and P3; and the anterior leaflet is labelled in relation to those scallops although there is no anatomical separation. The anterior leaflet surrounds about 2/3 of the valve opening, with the remaining 1/3 being covered by the posterior leaflet. The anatomy and relative location of the mitral valve are shown in Figure 1.

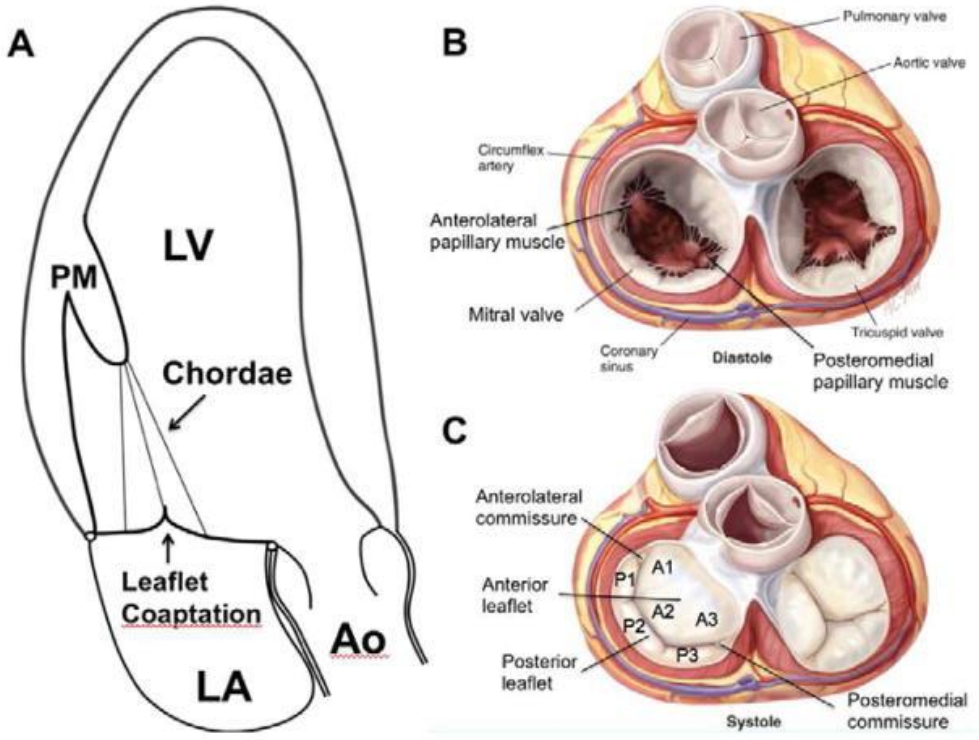

Figure 1: Anatomy of the mitral valve. A shows the apical long-axis view and the placement of the valve in relation to the Left Ventricle (LV), Left Atrium (LA), Aortic Valve (Ao) and Papillary Muscles (PM). B shows the open mitral valve from the surgical view through the left atrium, and C shows the surgical view of a closed mitral valve. Taken from (Dal-Bianco and Levine, 2013).

The mitral annulus is a fibrous ring which surrounds the leaflet insertion points around the whole valve structure. The annulus is not circular nor planar, as a number of commercially produced annuloplasty rings are shaped. It is, rather, a hyperbolic paraboloid with a flatter anterior side, producing a more D-shaped geometry (Mahmood *et al.*, 2013). It is a dynamic structure, and supports complete shutting of the leaflets during systole to prevent regurgitation of blood back into the atrium of the heart (Mahmood *et al.*, 2013).

The mitral valve is instrumental in controlling the flow of oxygenated blood out of the heart to the rest of the body, and as such degeneration or loss of function to the valve can have severe consequences if left untreated.

Mitral valve disease is classed into two categories: stenosis and regurgitation. The former refers to a tightening of the valve, the latter to a loosening of the valve apparatus.

1.1.2.1 Mitral valve stenosis

Mitral stenosis regards the tightening of the valve opening, preventing the free movement of blood from the atrium to the ventricle. It is most commonly caused by rheumatic fever, or more rarely by calcification of the mitral annulus. Mitral stenosis was the first cardiac valvular disorder that was corrected surgically, however its prevalence has decreased in developed countries(Sud *et al.*, 2016).

1.1.2.2 Mitral valve regurgitation

Mitral regurgitation results from the failure of the posterior and anterior leaflets of the valve to meet completely, resulting in backwards flow of blood through the heart (Enriquez-Sarano, Akins and Vahanian, 2009). Over time, the heart will compensate through left atrial hypertrophy, eventually resulting in heart failure. The causes behind this regurgitation can be congenital or acute and can achieve such damage through various mechanisms. Widely, the causes are classed as ischaemic, following an infarction of the surrounding tissue, or non-ischaemic. Non-ischaemic causes include primary myxomatous disease, a loosening of the annulus and leaflets, annular calcification and endocarditis (Enriquez-Sarano, Akins and Vahanian, 2009). Mitral valve disease regurgitation can also be classed into primary (directly caused by abnormalities of the mitral valve itself), or secondary (when a different event such as a myocardial infarction has led to a cascade of dysfunction in the heart eventually resulting in mitral valve failure) (De Bonis *et al.*, 2016).

Pharmaceutical interventions for primary mitral valve regurgitation are usually not recommended (De Bonis *et al.*, 2016). Some symptomatic management can be achieved

through medicine administration; however, the failure of the valve must be surgically addressed in order to rectify the disease. In secondary mitral valve regurgitation, where the mitral valve dysfunction has arisen from other diseases of the heart (such as myocardial infarction or endocarditis), pharmaceutical intervention should be used to reduce primary disease burden, however surgical repair or replacement of the mitral valve is also indicated to fully resolve symptoms (De Bonis *et al.*, 2016). Therefore, across all causes and types of mitral valve regurgitation, surgical intervention remains the most instrumental in resolving disease.

1.2 Mitral valve surgery

Depending on the mechanism of injury and the severity of regurgitation, the prognosis for patients with mitral valve regurgitation varies widely, as does the necessity for intervention and the method thereof (Delling and Vasan, 2014). Surgical interventions for treatment of mitral regurgitation are a continually evolving practice, having seen much change since the first implantation of the Starr-Edwards Valve in 1960 (Matthews, 1998). Broadly speaking, surgery can be split into two approaches: surgical repair of the existing valve, or entire replacement of the patient's valve structures, using long-term, implantable devices.

During the last two decades, replacement of the mitral valve has become less common, with repair of the existing valve now being favoured as a less invasive procedure and with better operative outcome (Gammie *et al.*, 2009; Sawazaki *et al.*, 2014; Lazam *et al.*, 2017). Operative mortality for mitral valve replacement surgeries (3.8%) has been found to be significantly higher than repair surgeries (1.4%), and long-term mortality rates follow the same pattern (46% versus 23%) (Gammie *et al.*, 2009; Lazam *et al.*, 2017).

In the years 2018-19, mitral valve repairs alone constituted 1955 cases in the NHS, with mitral valve replacements producing a further 1413 patient episodes (NHS Digital, 2019). The costs for surgery are high, with in-hospital estimates of costs in the USA standing at $78,216 for valve replacement and $72,761 for repair (Ferket *et al.*, 2018). Despite being the less expensive option, repair surgery clearly remains expensive. Common to both are long in-hospital recovery times, and for repair, annuloplasty ring devices themselves reaching thousands of pounds alone (Cohn *et al.*, 1997; Edwards Lifesciences LLC, 2010). In addition, sizers required to decide on the correct implant for use on patients must be purchased separately, and range from hundreds to thousands of pounds for a set (Edwards Lifesciences LLC, 2010).

1.2.1 Mitral valve replacement

Mitral valve replacement is more likely to be employed in patients who are older and with an increased number of comorbidities, or who have more severe disease (Gammie *et al.*, 2009; Lazam *et al.*, 2017). When replacing a cardiac valve, either a biological or a mechanical valve can be chosen for implantation. Biological valves have become more common in surgical use, despite their limitations in long-term placement (Gammie *et al.*, 2009; Madesis *et al.*, 2014). The reduction in use of mechanical valves is likely attributable to the higher risk of embolism, requiring more anticoagulant medication, which in turn then leads to an increased risk of haemorrhage post-surgery (Enriquez-Sarano, Akins and Vahanian, 2009).

Largely, however, repair surgery is now preferable to replacement due to its reduced negative outcomes and reduced frequency of reoperation, with one group expressing that replacement surgeries are performed "far too frequently" when alternative surgeries are available (Gammie *et al.*, 2009; Madesis *et al.*, 2014; Lazam *et al.*, 2017). Whilst mitral valve surgeries have increased by 31% overall over the past 10 years, the occurrence of repair surgery has greatly outpaced replacement: mitral valve repair has increased in frequency by 56% (NHS Digital, 2019).

1.2.2 Mitral valve repair

Novel developments of repair and annuloplasty surgeries of the mitral valve have included transcatheter and minimally invasive approaches to the surgical technique (Cohn *et al.*, 1997; Tatooles *et al.*, 2004). However, the scope of this thesis focusses on conventional mitral valve repair, which remains the more common surgery under employment, due to limited evidence of significant benefit to patients for these more expensive novel techniques. Further, most devices capable of conventional repair are also appropriate for use in minimally invasive techniques (Cohn *et al.*, 1997; Van Praet *et al.*, 2018).

The aim of a mitral valve repair surgery is twofold: to restore coaptation of the valve leaflets, and to restore the natural shape of the mitral annulus (Madesis *et al.*, 2014). The combination of these two factors should lead to a restoration of normal valve function and elimination of regurgitation. A view of presurgical, diseased and postsurgical mitral valve apparatus is shown in Figure 2.

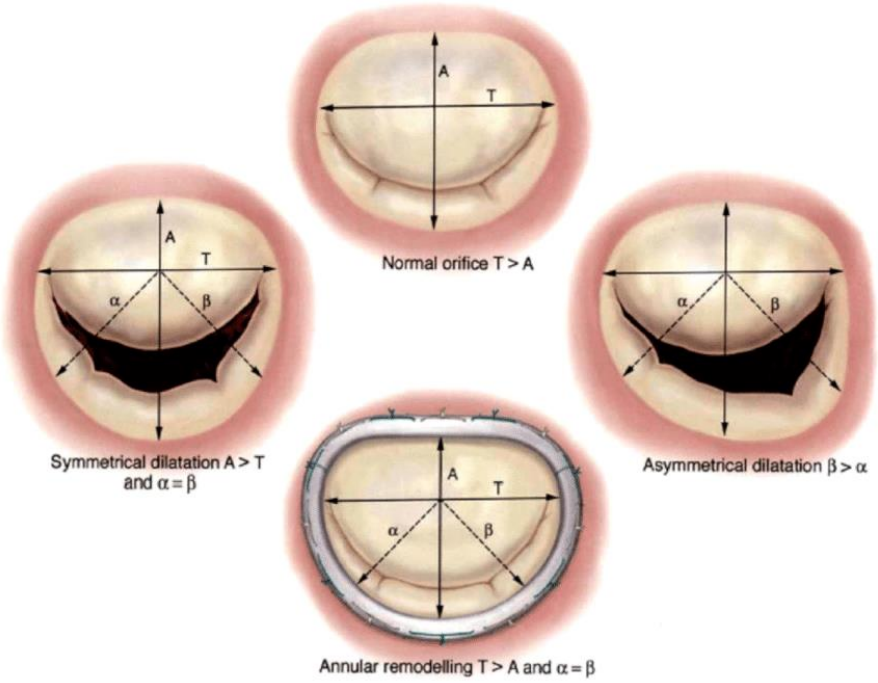

Figure 2: A view of mitral valve apparatus. From top: a healthy mitral valve; a valve with symmetrical dilatation across the posterior aspect; a valve with asymmetrical dilatation on one side of the posterior aspect; a reconstructed valve following repair. Taken from (Kheradvar *et al.*, 2015)

Where a valve prolapse is present amongst the disease, sections of the posterior valve leaflet will usually be removed (this is less commonly applied to the anterior leaflet), and the chordae tendinae may be shortened or added to with artificial chordae (Enriquez-Sarano, Akins and Vahanian, 2009).

In the case of functional mitral regurgitation however, surgery focusses more on the effect of annular dilatation and reducing this through introduction of annuloplasty devices intended to reduce the circumference of the diseased mitral valve opening (Enriquez-Sarano, Akins and Vahanian, 2009).

The discussion of respecting versus resecting the valve tissue during a mitral valve repair has been continual, with removal of valve leaflet tissue being discussed as a potential source of postoperative valve stenosis. However, both techniques are still employed at the discretion of the surgeon, with resection applied more commonly where there is an excess of tissue in the valve leaflets or where the mitral annulus has become calcified (Tomšič, Klautz and Palmen, 2018).

As mentioned previously, annuloplasty is employed as a final step in most mitral valve repair surgeries. This ties into the second aim of the repair surgery, in restoring the natural shape

of the annulus, particularly in reducing the circumference when dilated (Madesis *et al.*, 2014).

1.2.2.1 Mitral annuloplasty

The process of annuloplasty, shown in Figure 3 involves the insertion of a device over the mitral valve to restore a healthy annular shape and encourage coaptation of the valve leaflets. Dilatation of the mitral annulus can either be a cause or a result of mitral regurgitation, and therefore is commonly found in association with valvular disease.

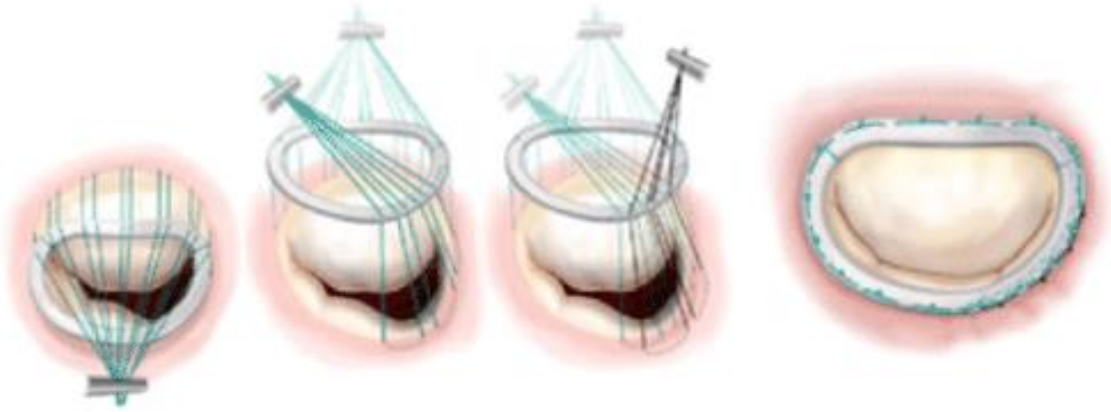

Figure 3: The steps of mitral annuloplasty. From left: sutures are placed through the anterior portion of the valve annulus and the annuloplasty device. Sutures continue around the device and the valve circumference and are pulled tight to fix the device in place over the top of the valve structure. Taken from (Kheradvar *et al.*, 2015)

Depending on the severity of disease and related conditions, the decision can be made to either true-size or under-size the ring according to the current dimensions of the mitral valve. True-sizing will replace the shape of the annulus and prevent further degeneration; whereas under-sizing will pull back together valve leaflets which have lost coaptation due to a dilated annulus. Inclusion of annuloplasty in mitral valve repair is a significant predictor of success rates of mitral valve repair, and exclusion of annuloplasty can result in recurrent regurgitation (Flameng, Herijgers and Bogaerts, 2003).

Current rings used in annuloplasty are composed of a titanium alloy or polymer (traditionally polyoxymethylene) core, surrounded by sponge and Dacron (polyethylene terephthalate) fabric for suturing. Rings have been designed with a range of minor modifications, including altering rigidity and increasing or decreasing the saddle-like shape (Jensen *et al.*, 2008; Silberman *et al.*, 2009). Some major commercial producers of annuloplasty rings include Edwards Lifesciences, Medtentia, St Jude Medical and Sorin. An example of a Medtentia

annuloplasty ring (with additional ventricular appendage under the main ring structure) is shown in Figure 4 (Konerding *et al.*, 2013).

Figure 4: Image of the Medtentia annuloplasty device, manufactured with a metal core and partially covered with a suture cuff. Taken from (Konerding et al.*, 2013)*

Current choice of annuloplasty ring is led primarily by surgeons' preference, influenced by the brands available at individual hospitals and training programmes (Arora and Anyanwu, 2015; Wan *et al.*, 2015). Few clinical or experimental studies have been performed to compare the efficacy and suitability of different rings for repairs, and this remains a limiting factor on the evidence-based approach to mitral valve repairs (Wan *et al.*, 2015). More studies are now being produced using techniques varying from augmented reality sizing (Ender *et al.*, 2008) to finite element analysis of forces on the valve (Votta *et al.*, 2007), however most of these focus only on one specific ring design or a direct comparison of only a small number of those available.

1.2.3 Recurrent disease

Whilst surgery is mostly successful in repairing or replacing the valves, repairs may not last over a lifetime and may require reoperation. The rate of failure for mitral valve repair varies widely between institutions, surgical technique, devices, and methods employed. However, within 10 years of surgery, figures of around 15-20% of patients experiencing a return of mitral regurgitation are not uncommon (Shimokawa *et al.*, 2011; da Costa *et al.*, 2018; Petrus *et al.*, 2019).

Modes of recurrent disease can be dependent on a range of factors, both biological and external. In some cases, underlying disease such as ischaemia or endocarditis will progress. In other cases, some portion of the surgical procedure will fail – this may be procedural or directly related to devices implanted during surgery. Historically, procedural complications were common, however in more recent times studies have shown that the majority of recurrent mitral valve regurgitation now arises from disease progression (Gillinov *et al.*, 1997; Shimokawa *et al.*, 2011).

Patients with recurrent regurgitation are at high risk of the disease progressing further, and significant risk of complications and death. Reoperation is usually necessary, to re-repair or otherwise rectify surgical failure. In cases where reoperation is attempted for recurrent disease, valve replacement may alternatively be attempted (Gillinov *et al.*, 1997).

Specifically relating to annuloplasty devices themselves, failure can arise from any portion of the surgical application. Devices themselves may break, sutures may come loose, or complications may arise from interactions on the surface of the device including infection or thrombi (Gillinov *et al.*, 1997; Dumont *et al.*, 2007; Shimokawa *et al.*, 2011).

In order to combat the concerns of failing annuloplasty devices, the design of bespoke annuloplasty ring implants for individual patients has been proposed, in place of the current system of near-sizing based on a limited range of commercially available sizes and shapes. These personalised devices aim to improve fit to patient anatomy to reduce the risk of complications such as dehiscence, stenosis or damage to other structures owing to under-, over-, or incorrect sizing.

1.3 Personalisation of medical implants

Historically, implantable medical devices have been manufactured using formative or subtractive techniques, including casting and milling (Sidambe, 2014; Dall'Ava *et al.*, 2019). These processes are limited in their ability to change designs and are suited predominantly to mass manufacture of a set design, with some small variation across a size range for example. Adaptation of these processes to produce wide variation or even individual designs would be complex and costly, owing to the need to produce new moulds and specific tooling for each design (Dall'Ava *et al.*, 2019).

In some cases where high personalisation has been a requirement of an implanted device, manual adjustments have previously been adopted. These would include processes such as hammering a plate or bending a wire into shape according to the needs of the application (Raisian *et al.*, 2017). In particular, this has been adopted for craniomaxillofacial implants, where aesthetics and functional shape specificity is of higher importance. However, these processes are both time-consuming and imperfect, being reliant on the precision of a surgeon to produce an implant matching the needs of the patient manually, and within the time frame of active surgery.

More novel manufacturing techniques developed in the late 20th and early 21st century allow for greater design freedom and greater ease in adapting individual or smaller groups of devices for a specific application. The addition of computer numerical control (CNC) machining allowed quicker manufacturing with reduced human input into a manufacturing process. In turn, as this process is controlled by computers, designs can be changed incrementally, and bespoke devices become easier to realise (Dall'Ava *et al.*, 2019). However, again this process remains cost prohibitive in most cases. The material wastage in such subtractive processes is high, resulting in high output costs for each individual implant compared to the material retained in the part. This becomes particularly the case as implant designs become more complex, when considering small individual anatomical variances or the inclusion of cell growth-promoting lattice structures. Thus, these adaptable but subtractive processes do not offer a sustainable option to the medical sector for wider adoption of bespoke implants.

Additive manufacturing technologies present a promising outlook to bespoke medical implants in comparison to other available technologies. The ability to produce complex and rapidly adaptable computer-based designs, as found in CNC milling, is retained, with further improvements on precision and reduced material wastage (Gibson, Rosen and Stuker, 2013).

The potential for recycling of unused materials across a number of additive technologies reduces the cost output associated with subtractive techniques, and fine internal details are manufacturable in-process as a part builds from “ground-up” (Dall’Ava *et al.*, 2019).

1.4 Additive manufacturing

Additive manufacturing (AM) has presented an upheaval in manufacturing and research and is quoted as being part of the "third industrial revolution". AM encompasses the production of parts from 3D computer models, normally in a layer-by-layer manner, in contrast to traditional or subtractive manufacturing techniques (Gibson, Rosen and Stuker, 2013).

The benefits of additive manufacturing include increased freedom of design, production on demand and simplification of supply chains. In the production of small-volume, complex objects, AM can both speed up and decrease the cost of manufacturing. As a result, the financial impact of AM introduction has been significant: the industry saw an annual growth rate of 30% in the years 2010-2015 and an annual growth of 21% in 2017 alone (Bourell, 2016; SME, 2018). Further, industry experts are almost unanimously agreed that this growth is set to continue and likely accelerate, driven by increased AM of end-use devices and bioprinting (SME, 2018).

Methods of additive manufacturing are divided into seven categories based upon the form of the starting material and method of consolidation. These categories include: binder jetting, directed energy deposition, material extrusion, material jetting, powder bed fusion, sheet lamination and vat photopolymerization (Gibson, Rosen and Stuker, 2013). The seven methods of AM provide different benefits for different applications: some provide higher accuracy, whilst others are more accessible to the wider market or are able to be applied to a wider range of materials. Interest in additive manufacturing has been raised across a number of sectors including medical, aerospace, and automotive applications.

A brief overview of the major additive manufacturing methods and their application in medical uses is shown in Table 1. In this research, selective laser melting was chosen as the method of manufacturing. Selective laser melting has been trialled for a number of medical applications, as discussed in Section 2.5.5, and has promise in manufacturing materials which have historical evidence of biocompatibility in various medical applications. Metals such as Ti6Al4V, CoCr and stainless steels are common in medical devices and thus a metal manufacturing method is beneficial to this research. Other metal AM technologies listed in Table 1 are less appropriate for small device manufacturing, such as DED which is typically contained to larger bulk deposition of material in applications such as cladding or large AM builds.

Table 1: Overview of Additive Manufacturing Processes in medical applications (Gibson, Rosen and Stuker, 2013)

Process category	Benefits	Downfalls	Common materials	Employability in medicine
Binder jetting	Wide range of binder and material combinations available Comparatively faster than some other AM techniques	Requires post-processing Struggles with structural components due to spaces without binder present within layers	Metals, polymers, and ceramics Powder-based material	Employed in manufacture of implants and drugs
Directed energy deposition	Greater control over material microstructures Hybrid systems are in development for deposition-processing combinations	Requires post processing Currently limited to near-net shapes	Metals Powder or wire-based material	Employed rarely in manufacture of implants
Material extrusion	Cheaper and more accessible than many other AM processes	Comparatively slow process Low accuracy and precision compared to other processes	Polymers Filament-based material	Employed in the manufacture of guides and models
Material jetting	High accuracy deposition of material droplets	Greater reliance on support structures than other processes	Polymers Droplet-based material	Employed in the manufacture of guides and models Some use of biocompatible resins for dentistry
Sheet lamination	High-speed AM process	Limited applications and materials available	Metal, polymers, and paper Sheet-based material	Uncommon in medical applications
Vat photopolymerization	High accuracy process Comparatively good surface finish of AM parts	Requires extensive post-processing Reliant on support structures Expensive process	Polymers and resins Liquid-based material	Employed in the manufacture of implants and tissue engineering
Powder bed fusion	Some self-supporting ability Comparatively inexpensive when including powder recycling	Often requires post-processing Limited size	Metals, polymers, and ceramics	Employed in the manufacture of implants and tissue engineering

1.4.1 Selective laser melting

Selective laser melting (SLM), shown schematically in Figure 5, is a powder bed fusion technique of additive manufacturing used primarily in the fabrication of metal parts. The process involves a powdered material melted together in layers by a laser, controlled via a computer holding a CAD model of the final part.

SLM is normally carried out in an inert gaseous environment to minimise oxygen content and increase purity of the material. Inside the machine is a scanning laser, a moving build platform, and a powder recoater, as shown in Figure 5. The recoater spreads material powder over the build platform at a defined thickness (dependent on the material), after which the laser passes over the powder in patterns dictated by a single layer of the CAD file to fuse the powder in those areas. The build platform then lowers, another layer of material is spread over the top, and the process repeats.

Specific to biomedical applications, SLM parts can be produced with porous structures beneficial to the growth of cells on and into them. Previous *in vitro* studies have shown that SLM-manufactured Ti6Al4V and stainless steel provide beneficial mechanical properties and cellular integration, including improvements over material manufactured by non-additive techniques (Hollander *et al.*, 2006; Wei *et al.*, 2015). In addition, porous structures provide improved mechanical properties for bone applications compared to traditional metal parts, as they minimise the risk of stress shielding around the implanted part (Arabnejad *et al.*, 2017). The freedom of design and manufacturing offered by additive manufacturing can provide greater ability to fabricate these internally porous components, aiding the reduction of stress shielding.

Over alternative methods of additive manufacturing, SLM also provides some process benefits. The lack of binding material required means that parts produced can be more dense than, for example, produced using binder jetting where the binding material is removed to complete manufacturing of the part. In addition, the material which is left unmelted provides some support to overhanging or internal structures, reducing the number of support structures required in other methods such as fused deposition modelling. These support structures provide areas of extra material which must be removed during post-processing of the build, however due to the geometry of an annuloplasty ring not involving large overhangs or lattices, the build orientation can be optimised to minimise the impact of these supports. Unused material inside the SLM machine after a part is finished can also be recycled and reused for a next build. Finally, SLM is capable of achieving very good mechanical properties in finished pieces. SLM manufacture of Ti6Al4V alloy is now capable of meeting and

exceeding mechanical properties achievable with wrought and cast material, even without the need for post-processing treatments (Liu *et al.*, 2019). In this study, parameter optimisation led to increases in ultimate tensile strength, ductility and hardness when porosity was well controlled (Liu *et al.*, 2019).

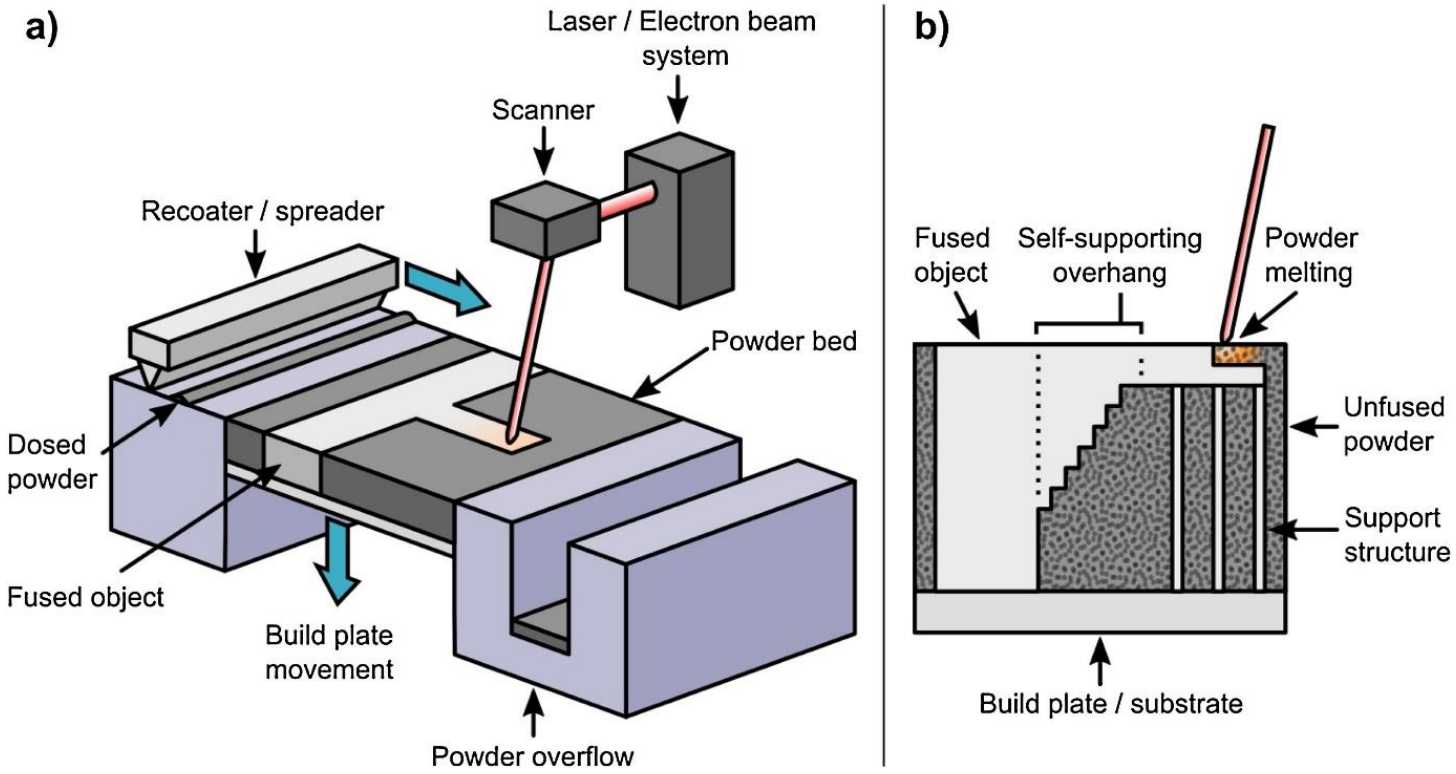

Figure 5: Overview of the powder-based fusion method of metal additive manufacturing, used in some medical applications. (A) shows the overall internal workings of a powder bed fusion machine including the powder bed, material powder, and laser used to fuse particles together. (B) shows a cross section of the build area during manufacturing, exhibiting the freedom of design owed by AM techniques allowing for overhanging parts within the build. Taken from (Lowther *et al.*, 2019).

1.5 Personalised implants by selective laser melting

A number of methods of design, production and implementation of personalised implants have been investigated. Depending on the aim and application of the device, appropriate material properties needed vary. Examples of AM parts in the literature include skull plates, jaw replacements, neck of femur replacements and more (Cohen *et al.*, 2009; Jardini *et al.*, 2014; Rotaru *et al.*, 2015; Wong *et al.*, 2015; Lu *et al.*, 2018; Goodson *et al.*, 2019)

Titanium and its alloys have been the material of choice in most additively manufactured implanted medical devices to date, with other materials in use including CoCr, polymers such as PCL, and ceramics for dental applications (Lowther *et al.*, 2019). Titanium has a long history of development in selective laser melting processing and is now able to be additively manufactured with ease and success. In addition, it boasts good biocompatibility, specifically in the Ti6Al4V alloy (Sidambe, 2014).

With regards to mechanical properties during SLM production, Ti6Al4V has proven to be capable of additive manufacture to similar properties as those found in conventional manufacturing, especially when including post-processing methods such as heat treatments (Liu *et al.*, 2019). Alternatively to heat treatments, various scanning strategies can be employed to reduce issues such as residual stress or porosity commonly found with SLM-manufactured titanium alloys (Liu *et al.*, 2019). With the employment of one or both of these activities, mechanical properties within range of conventionally manufactured material is possible, and in some cases strength and hardness can be higher, for example compared to wrought material (Shunmugavel *et al.*, 2017; Liu *et al.*, 2019).

Titanium alloy has been used in additively manufactured skeletal implants due to its good biocompatibility and mechanical properties, especially when taking into account the potential for complex internal structures (Kaur and Singh, 2019). Inclusion of these structures in the place of a fully solid part lowers the density of an implant and matches the mechanical properties closer to that of the patient's own bone, avoiding stress shielding from the metal part (Kaur and Singh, 2019). The elastic modulus of solid Ti6Al4V, for example, is 110GPa, whereas human cortical bone only approaches 20GPa. In addition to single lattice structures to move the overall modulus closer to matching the surrounding bone, functionally graded materials using SLM technology allow for a gradient of properties to exploit the benefits of a strong material while not damaging other body tissues (Xiong *et al.*, 2020).

With regards to annuloplasty devices, the *LivaNova Memo 3D ReChord* device is manufactured using a combination of titanium alloys at its core (namely, Nitinol and

Ti6Al4V). This device is designed for “selective flexibility” in the posterior portion of the device, allowing for movement of the valve in this area (Prinzing *et al.*, 2018). The nitinol alloy alongside silicone surroundings allow for flexion in the ring, with Ti6Al4V core components providing rigidity and support.

Further to the general application of additively manufactured Ti6Al4V in medical devices, material development and improvement of biocompatibility through integration of novel technologies has been attempted. Fine control over the size and number of pores present in an additively manufactured part has been asserted, providing improved design techniques for enhancement of osseointegration (Murphy and O’Brien, 2011). Surface coatings and material additives, including active biomolecules such as vascular endothelial growth factor (VEGF) and passive coatings like hydroxyapatite, have been applied to increase the speed at which cellular integration takes place (Matena *et al.*, 2015; Wei *et al.*, 2015).

By comparison, long-term soft tissue devices are less well investigated, owing likely in large parts to the lack of availability of safely implantable materials used in 3D printing with appropriate mechanical properties. In addition, soft tissues present challenges in imaging clearly for design as the densities relied on by most medical imaging software are too similar to distinguish features across organs. In their place, a large area of research for organs and other soft tissues resides currently in preoperative assessment and planning of surgeries (Birbara, Otton and Pather, 2019).

1.6 Challenges of the cardiovascular environment

The needs of the cardiovascular environment with regards to long-term implantable devices are in many cases more challenging than other organ systems. Imaging of the cardiovascular system is often difficult or invasive, risks of complications are high, and the potential outcomes of such complications can be life threatening.

As the heart is encased within the chest cavity, it is secluded behind both the ribcage and surrounding organs. Imaging the heart therefore is challenging, especially as a soft tissue which does not provide significant density differences from surrounding areas, as is found with bone. The activity and movement of the heart can also provide challenge in imaging the heart clearly before or during surgery (Cawley, Maki and Otto, 2009).

Compared to skeletal implants, the impact of blood flow on cardiovascular implants is much greater. Cardiovascular implants are in direct, constant contact with blood throughout their lifespan, and in the majority of cases they are subject to high-pressure and turbulent flow of blood. This provides potential for complications through more than one avenue: the high pressure puts strain on the tissues and sutures used to hold the implant in place, and the inclusion of a foreign object in the blood provides infection and thrombotic risk (D'Souza *et al.*, 2008; Anyanwu and Adams, 2009). This risk is heightened with comparison to other devices, as the direct blood contact allows for any infective or thrombotic agents to be moved quickly around the body and spread more easily than would be found in local systems.

Although the cardiovascular environment provides numerous challenges, there are also some benefits of working with softer tissues. Unlike skeletal tissue, which is highly active with fast cellular turnover and constant growth, the heart and vessels are comparatively less active in dividing and replacing the tissue. As a result, the potential for stress shielding and other issues of damage to renewing tissue associated directly with material properties is reduced (Lowther *et al.*, 2019). The load-bearing nature of the implant is also reduced, and in the case of annuloplasty devices, the lack of articulating parts avoids issues associated with material-on-material contact within devices (Nuevo-Ordóñez *et al.*, 2011).

Assessment of cardiovascular devices remains stringent, with a wide range of expected conditions to be tested before market (ISO, 2017). An annuloplasty device is regarded as a Class 3 Medical Device under the EU Medical Devices Directive, alongside other long-term implantable devices such as hip stems, tissue scaffolds or bone plates (Publications Office, 1993). This places annuloplasty rings in the highest risk category of device (excluding active

devices) and opens them to stringent testing and validation needs before being allowed into clinical use.

In most cases, personalised medical devices, including those such as annuloplasty devices and other Class 3 devices, are exempt from the EU Medical Devices Directive. Additively manufactured, bespoke items did not previously fall into the categories of legislation as they could not be widely verified on a batch-wide basis and did not fulfil the requirements of the directive. Some of this discrepancy was cleared through the updated guidelines provided in the 2017 update to the Medical Devices Regulations, however in large part, bespoke devices remain outside of the regulatory framework (Publications Office, 2017). In fact, the explanatory notes of the new Medical Devices Regulations agrees that "*Manufacturers of medical devices for an individual patient, so called 'custom-made devices', must ensure that their devices are safe and perform as intended, but their regulatory burden remains low"*(Publications Office, 2017). In such cases, an individually designed and prescribed device can be given to a patient at the behest of clinicians and with appropriate supporting documentation to show evidence of efficacy of the device.

Regardless, the appropriate measures to take when developing a novel device for wider use remain to test stringently on at least the material and prototype level, even if rigorous testing of the final part is not possible. Later validation of final products can be supported using witness specimens and sacrificial copies of the device on the same build. Whilst guidelines are variable for individual devices and dependent on previous experience of the device, material biocompatibility, haematology and thrombotic potential are all expected amongst blood contacting devices, with variations based on duration of blood exposure and purpose of the device as well as the novelty of material or application (ISO, 2017).

2 Literature Review

2.1 Personalised cardiovascular surgery

Previous examples of personalised cardiovascular devices have included early investigations into vascular stents, balloons and valve repairs (Demir and Previtali, 2017; Robinson *et al.*, 2018). Further developments have also been made in tissue engineering associated with additive manufacturing, dubbed "bioprinting" (Alonzo *et al.*, 2019; Vashistha *et al.*, 2019), however this will not be a focus in this thesis.

Other developments in patient-centred care have included the personalisation of existing surgeries and imaging to provide individualised plans and outcomes in contrast with assumptions about patient needs across populations. Computational modelling of therapies and devices has been undertaken, addressing diseases such as heart failure, aneurysms and valvular disease among others (Gray and Pathmanathan, 2018).

Additive manufacturing, for its part, provides other avenues of personalisation for surgery and disease control, owing to the ability to replicate complex structures quickly and cheaply.

2.1.1 Additive manufacturing in cardiovascular disease

A large portion of previous work using additive manufacturing in medicine has been in skeletal applications, owing to both the availability of appropriate materials and the ease with which these structures can be imaged and processed using available computer programs. However, soft tissue applications have been investigated more recently, covering a number of potential areas for work. Cardiovascular interventions are particularly benefiting from this technology given the complexity of the heart and its related structures, giving the chance to visualise internal parts before surgery has begun.

2.1.1.1 Education and training

For the purposes of training surgeons, nurses and other healthcare professionals, additive manufacturing provides an effective method of producing anatomical models based on real patients and incorporating the naturally occurring differences in anatomy. These models can be produced quickly and relatively cheaply, providing a wider range of diseased and normal anatomies to inspect and minimising patient risk during training periods.

Models have been produced of whole mitral valves comparing diseased and healthy states (Witschey *et al.*, 2014; Mahmood *et al.*, 2015) as well as specifically the mitral annulus alone (Mahmood *et al.*, 2014).

One such example in which a significant impact on student learning has been found was a comparison between cadaver donations and additively manufactured models in cardiac anatomy teaching (Lim *et al.*, 2016). The inclusion of additively manufactured models in education resulted not only in a significant improvement in post-learning test scores compared to pre-learning tests, but also provided a significantly higher average post-test score in the group using additively manufactured models compared to those using cadaver-only or combined learning techniques (Lim *et al.*, 2016).

2.1.1.2 Presurgical planning

With regards to cardiovascular disease, visualisation of internal structures that are not easily accessed outside of the operating theatre can be hugely beneficial in the planning of surgery. In particular the visualisation can aid surgeons in predicting complications to the surgery and decide on which route or method of access will be most appropriate: in one study it was found that the majority (85%) of cardiac health professionals asked would likely use additively manufactured valve models in future practice (Birbara, Otton and Pather, 2019).

A number of groups have applied additive manufacturing technology specifically to the preoperative planning of valve surgeries. These have included the planning of transcatheter and percutaneous surgical interventions as well as paediatric cases (Dankowski *et al.*, 2014; Izzo *et al.*, 2016; Ilina *et al.*, 2017; Scanlan *et al.*, 2018). Due to the obvious anatomical size differences between adult and paediatric cardiovascular systems coupled with the more subtle structural differences, being able to print 3D models of valves and other structures represents a significant development in the preoperative planning process.

2.1.1.3 Testing of interventions

Methods for effective testing of new medical and surgical interventions are constantly evolving, and in particular there is a need for effective alternatives to animal and human testing of devices at early stages. In this vein, additive manufacturing has continued this trend, as the reproduction of minor variations in cardiac anatomies allows for testing of new devices across a number of possible situations. In addition, different surgical techniques and equipment can be tested on one patient's anatomy to decide the best course of action for that individual.

"Indirect printing", or using additive manufacturing for the production of bespoke negative moulds, has been used frequently to work around the limitations of existing AM materials when mimicking human tissue. For example, (Ginty *et al.*, 2017) used a final silicone piece produced from a printed mould. The hope was in these cases that using actual patient valve

dimensions produced by additive manufacturing, the chambers would be more accurate at testing individual cases by avoiding use of a generalised shape from a large population (Mashari *et al.*, 2016). However, with a total process time of 19 hours from image acquisition to a finished silicone piece, this method proves inefficient when compared to the direct printing achieved by studies above. A similar method of indirect printing was used to produce a model of an aortic aneurysm for stent design in a vascular phantom (Sulaiman *et al.*, 2008). In addition, (Vukicevic, Puperi, *et al.*, 2017) used directly printed mitral valve models to test the new MitraClip device in the lab without using human or animal tissues. The study by (Vukicevic, Puperi, *et al.*, 2017) in particular is of note as the group made use of a multimaterial printer which allowed for closer representation of tissue properties, but also variation to accommodate for other needs, such as calcified deposits in a harder material. Both studies concluded with the use of the chosen device in surgery with the patients concerned, and both provided positive outcomes to the patient.

As technologies develop and further software capabilities become easily accessible, it is likely that these workflows will become more appropriate for common clinical use. In the meantime, methods of indirect printing are useful for widening the pool of materials for use to better mimic human tissues.

2.2 Limitations of existing annuloplasty rings

Up to 20% of patients will require further surgery following mitral valve repair, often due to relapse or progression of disease (Enriquez-Sarano, Akins and Vahanian, 2009; Shimokawa *et al.*, 2011; da Costa *et al.*, 2018; Petrus *et al.*, 2019). Whilst the mechanism of secondary damage is most commonly new or worsened disease in the valve, technical failure of the initial surgical procedure still constituted nearly half of all reoperations in one study (Suri *et al.*, 2006). Issues with the surgical procedure are seen as preventable, but still occur and in some cases require more than one revision surgery following the original repair (Dumont *et al.*, 2007).

Dehiscence, or a complete failure of sutures to hold the annuloplasty ring in place leading to tearing of the stitches through the tissue, represents a medical emergency which must be operated on immediately. It has been quoted as the most common technical or procedure-related postoperative complication (Dumont *et al.*, 2007). Whilst this often occurs from undersizing of the annuloplasty ring, a device which appears to be correctly sized may have unequal forces exerted around its circumference, leading to the same outcome.

More common but less severe complications of annuloplasty surgery include left ventricular outflow tract obstruction and systolic anterior motion of the valve (Dal-Bianco and Levine, 2013). These may or may not require further intervention or reoperation, however, often lead to decreased efficiency of the heart, and may decrease quality of life in those affected.

Although a range of sizes is available in varying models of annuloplasty ring, few are available in sizes suitable for small paediatric hearts. In part this is due to a lack of demand, as a fixed annuloplasty ring is unable to grow with the developing paediatric heart, potentially leading to pathological stenosis. In addition the risk of embolism associated with foreign bodies within the heart is extended due to the longer lifetime with the implant in situ (Kazaz *et al.*, 2005; Cikirikcioglu, Cherian and Kalangos, 2012).

Of the repairs performed in the NHS during the years 2018-19, 54 cases were in patients under the age of 18, constituting just over 2.6% of procedures (NHS Digital, 2019). In these patients, annuloplasty without an annuloplasty ring is usually performed (Komoda *et al.*, 2009). Procedures like the De Vega or Paneth annuloplasty can be used to reduce the size of the native annulus by suturing through the tissue itself, or annuloplasty can be avoided entirely (Wood *et al.*, 2005). Whilst this avoids the need for reoperation to replace annuloplasty rings as the heart grows, it can leave an incomplete repair and restoration of the healthy annulus may not be successful in the long term.

Other limitations to the availability of annuloplasty devices include bariatric surgery as well as disease which has progressed past a point of successful reparability. Similarly, to paediatric surgery, the sizes of annuloplasty ring required for some of these surgeries are not currently produced. In addition, patients who are older or have greater body surface area undergoing mitral valve replacement are at a greater risk of mismatch between device size and the native valve (Akuffu *et al.*, 2018) . In the case of severe disease, modelling of the valve and forces exerted on it by implants could better inform surgery. Then, by using personalised implants, valve repair could be undertaken within acceptable limits of regurgitation recurrence and ring dehiscence risk. Larger sizes could also be produced as they would not bear the economic loss of mass-producing underused sizes as they would still be manufactured on an individual basis for patients.

2.3 Essential functions of annuloplasty devices

Mitral annuloplasty, as discussed in Section 1.2.2.1, is commonly applied in mitral valve repair, and requires the use of a ring or near-ring annuloplasty device. These devices provide the mechanical support for a mitral valve repair, however in order to provide this support safely and effectively inside the heart they must fulfil several functions:

2.3.1 Form the appropriate size and shape for a patient's mitral valve

Correct sizing of an annuloplasty ring is of vital importance, as incorrect size or shape can lead to negative consequences, including mitral stenosis or recurring regurgitation (Magne *et al.*, 2008). Whilst sizing is generally successful in most patients, it requires interoperative assessment by the surgeon, leading to a subjective decision which can be affected by the experience of the surgical team, as well as extended time on bypass and under anaesthesia for the patient (Graser *et al.*, 2014). Previous studies have shown that different methods of manual intraoperative sizing commonly employed result in significantly different size suggestions (Al-Maisary *et al.*, 2017). In this research it was shown that based on five different methods employed by surgeons, the average size suggestions produced for a cohort of 43 patients ranged between 29.9mm and 37.5mm (Al-Maisary *et al.*, 2017).

Even when rings are sized correctly however, animal studies have shown that the implantation of currently available annuloplasty rings may still lead to an imperfect repair of the valve and annulus. In one study the implantation of annuloplasty rings led to a reduced maximal opening of the valve leaflets when compared to normal, healthy diastole (Bothe *et al.*, 2010). In addition, some models increased the excursion of valve leaflets or decreased the distance between the left ventricular septum and the anterior aspect of the mitral valve (Bothe *et al.*, 2010). The latter of these is considered a risk for future regurgitation of the anterior leaflet, and the former was found to increase bending stresses on the valve leaflets, suggesting that fully rigid rings may be detrimental to the success of long-term repair (Bothe *et al.*, 2010).

Some of the issues described above with current annuloplasty rings have been improved through the design of a "saddle-shaped" ring (Bothe *et al.*, 2010). These rings are designed to reproduce the natural three-dimensional shape of patients' healthy annulus more effectively. Saddle annuloplasty rings have been shown to distribute stress more effectively, leading to lower overall forces than traditional flat rings (Jensen *et al.*, 2008). Shapes bespoke to the patient and their individual disease mechanism, however, are likely to be even more successful in treating mitral regurgitation. The Geoform annuloplasty ring was designed

specifically for functional mitral regurgitation, avoiding the need to downsize rings to provide support for severe lack of coaptation in some patients (Votta *et al.*, 2007). These rings have been successful in surgical use, and have suggested that disease-specific design could improve outcomes of current surgery (Votta *et al.*, 2007; Timek *et al.*, 2014).

The mitral valve is commonly described as adhering to a 3:4 ratio between the anteroposterior and transverse diameters (Carpentier, Adams and Filsoufi, 2010), and examples of existing surgical implants being designed according to this ratio can be found, such as the Carpentier-Edwards Physio Ring. This ratio stems from the experience of Carpentier and surgical textbooks, however few papers have been published investigating the relationships between the healthy dimensions of a mitral valve (Carpentier, Adams and Filsoufi, 2010). If accurate, this ratio could be instrumental in the prediction of mitral valve dimensions post-intervention and could allow for design of patient-specific implants based on preoperative scan data. However, limited evidence has been published to support this ratio, and as such it is not clear how much value this relationship could provide in predictive settings.

2.3.2 Prevent coagulopathies leading to cardiovascular deterioration

A major concern of long-term implantable devices in constant blood contact is the risk of thrombosis instigated by the device itself. Whilst coagulation is a normal part of circulatory system upkeep, erroneous clots can result in catastrophic consequences, leading to myocardial infarction or cerebrovascular accidents.

Foreign objects in the bloodstream pose risk for this, as they interrupt the flow of blood, causing turbulent and high-pressure blood to come into repeated contact with the artificial surface of the device. These devices are lacking the natural anticoagulant factors found in endothelium that protect healthy tissue from activating the extrinsic clotting cascade, as well as actively encouraging the intrinsic pathway (as shown in Figure 6), and as such they can result in erroneous activation in otherwise healthy tissue (Smith, Travers and Morrissey, 2015).

The consequences of such clotting activation are severe: if a clot forms within the vessel containing the device, it may interrupt normal function of the device. For example, if a stent has been inserted to open an atherosclerotic vessel, coagulation on the internal surface of the stent would lead to reocclusion of the vessel and could cause further angina or myocardial infarction. Alternatively, the clot may travel through the circulatory system past the initial point of formation. In these cases, thrombi can become lodged in vessels anywhere

within the body and occlude blood flow to a different organ or tissue, resulting in deep vein thrombosis or pulmonary embolism, among others.

The process of coagulation involves a vast number of factors, cells, and enzymes. Various different branches of the coagulation cascade (shown in Figure 6) respond to different types of interruption, including external damage and foreign objects including glass or clay (Smith, Travers and Morrissey, 2015). The extrinsic pathway is activated primarily in natural haemostasis and involves release of tissue factor into the blood stream, most often by damage to cells of the endothelium. The intrinsic pathway, comparatively, is directly activated by blood contact against an artificial surface resulting in activation of blood clotting factors.

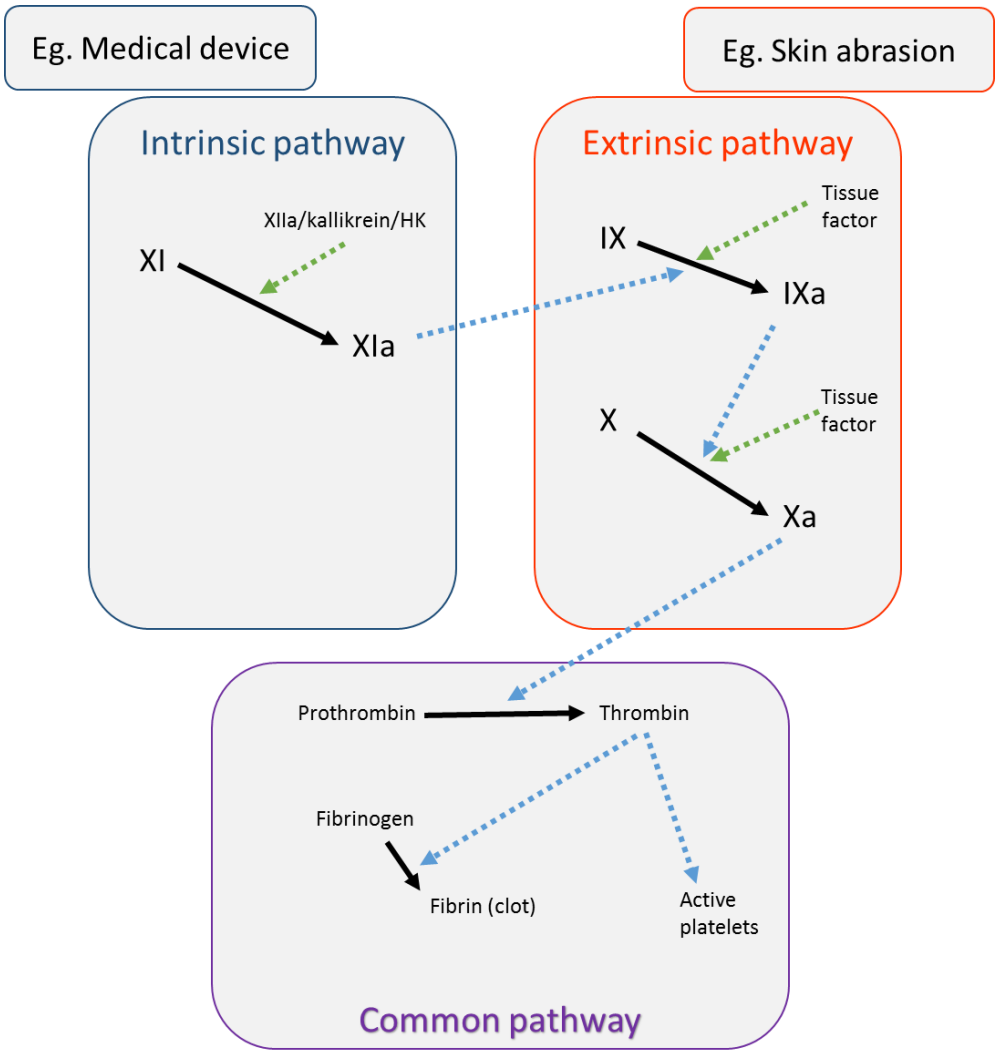

Figure 6: Simplified diagram of the intrinsic and extrinsic pathways of the coagulation cascade, adapted from (Smith, Travers and Morrissey, 2015)

Common to both pathways is the reaction of platelets within the blood vessel. Platelets represent a late step of the coagulation pathway and their activation results in formation of platelet plugs (Davie, Fujikawa and Kisiel, 1991; Palta, Saroa and Palta, 2014). Active platelets then in turn release factors which activate the clotting cascade further, leading to a positive feedback loop and the potential for significant thrombus formation.

2.3.2.1 Platelet activation on medical devices

In general, artificial, non-biological materials directly in the bloodstream lead to activation of the intrinsic pathway of coagulation. Particular materials have been found to be more potent activators, including clay and diatomaceous earth, which have been applied to benefit in haemostatic gauzes and blast dressings (Smith, Travers and Morrissey, 2015). However, for the purposes of long-term blood-contacting devices, this activation is significantly less beneficial and poses great risk to patients. In addition to the material itself, properties of the device and the material used can contribute to the thrombotic potential of the device, through shape (inclusion of corners that trap blood), surface chemistry (chemicals which encourage conformational change and activation of clotting factors) or surface profile (rough surfaces which catch and activate or damage platelets, cells and blood constituents).

Surface topography can influence the coagulation cascade through a number of media: protein adsorption, cell behaviour and direct platelet adhesion are all affected by the topography of a material introduced to the blood. In turn, the topography can also affect surface chemistry reactions of blood constituents against the material (De Mel, Cousins and Seifalian, 2012). Previous investigation into the surface features of Left Ventricular Assist Devices (LVADs) found that unevenness on the surface of blood-contacting parts resulted in an increased thrombogenic risk, although all those included in the study still fell within acceptable limits (Linneweber *et al.*, 2007). This impact is produced through interactions with a number of blood constituents, including platelets as well as factors of the coagulation cascade themselves. In addition, research into plastics used in intravascular catheters showed that within individual types of plastic, more thrombogenesis was found on samples with greater surface roughness (Hecker and Edwards, 1981; Hecker and Scandrett, 1985).

Guidelines for mitral valve annuloplasty include the provision of a period of anticoagulation post-surgery (Asopa, Patel and Dunning, 2006). However, it is acknowledged that in many cases this guideline is not followed. Whilst many patients are safely discharged post-operatively, some will experience a thromboembolism directly caused by the repair surgery in the period following operation. Annuloplasty devices pose particular risk due to their long-

term insertion directly inside the heart, which can lead to highly motile thrombi which may form even despite the presence of anticoagulation medication (Aytekin *et al.*, 2011).

2.3.3 Integrate fully with the patient's body

Endothelialisation is a process undertaken by most long-term medical implants in the cardiovascular environment. During this process, endothelial cells migrate onto the surface of an implanted device, along with cell growth promoted by clotting and trapping of blood-borne progenitor cells differentiating into endothelial-type cells (Heath, 2017).

In many cardiovascular implants, the endothelial layer produced over the top of the device provides mechanical support in addition to sutures and a layer of immune protection from rejection. In addition, the finished endothelial layer is strongly anti-thrombogenic, resulting in a significantly reduced risk of clotting-related adverse effects after the endothelium has encased the device completely (Post, Wang and Cosgriff-Hernandez, 2019).

Endothelialisation is so central to the longevity of cardiovascular repairs in particular, that devices designed solely to initiate the endothelialisation process and then dissolve have been developed both for stents and annuloplasty devices (D'Souza *et al.*, 2008; Cikirikcioglu, Cherian and Kalangos, 2012; Myers and Kalangos, 2013). Other methods of encouragement of endothelialisation have included microporous materials, surface coatings, and drug elution (Heath, 2017; Post, Wang and Cosgriff-Hernandez, 2019).

2.3.3.1 Endothelialisation of existing annuloplasty devices

In the case of annuloplasty devices, the sewing cuff provided to enable suturing of the device to the valve annulus also provides an environment for aggregation and growth of endothelial cells. This sewing cuff fulfils the needs for endothelialisation by providing anastomoses at suturing points for cell migration, and space for clots or trapping of circulating progenitor cells in the fabric or sponge layers (Carpentier, Adams and Filsoufi, 2010; Heath, 2017).

Current guidelines of mitral valve repair recommend the inclusion of a 3-month period of anticoagulation for patients after annuloplasty. This temporary measure is largely included as by 3 months post-surgery, it is expected that endothelialisation of the device will have taken place and will then provide protection and antithrombotic properties of its own accord (Asopa, Patel and Dunning, 2006).

Therefore, in producing novel annuloplasty devices which may not be regularly covered in suturing fabric due to their bespoke shape and size, it is of vital importance that an alternative method of encouraging endothelialisation onto the device is investigated. Whilst

this could be achieved by addition of a suture ring or other material similar to current workflow, technological advances and material capabilities mean that cell growth could be achieved on the bare metal ring without the additional part. This therefore reduces the potential sources of infection within the device and could pave the way to future advancements such as pre-seeding cardiovascular devices with patient stem cells to promote integration before surgery begins.

2.3.3.2 Cell growth on uneven surfaces

It has long been discussed that uneven or porous surfaces can provide preferential surfaces for cell growth into implant and scaffold parts. Previous studies have utilised acid etching, sand blasting, and oxidising to increase the surface micro-roughness of materials under investigation, leading to increases in cell attachment and cell proliferation (Zareidoost *et al.*, 2012; Tejero, Anitua and Orive, 2014). These studies have shown improvements in cell viability over long periods of time as well as in initial growth stages, suggesting that this improvement in cell growth is maintained in the long term, not just attributable to an initial promotion of growth.

This therefore provides benefit to the integration and maintenance of medical implants throughout the body system, although the majority of existing studies has focussed on osteoblast growth in skeletal implants. Aside from long-term medical implants, tissue scaffolds can also benefit from the same promotion of cell growth according to surface profile, including using cell types other than osteoblasts.

2.3.3.3 Surface functionalisation of devices

Surface modification of medical devices goes past simply material or topological adjustments and now includes the use of coatings and bioactive compounds to augment the interaction between device and body (De Mel, Cousins and Seifalian, 2012; Jaidev and Chatterjee, 2019; Florea *et al.*, 2020). In particular, bioceramics and biological peptides have been used to actively encourage interaction or behaviour of cells surrounding an implanted device. Biomolecules like collagen and growth factors can be immobilised on the external surfaces of manufactured devices, and have been shown to improve osseointegration as well as reducing inflammation at the site of insertion (Florea *et al.*, 2020). The inclusion of active biomolecules is attractive, as whilst materials may be more or less hospitable towards cellular growth, the inclusion of biological peptides renders an implant *actively* encouraging to the promotion of integration at a cellular level.

Again, the majority of published work centres these investigations on osseointegrative properties, aligned with the production of skeletal implants. Thus, whilst it can be agreed that a large number of potential methods of biofunctionalization exist which can improve outcomes with regards to bone formation and fixation, it is not fully understood what behaviour these surfaces may exert with other cell types. However, considerations applicable to both settings, such as incidental amplification of bacterial growth leading to infection, have been shown to be of minimal concern (Florea *et al.*, 2020).

However, whilst they may show promise in novel implant improvements, many biological surface functionalisation techniques require a long and costly process to adhere to device surfaces. Such processes are likely to render them inappropriate for widespread adoption (Henry *et al.*, 2018). In their place, single-step biotinylation has been developed and tested across a wide range of conventional materials including metals, polymers and glass, showing reasonable adherence to these surfaces (Williams *et al.*, 2016; Henry *et al.*, 2018). This novel technique provides an interesting development in rapid surface functionalisation for a number of uses, however significant application-relevant investigation must still be undertaken as the technology remains in early *in vitro* study.

2.3.4 Avoid secondary infections leading to cardiovascular deterioration

A final consideration of any surgery or implantable device is the avoidance of inducing or worsening infection in the patient. This is a frequent topic of research amongst both conventional and novel manufacturing techniques, across all body systems where devices may be implanted. In the case of annuloplasty devices, some devices have been specifically designed with the avoidance of provoking endocarditis during or after surgery, however typically cases of mitral regurgitation involving endocarditis are managed with antibiotics as a first line intervention (Kazaz *et al.*, 2005; Myers and Kalangos, 2013; Rostagno, Carone and Stefàno, 2017). Should this fail, replacement is generally seen as preferable owing to high risk of repair failure in these patients (Rostagno, Carone and Stefàno, 2017).

In the majority of mitral repairs with annuloplasty, secondary endocarditis is a rare complication. Whilst this risk must not be overlooked, by mitigating the risk of coagulopathies and inducing cellular integration, a large portion of complications relating to infection can be diminished. Therefore, the reduction of infection in mitral valve repair will not be a direct focus of this thesis, however it remains an area for further future investigation.

2.4 Mitral annuloplasty rings as bespoke additively manufactured implants

In 2010, Díaz Lantada et al. described their method for designing a bespoke annuloplasty ring according to patient data acquired by cardiac CT. This group noted the difficulty of segmentation by density, given the Hounsfield scale differences in portions of the mitral annulus are small and thus challenging to distinguish. As an alternative, they used Philips TC software to locate the exact point of intersection between valve parts, then exported the Cartesian coordinates to a separate CAD program (Díaz Lantada *et al.*, 2010). A curve can then be drawn to produce a ring in the exact shape of the patient's own annulus. However, as the authors note, this file must be further altered to provide a supportive structure able to reinstate leaflet coaptation, the extent of which can be dictated by the severity of disease. Further, whilst this study made use of additive manufacturing technologies, the ring was printed using a 3D Systems SLA-350 printer and an epoxy resin, rendering it clinically inappropriate due to the toxicity of the material (Díaz Lantada *et al.*, 2010).

Owais et al. 2014 followed a protocol of creating an annulus shape based on patient scan data to assess whether this concept is feasibly applicable to the clinical setting. Patients were assessed using 3D transoesophageal echocardiographic (TOE) scan data acquired during usual procedures to best replicate normal inpatient treatment. The group used TomTec's Image Arena software for mitral valve analysis, to automatically segment the mitral valve and distinguish the annulus from surrounding areas (Owais *et al.*, 2014). Following this analysis, Cartesian coordinates of the annulus were exported to SolidWorks to produce a 3D curve based on the data taken from the scan, and a cylindrical surface was created. This 3D model was printed on a MakerBot Replicator 2 using "an inflexible bioderived plastic" but was not used for further analysis or production of a supportive implant. Whilst the authors noted the potential for personalised implants in the future, they described the primary use of their model to be in surgical assistance through planning and visual confirmation of repair (Owais *et al.*, 2014).

Later however, (Graser *et al.*, 2014) improved upon this procedure, providing both a method for adjusting the CAD file to produce a supportive implant, as well as producing the final ring in a biologically safe material. 3D echocardiography was again used as the primary source of data acquisition for the model, averaging measurements throughout the cardiac cycle to give a representative likeness. Although the software is not named, a semi-automatic method of identifying areas for measurement is described, and is reported to only take 74 seconds to create the shape according to an input scan (Graser *et al.*, 2014). The ring produced could then be sized down overall, adjusted according to the assumed 3:4 ratio of the natural

annulus, or calculations made of the deformation stresses to reduce the risk of device dehiscence or fracture owing to high stress (Graser *et al.*, 2013, 2014). After production of an appropriately adjusted ring file, this design was manufactured in “biocompatible titanium” (likely Ti6Al4V, as this alloy is used frequently for medical implants). Ti6Al4V boasts a proven safety record when manufactured conventionally and used as the core of some currently commercially available annuloplasty rings (Prinzing *et al.*, 2018). Whilst the biocompatibility of a material cannot be assumed to be consistent across different manufacturing or processing techniques, there has been clinical evidence of the use of additively manufactured Ti6Al4V alloy with no reported adverse events (Sidambe, 2014). It is, however, important to note that this biocompatibility is dependent in large part on the specific device and application, not the material alone.

The most complete end-to-end procedure for producing these devices using additive manufacturing has been achieved in animal studies by (Sündermann *et al.*, 2013) during which personalised, additively manufactured Ti6Al4V annuloplasty rings were implanted into healthy pig models. The data used to produce ring designs were taken from CT angiography scans in this instance and 50% of manufactured rings were found to match the exact shape of the annulus in the studied pig intraoperatively. The failures were attributed to a systematic computing error in modelling software leading to a 10mm discrepancy in all directions and was corrected for later models. Figure 7 shows five of the differing designs produced for five pigs in the study, displaying a large variation in the exact shape required for each individual. Given that these studies were produced on healthy pigs and that the ring design involved no patient- or pathology-specific downsizing or other morphological alterations, there remains work to do in effectively treating mitral insufficiency with personalized implants. A summary table of existing studies describing design or assessment of additively manufactured annuloplasty devices is shown in Table 2 below:

Figure 7: Five personalised annuloplasty ring designs, produced from CT imaging of porcine hearts. Taken from (Sündermann et al. 2013)

Table 2: Summary table of published studies discussing additively manufactured annuloplasty devices

Author and year	Summary of actions	Limitations
Díaz Lantada et al. 2010	• Described method of designing a bespoke annuloplasty device from medical scan data, using existing cardiology software paired with CAD software.	• Used CT scan data which carries greater risk to patients and is not a usual part of patient care. • Did not account for the pathological state of a patient's annulus pre-surgery. • Produced a model in SLA epoxy resin, an unsuitable material for implantation or biological applications.
Graser et al. 2013	• Developed a semi-automated method of identifying and modelling the human mitral valve on individual medical images for design purposes, using leaflet insertion points.	• Did not evaluate success *in vivo* or compare to existing devices. • Did not produce or evaluate physical models themselves, only highlighted the possibility of using additive manufacturing to do so.
Sündermann et al., 2013	• Scanned pig hearts, designed bespoke annuloplasty devices for their anatomy, additively manufactured the devices in biocompatible Ti6Al4V alloy, and surgically implanted the devices into the respective pigs.	• No follow-up for survivability post-implantation • Significant systematic error in design program. • Pig hearts were not diseased prior to study starting. • No accounting for changes in anatomy post-surgery. • Used CT scan data which carries greater risk to patients and is not a usual part of patient care.
Graser et al. 2014	• Developed a semi-automated method of identifying and modelling the human mitral valve on individual medical images for design purposes, using leaflet insertion points.	• Did not evaluate success *in vivo* or compare to existing devices. • Did not produce or evaluate physical models themselves, only highlighted the possibility of using additive manufacturing to do so.
Owais et al. 2014	• Existing clinical software TomTec ImageArena was used to identify mitral annulus and produce a 3D model of the annulus for device design. • Using Solidworks to produce the design, a plastic annuloplasty device model was additively manufactured.	• Produced a plastic (FDM) model of the annuloplasty device, not a biocompatible material. • Identified the application of their model to be primarily education or surgical planning, not looking towards implantable devices.

2.4.1 Additively manufactured devices and design considerations

The access to data for design of cardiovascular devices is more challenging than other implantable devices, particularly those in the skeletal system. The heart is not only entirely made of soft tissue of similar density throughout, it is constantly in movement and cannot be held still for imaging purposes, and is also trapped inside the thorax, behind the ribcage and other tissues. Therefore, it must be considered which imaging modalities are best suited to the production of accurate and detailed data for personalised devices in the cardiac system.

2.4.1.1 Cardiac CT

CT scans are employed in some preoperative planning stages of structural heart disease, including transcatheter valve replacements, and particularly in the case of the aortic valve. Assessments of aortic regurgitation by CT scan compared to transthoracic echocardiography have shown similar results (Alkadhi *et al.*, 2007). However, the inclusion of CT scans must be considered carefully in any treatment plan as patients are exposed to significant levels of radiation which would not otherwise be necessary.

2.4.1.2 Cardiac MRI

Cardiac MRI has been posed for improvement on the current standard of echocardiography (Cawley, Maki and Otto, 2009). Its proponents pose a greater resolution of scans less dependent on operator experience, and less influenced by the presence of other body structures or internal devices. However, in practice, cardiac MRI is a more expensive method of imaging, which is less widely available in institutions. In addition to this, it is a more invasive experience for patients, leaving them in potential discomfort for a longer period of time, and MRI cannot be used if patients already have magnetic devices from previous surgeries (Cawley, Maki and Otto, 2009).

2.4.1.3 Cardiac ultrasounds

Echocardiography is already commonly employed in preoperative and perioperative assessment of mitral valve disease (Dal-Bianco and Levine, 2013). Echocardiography is possible from two routes of imaging: transthoracic and transoesophageal. The balance of choice lies between the comfort of patients and the accuracy of imaging. Whilst transthoracic ultrasound provides a less invasive procedure, it suffers from the presence of the ribcage between the equipment and the heart itself.

Overall, ultrasound remains the imaging modality of choice, with good resolution for imaging and allowing for temporal changes over the cardiac cycle as opposed to a single static image (Dal-Bianco and Levine, 2013).

2.4.2 Additively manufactured devices and coagulation

Powder bed fusion is known to produce parts with rough and uneven surfaces, owing to the powder from which parts are created and the layer-by-layer formation of parts (Townsend *et al.*, 2016). Previous investigations using electron beam melting of titanium alloy powder has shown that as-built powder bed surfaces are significantly more thrombogenic than machined surfaces of the same material (Klingvall Ek *et al.*, 2017). As yet, however, the effect of specifically SLM-produced materials and surfaces on blood activity has not been investigated.

In addition to the general activation of intrinsic coagulation pathways by the foreign material, additively manufactured parts' rough topography pose an increased thrombogenic risk due to the increased protein adsorption and platelet activation on these rough surfaces (Linneweber *et al.*, 2007; De Mel, Cousins and Seifalian, 2012).

In addition, the presence of any unsintered loose particles on the surface could provide environments for the attraction and activation of platelets, after which they could also dislodge and travel through blood vessels. This would therefore increase the risk of thrombi forming away from the device surface, resulting in other infarctions.

2.4.3 Surface post-processing of additively manufactured medical devices

It is well known that the majority of additive manufacturing methods require at least some, and often extensive, post processing procedures to produce a functional component, regardless of application. This ranges from full re-machining of near-net shapes achievable in some DED processes, through to removal of support structures in SLA builds (Gibson, Rosen and Stuker, 2013). More often than not, additively manufactured components are left with significant surface roughness owing either to the layer-by-layer manner in which they are fabricated, or the feedstock from which they are built. Whilst some surface finish can be compensated for through process optimisation and part orientation, more work is required to provide surface finish comparable to that possible with conventional manufacturing such as turning, in a reliable manner (Townsend *et al.*, 2016).

This need is augmented in medical devices where any rough surface can lead to coagulopathies, and any material that is not fully integrated with the part could come loose and induce significant health risks. Post-process finishing of AM surfaces remains an active

field of investigation, and some techniques do show promise for matching surface finishes achievable by conventionally manufactured and finished components.

Existing, traditional methods of polishing available to use, however, are largely time- and resource-consuming and are only capable of providing one surface finish across a whole part. Mechanical polishing by hand, for example, despite resulting in excellent surface finishes, is extremely time-consuming and labour-intensive. Alternatively, mechanical polishing could be achieved by tumbling, which would not require the resource of an individual polishing each part, but is only capable of polishing the whole part in its entirety, and cannot allow for different surface finishes for different areas of a device. Further, tumbling cannot account for complex shapes and may miss portions of a part which would be caught with an operator manually polishing the device. Similarly, whilst traditional electrochemical polishing would overcome the issue of complex geometry, and even allows for polishing within internal structures like lattices, it can only be applied equally across the entire part.

2.4.3.1 Electrochemical jet machining

Electrolyte jet machining (EJM) is a form of electrochemical machining focussed on one specific area through a small jet of electrolyte solution which can be moved over the surface of a part and be targeted to specific areas (Mitchell-Smith and Clare, 2016). During this process, the top layers of material can be removed through the application of an electrical potential across the surface, leading to anodic dissolution.

EJM provides a number of benefits over conventional machining; however the production of surfaces with low Ra is of particular interest in this particular application (Speidel *et al.*, 2016). In addition, the specificity of EJM over other polishing methods can provide benefit in biomedical applications for surface preparation of medical devices.

Whilst polishing of metal parts can aid in prevention of detrimental clotting on device surfaces, it also diminishes the potential benefit gained from rough and porous AM parts in growth of beneficial cells. By using EJM, surfaces can be patterned and selectively polished to allow different areas of a device to remain roughened or smoothed as necessary for the application (Zhao and Kunieda, 2019). In the case of cardiovascular devices, this may take the form of a polished internal surface through which blood can flow safely, and an as-built, rough surface on external faces which can then integrate in surrounding tissues of the heart or blood vessels. In addition to this, the multi-axis potential of electrolyte jet machining allows for this patterning to be successful over complex shapes, including those manufactured by additive manufacturing techniques (Zhao and Kunieda, 2019).

Previous application of EJM has included investigation into a range of metals and alloys including steels, titanium, and aluminium, however there is currently no published research specific to its use on SLM-produced surfaces. In addition, the biological blood response to surfaces processed using EJM has not previously been investigated. Previous work has applied the use of EJM to osteogenic functions in providing microstructuring of metal surfaces (Mitchell-Smith *et al.*, 2018), however investigations have not included the effect of these changes on blood activity.

2.4.4 Additively manufactured devices and integration

Additive manufacturing can produce objects that benefit cell growth in three ways: through design, through additional exogenous surface treatments, and through existing material properties. Additively manufactured parts are known to be rough and potentially porous dependent on the material and AM method applied, and can also be expressly designed to include internal porosity or channels for cell growth (Cheng *et al.*, 2014; Matena *et al.*, 2015; Arabnejad *et al.*, 2017; Demir and Previtali, 2017). These methods have previously been shown to promote cell growth with comparison to traditionally manufactured materials with regards to the surface profile, and internal pores are significantly easier to produce given the self-supporting nature of powder bed fusion methods.

Despite improvements which can be achieved directly using additive manufacturing techniques alone, further developments have been investigated applying methods which promote cell growth to the additively manufactured surface, providing a benefit twice over. Addition of materials to existing filaments, post-processing as discussed in 2.4.3, and surface modification or annealing of bioactive molecules could all promote cell growth on a surface and in a 3D part which is already primed to improve biocompatibility (Kotlarz *et al.*, 2018).

Within the extracellular matrix, different cell types benefit from different environments in promoting their growth. This is particularly true of progenitor cells which can be encouraged down differential pathways according to the niche in which they are placed (Murphy and O'Brien, 2011). Therefore, it may be that the specific environments produced so far with AM parts for osteoblast growth may not lend themselves to growth of other cell types, such as endothelial cells. Thus, it cannot be assumed that methods which have previously been successful *in vitro* for promotion of osteoblastic proliferation will also benefit devices designed for use outside of the skeletal system.

As discussed in 2.4.3.1, the selective surface patterning ability of EJM allows for the provision of differing surfaces across a single component part. This feature lends itself to the potential

for fine control over biological response to implanted devices. The provision of highly patterned surfaces with niches available for fibroblastic adhesion may encourage cell growth where needed for integration, whilst avoiding the same topologies where coagulation needs to be avoided. This may be possible through either different processing parameters or through simply not polishing areas where the AM process has left a beneficial surface for this application.

Further, as discussed in 2.3.3.3, a number of developments are underway for rapid biological functionalisation of inorganic surfaces (Williams *et al.*, 2016; Henry *et al.*, 2018). Rapid and simple surface functionalisation may be capable of augmenting further the expected cellular responses to surface topologies. However, the interaction between the surface features seen in additively manufactured components (or those processed by EJM) and the activity induced by active biotinylation, is not yet known.

2.5 Material Choice

2.5.1 Materials choice for novel annuloplasty devices

Annuloplasty devices, as discussed previously, vary widely in the material and design choices applied to their manufacture. A range of materials have been used in their production, spanning both polymer and metallic materials. Similarly, there is a limited range of materials which can be processed by different additive manufacturing methods, and therefore the choice of material used to produce a novel annuloplasty design must take into account both these needs. Amongst potential materials, additional properties have been investigated such as deliberate device resorption (Myers and Kalangos, 2013) or shape memory for semi-flexible or minimally invasive devices (Purser *et al.*, 2010).

2.5.2 Ceramics

Ceramics and bioceramics hold significant importance in implantable medical devices. In particular, hydroxyapatite is a common material used in conjunction with metals and other materials to improve performance of skeletal implants (Wei *et al.*, 2015). Many ceramic materials are applied to improve the biocompatibility and integration potential between the device and the human body, including silica and titanium dioxide (Kaur and Singh, 2019).

Additive manufacturing of ceramics has been in development for some time and is particularly active in research relating to tissue engineering scaffolds as well as the above skeletal implant applications. In many cases, these investigations involve the development of composite materials between metals and ceramics, as above (Wei *et al.*, 2015; Kaur and Singh, 2019).

As pertains to cardiovascular devices, some ceramic materials have been investigated for their application in implantable devices such as stents, given their high strength and potential for low thrombogenic risk, however this remains under investigation (Parlak *et al.*, 2019).

2.5.3 Polymers

Polymers are used in the core of some annuloplasty rings. They are used in both flexible and semi-rigid rings, and are sometimes thought to allow a more “natural” movement of the annulus than with the insertion of a rigid ring (Silberman *et al.*, 2009).

PTFE, known by its brand name of Teflon, is most well-known for its hydrophobic use in creating non-stick pan coating. However extended PTFE is currently used in surgical meshes and for ligament repair, and forms part of the structure of the Koehler Mitral Repair System. Whilst additive manufacture of PTFE products has proven challenging due to high melt viscosities preventing extrusion, the material has been processed in an extrusion-based

process, through mixing of PTFE nanoparticles and a sacrificial "gum" additive (Maitz, 2015; Jiang *et al.*, 2019). Following post-processing, the mechanical properties of the remaining PTFE structures were shown to be comparable to compression-moulded PTFE and could be adjusted to fulfil precise mechanical requirements (Jiang *et al.*, 2019).

Thermoplastic polyurethanes (TPU) present a biocompatible material useful primarily in the production of temporary internal scaffolds. One group has printed medical grade TPU using fused deposition modelling (FDM) and electrospinning to produce a blood vessel scaffold for use in coronary artery bypass grafts (Owida *et al.*, 2011). However, despite the TPU studied being more stable than others available, it was still subject to hydrolytic and enzymatic degradation, and could break down over a long period of implantation (Owida *et al.*, 2011). In addition to manufacture by FDM, TPU powder has also been manipulated using a laser sintering process, which allowed recycling of the powder bed, potentially reducing manufacturing cost (Plummer *et al.*, 2012).

PET is a biostable polymer used in cardiac surgery for vascular grafts and surgical meshes (Stone *et al.*, 2012; Maitz, 2015)**.** This polymer has also been used for fabrication of improved artificial ligaments (LARS) with high strength for repair of ruptured ligaments (Pan *et al.*, 2013). Under the brand name Dacron, it is currently used as the surrounding suture material on current annuloplasty rings.

Polyetheretherketones (PEEK) have been developed for use in medical devices as they produce similar mechanical properties to bone, and are very biocompatible (Vaezi and Yang, 2015). It has previously been manufactured using laser sintering, and has recently been investigated for extrusion manufacture to produce parts at lower cost (Vaezi and Yang, 2015).

2.5.4 Shape memory materials

Shape memory materials have been investigated for use in minimally invasive and other newer techniques of mitral valve repair surgery. These implants encompass two concepts of benefit. The first is the ability of flatter rings to be inserted through the ribcage, thus allowing minimally invasive and robotic surgeries to be undertaken, with faster recovery and a shorter hospital stay. Once inserted, the shape memory ability allows the ring to reform in the annular shape upon returning to warmer temperatures induced by the patient's own body heat (Purser *et al.*, 2010). An alternative school of thought involves shape memory rings which are more permissive of movement of the mitral valve, however, will always return to their "programmed" shape to provide adequate support.

Thermoplastic polyurethane, discussed previously in its use for printing a scaffold for blood vessels (Owida *et al.*, 2011), is also applicable to shape-memory functions according to its semi-crystalline structure (Wache *et al.*, 2003). TPU has also been used experimentally to produce a vascular stent with the possibility of direct drug delivery, allowing for up to 35% drug content by weight (Wache *et al.*, 2003). These stents may reduce the risk of stenosis and thrombosis compared to traditional metal stents and propose a viable plastic alternative in temperature-sensitive implants (Wache *et al.*, 2003).

A Nickel/Titanium (Nitinol) alloy has been used to produce a shape-memory ring which can be used in minimally invasive annuloplasty (Purser *et al.*, 2010). This ring is viable for use in minimally invasive procedures owing to its ability to be straightened and pass through small incisions at low temperatures, and return to its designed ring shape at body temperature once in situ (Purser *et al.*, 2010). Nitinol has been explored for additive manufacture, particularly using powder bed techniques like SLS and SLM (Elahinia *et al.*, 2016; Taheri Andani *et al.*, 2016). Investigations into the composition of powder for this technique concluded that a powder containing greater concentrations of Titanium exhibit the favoured shape memory effects, whereas a greater amount of Nickel leads to a superelastic product (Elahinia *et al.*, 2016). Either function may be a useful addition to the design of cardiovascular devices: superelastic properties could produce semi-flexible devices which provide support with greater valve freedom, and shape memory properties lend themselves towards the provision of minimally invasive surgical techniques (Purser *et al.*, 2010; Prinzing *et al.*, 2018). This material has already been used for the production of conventionally manufactured, selectively flexible annuloplasty devices by Sorin and LivaNova (Prinzing *et al.*, 2018). Further research into the modulation of these properties by varied powder content would be beneficial given the potential for functionally graded materials in additive manufacturing techniques.

Porous Nitinol parts have been manufactured using SLM for biological applications, mimicking the porosity of additively manufactured Ti6Al4V implants mentioned previously (Taheri Andani *et al.*, 2016). This study showed that, similarly to titanium implants, it is possible to manipulate stiffness through porosity to improve bone healing and decrease stress shielding around bone implants (Taheri Andani *et al.*, 2016). The inclusion of these prospects through additive manufacturing techniques could open up new methods of encouraging endocardial ingrowth and implant integration, as well as improving the material properties of rings to provide a compromise of stiffness and flexibility in different areas.

2.5.5 Metals

Metals are frequently used for a number of surgical implants already and are in development for serving the same purposes through additive manufacture. Metal alloys are already used to produce the structural core of commercially available rigid annuloplasty rings, as well as some semi-rigid rings, such as the shape memory alloys discussed in 2.4.3 (Prinzing *et al.*, 2018).

Stainless steels, predominantly grades 316 and 316L, are used in medical implants where strength of material is required, and shows reasonable biocompatibility (Müller *et al.*, 2005). Stainless steel has been combined with hydroxyapatite and manufactured through selective laser melting, for the purposes of improved integration of bone implants (Wei *et al.*, 2015)**.** The addition of the biological hydroxyapatite molecules provided a better integration into existing anatomy, but also led to greater cracking of the finished product, which suggests that it may not survive repeated stresses (Wei *et al.*, 2015).

Cobalt chrome has recently gained interest in the additive manufacture of cardiovascular, skeletal, and dental devices (Tejero, Anitua and Orive, 2014; Demir and Previtali, 2017). In studies, selective laser melting of CoCr has been shown to be an acceptable manufacturing method producing cardiovascular stents with material properties comparable to conventional manufacturing. However the authors advise caution on assumptions of biocompatibility being consistent between manufacturing processes, recommending further specific study (Demir and Previtali, 2017). However, both cobalt and chromium ions have been linked to potential toxicity in the body when corrosion frees these elements from the component into circulation (Florea *et al.*, 2020). Documented risks include anaemia and central nervous system disturbances, which may be augmented by the possibility of loosening of powder material in an SLM part.

More commonly, Ti6Al4V has been the material of choice for its abilities in load-bearing, oxide passivation for biocompatibility, and its success in integration with bone (Tejero, Anitua and Orive, 2014). Ti6Al4V has been additively manufactured through electron beam melting for the application of complex meshes to medical implants in orthopaedics (Murr *et al.*, 2010). In addition, selective laser melting (SLM) has been used to produce titanium craniofacial implants following trauma (Rotaru *et al.*, 2015). Porous parts are used to mimic natural bone, and as a result ingrowth and integration of the part to the body have been shown to be successful (Rotaru *et al.*, 2015). Whilst the alloying elements of vanadium and aluminium pose some risk of cytotoxicity when free ions traverse the body, the low

concentrations of these elements results in an acceptably low risk (Florea *et al.*, 2020). The success of Ti6Al4V in soft tissue applications may be less fruitful as requirements may demand less rigid structures and are subject to greater chemical insult within direct blood flow.

Given the proven track record of Ti6Al4V applications in additive manufacturing and in biomedical implants, alongside the presence of titanium alloys in some modern annuloplasty devices, the work of this thesis has been undertaken using SLM manufacture of Ti6Al4V devices (Purser *et al.*, 2010; Sidambe, 2014; Tejero, Anitua and Orive, 2014; Prinzing *et al.*, 2018). The majority of frequently used annuloplasty devices are fully rigid, as they are more trusted in providing a long-term repair which will not deteriorate in future leading to re-operation (Silberman *et al.*, 2009). In addition, the potential for cell growth on titanium alloy devices provides a promising capability in promoting integration between the patient and the device, ensuring longevity of repair and reducing rejection risk of the device (Matena *et al.*, 2015).

2.6 Gap in Knowledge

As has been shown, some early work relevant to the development of bespoke, additively manufactured annuloplasty devices has been undertaken. However, a number of questions remain across the various functions which must be upheld by the device.

Whilst current devices are designed with a 3:4 “natural” annulus geometry in mind, it is not known whether this is an accurate design basis for either mass-produced or bespoke devices. Further, when manufacturing a bespoke device, a simple and effective design workflow from patient to data to device has not yet been agreed upon, with a number of investigators working with their own in-house software packages.

Whilst the impact of additively manufactured titanium alloy devices has been reasonably well documented in skeletal applications over recent years, there is less evidence available pertaining to cardiovascular-specific settings. Work remains in the effects of surface processing for AM parts particularly relating to blood clotting risk and non-osteoblastic integration.

In particular, novel processes in selective surface processing of AM parts are in development, and the effect of processes such as EJM have not yet been investigated for AM components nor for their potential biological effects. Further, whilst surface functionalisation of components has shown promise in device integration, its application with regards to non-osteoblast cells is less well investigated, as is the impact of combining functionalised and additive surfaces, which are both known to augment cell growth separately.

2.7 Aims and Objectives

The overall aim of this research was to **investigate the use of additive manufacturing to develop bespoke annuloplasty devices for improved patient care**. Based on the gap in knowledge identified in 2.5, it was proposed that this be investigated through the following objectives, divided into individual technical tasks:

Objective 1. Develop a design protocol for design of personalised annuloplasty devices, ensuring that it is compatible with existing patient pathways and does not produce unnecessary burden on clinician or patient.

Task a. Assess *commercially available annuloplasty device* shapes and sizes for suitability against natural human anatomy

Task b. Assess the suitability of *commercially available software* for use on soft tissue, ultrasound applications

Task c. Compare *methods of interpreting ultrasound* data to provide information appropriate to patient-centred design of annuloplasty devices

Task d. Consider methods of producing an *appropriately sized and shaped* annuloplasty device from the data extracted

Objective 2. Investigate the safety of materials for use in annuloplasty devices produced using additive manufacturing, particularly ensuring that coagulatory risk is considered and steps are taken to mitigate risk in changing from existing manufacturing techniques.

Task a. *Consider the material properties* of AM material compared to conventionally manufactured (e.g. wrought or cast) metals

Task b. Evaluate the success of a novel polishing method for selective surface finishing of AM titanium alloy to *reduce blood clotting*

Objective 3. Investigate the possibility of active biological integration between additively manufactured materials and live cells for annuloplasty repair longevity using novel technologies.

Task a. Evaluate the success of a novel polishing method for selective surface finishing of AM titanium alloy to *induce cell growth*

Task b. Compare the effects of selective surface finishing on *AM and conventionally manufactured* titanium alloy

Task c. Investigate the effects of active biological surface treatments to *induce cell growth* on the surface of AM titanium alloy

Task d. Compare the effects of active biological surface treatments to induce cell growth on the surface of *various AM materials*

2.8 Structure of Work

Chapter 1 has opened the discussion of cardiovascular disease and surgery, personalised medicine, and the part that additive manufacturing has to play in potential avenues of medical developments. **Chapter 2** has specifically discussed the application of AM technologies currently in use for cardiovascular disease along with the identification of mitral annuloplasty as a field with open potential for investigation of personalisation with additive manufacturing.

Chapter 3 describes the methods utilised throughout this research, across the remainder of objectives and chapters. The ensuing chapters hold results for each of the aims described above. **Chapter 4** shows development of an early design process for a bespoke annuloplasty device, including the challenges of imaging the heart compared to other organs and structures, aligned with **Aim 1**. In addition, evidence for the benefits of personalising this device is presented.

Chapter 5 discusses employing novel polishing techniques to prepare additively manufactured parts for implantation in the cardiovascular environment without inducing excessive coagulation, as targeted in **Aim 2**.

Chapter 6 exploits the 3D structure of additively manufactured parts along with novel surface treatment options to encourage integration between implants and recipients, aligning with **Aim 3**.

A discussion on the work presented and final conclusions are drawn with proposals for future work in **Chapter 7** and **Chapter 8.**

3 Experimental Procedures

In this chapter, the overall methodology is described, including the reasons for its selection. The experimental procedures undertaken to address each objective specified in Chapter 2 are laid out consecutively.

3.1 Overall Methodology

Whilst a relatively simple design in concept, in the correctly applied annuloplasty ring, several functions are undertaken by various components of the device. Therefore, the redesign of such a device using novel technologies should not only encompass the shape of the device itself but other functions it upholds, as discussed in Section 2.3. The layout of work done in this thesis is shown diagrammatically in Figure 8.

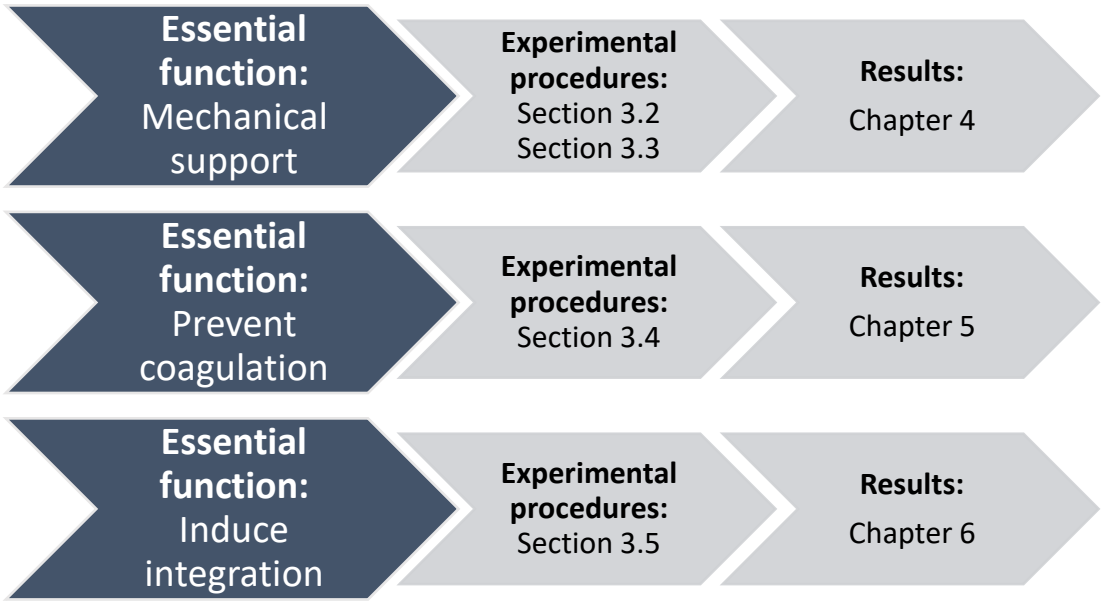

Figure 8: Layout of thesis

Initially, assessments of the human mitral valve were undertaken to validate the design and sizing of the device. In order to confirm that bespoke devices produced by additive manufacturing would be beneficial to patients, a series of cadaveric studies were undertaken to investigate the variation of natural human mitral valves. The design of the device was then progressed through the use of patient data and commercially available software to construct a method of extracting dimensions of the patients' anatomy to inform the design of the personalised annuloplasty ring for that patient. The experimental procedure is described in section 3.2 and 3.3 and the results are presented in Chapter 4.

Secondly, given that the device resides constantly within blood contact, the risk of blood clotting to patients was investigated. A novel method of controllable surface polishing for additively manufactured metal components was trialled to allow for selective polishing of surfaces to be in contact with blood.

Trials were first conducted using whole blood studies in flow cytometry, however the inability to qualify the effects of different areas of processed material led to further studies being conducted using alternative methods. This was also informed by the disagreement between visual and quantifiable data produced, and the potential for interaction between blood constituents posing a large number of uncontrollable variables. These second trials were undertaken using only human platelets as an indicator of clotting potential, with quantifiable and visual data produced using activity assays, cell counts and microscopy. The experimental procedure is described in section 3.4 and the results are presented in Chapter 5.

Finally, state-of-the-art annuloplasty devices include a sewing cuff, which in addition to providing suture placement in the device, allows for fibroblast and endothelial cell ingrowth. This cell growth acts as a protective layer of patients' own cells over the device, avoiding immune response and providing mechanical support. The novel polishing method described previously was performed again with altered parameters to provide a pitted surface to encourage fibroblastic growth on areas of the device in contact with soft tissue. This method was assessed using cell culture of fibroblastic cells alongside proliferation and morphology assays. The experimental procedure is described in section 3.5 and the results are presented in Chapter 6.

3.2 Assessment of the human mitral valve and commercially available annuloplasty devices

An investigation was undertaken to examine the relationship between the transverse and anteroposterior diameters of healthy human mitral annuli using measurements taken from donated cadavers. Whilst a preference would be given to the use of healthy, living human samples, it was decided that unnecessary medical imaging was not ethically justifiable in this case, and physical measurements would not be possible outside of a surgical setting, which would only occur in the case of cardiac disease. Thus, donors were screened for cardiovascular disease in life and only those with minimal evidence of cardiac dysfunction were included in the study (see Section 3.2.2).

3.2.1 Preliminary Investigations

To rehearse the methods of dissection, measurement and comparison, the experiment was first undertaken on bovine heart samples. The major vessels of the heart were first removed from the top of the heart, followed by a cut across the apex of the heart to provide support to stand upright on the table. The majority of dissection using the bovine organ was successful, however concerns with the structural integrity of tissue and holding shape during cutting were raised. It was further discussed that given the bovine tissue was not fixed, this was likely to be less of an issue when working with fixed human tissue. Visualisation of the valve was successful, however required removal of more tissue from the top of the valve than expected, further informing tool choice and decisions about how far down cuts on the organ should be made to avoid damaging the valve. As shown in Figure 9, loose tissue over the top of the valve sometimes occluded vision of the valve leaflets, an issue which was later identified as occurring in human samples also, and required the use of needles to pin away tissue for visualisation without manually pulling on the organ.

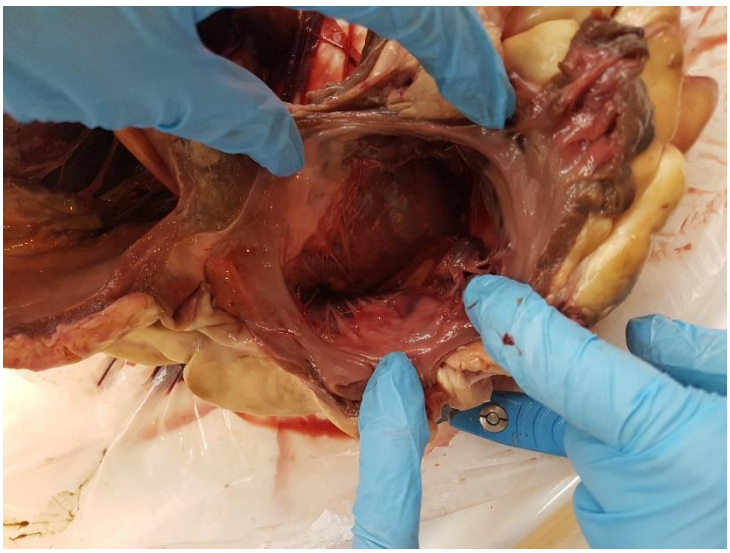

Figure 9: Visualisation of the bovine mitral valve after dissection

3.2.2 Cadaver Study

Human hearts (n=38) were collected from cadavers donated for the purposes of anatomical teaching and study. The hearts were dissected to isolate and visualise the mitral valve and annulus from a superior angle by removal of the apex and atria of the heart.

Manual measurements were taken of the transverse and anteroposterior dimensions of the mitral annulus using digital callipers. The structures of the mitral annulus were identified visually as the intersection between valve leaflets and the surrounding heart tissue, along with tactile identification of a fibrous tissue. The points of measurement were identified as the central points at the peak and lowest point of the annulus for an anteroposterior diameter, and the widest points of the transverse diameter by vision for the transverse dimension. These points are shown diagrammatically in Figure 10.

Figure 10: Image of a dissected heart showing the mitral valve opening. The positions of measurement taken are shown; anteroposterior positioning is shown in green circles and transverse positioning in blue squares.

Eleven hearts were excluded from study according to medical history or visual inspection. To exclude hearts which deviated significantly from health in life, or that had been damaged during storage, the mitral valve was scored visually. Those which appeared to have been physically damaged were excluded from study. In addition, the medical history of donors was taken into account: hearts that had recorded cardiac events in life or showed obvious signs of damage from storage or significant valvular disease were also excluded.

3.2.3 Statistical Analysis

SPSS Statistics version 24 was used for all statistical analysis. Graphical plots were also produced using Microsoft Excel. Regression analysis of the data presented graphically was calculated using Microsoft Excel, and a root mean square analysis was performed using SPSS to compare the expected 0.75 value and the values measured.

3.3 Device design from patient data

Once a cardiac scan has been taken, methods to produce a digital representation of the mitral valve and mitral annulus from which an annuloplasty ring could be designed must be employed. In existing examples of bespoke medical devices, the design is usually produced using thresholding methods available in commercial software packages (Wong *et al.*, 2015). Thresholding in this manner was initially investigated for design from an echocardiogram taken preoperatively, alongside alternative novel design methods which were reproduced in commercially available software.

3.3.1 2D thresholding

Thresholding involves the segmentation of scan data according to the density of tissues presented in the image, according to the Hounsfield units of density. This density is represented on medical images through a gradation of black to white pixels as the density of tissue increases. A range of densities can be selected for and limited to or excluded from the three-dimensional part being produced, after which manual editing of the produced "mask" can take place to fine-tune the design.

Given that most cases of personalised implants or medical devices are currently centred on bone and joint structures, the method of thresholding imaging data is sufficient to design with. Owing to the differing densities between bone and its surrounding tissue, this method is effective at isolating bone structures to design bespoke implants. However, as the heart is an entirely soft tissue organ, the delineation between individual structures is much less clear.

In addition, whilst CT and MRI images are single, still images taken at one point in time, an echocardiogram is made up of continuous imaging of moving objects. Thus, the quality of individual images can vary as the position of the heart structures move. In addition, there is potential for the camera itself to move during the imaging process as it is manually operated, and the experience of operators can impact the quality of image produced.

Initially, a design for bespoke annuloplasty device was attempted using these traditional thresholding methods. A mask of the cardiac tissue at the point of valve leaflet insertion was created, providing a two-dimensional outline of the inside of the mitral valve.

3.3.2 Single-layered thresholding

Thresholding was initially applied to the echocardiogram as would be for other bespoke medical designs, relying on the in-built capabilities of Materialise MIMICS 17.0 software for these designs. The area of the valve leaflets and annulus was identified visually, and choice

of thresholding limits was decided based on the density of tissue in these areas. Once segmentation of the valve circumference was completed to a sufficient standard, the 3D object created was exported to 3-Matic, the CAD software associated with MIMICS.

The scan was revisited using MIMICS 17.0 and the thresholding reapplied at less stringent parameters. In place of manual addition of required areas, this method relied more heavily on manual removal of non-valve structures. Overall, it appeared that this method required more human input and as such took longer to complete. It was also dependent on personal knowledge of cardiac anatomy. In order to minimise time expenditure, only a small selection of slices of the scan data were included in the segmented part, chosen by the clearest image of the open valve area from an axial view.

The segmented 3D object produced was exported to 3-Matic for CAD manipulation. The "create curve" tool was used to produce a curve attached to the inside surface of the object, following the shape of the model. A 2D sketching plane was created to produce a guide circle of circumference 2mm, and the "sweep" tool was used to expand this around the curve to produce a 3-dimensional ring shape.

3.3.3 Multi-layer thresholding

Later iterations were produced having included the full 3D shape of the valve apparatus when thresholding, as opposed to only including a small number of layers near the annulus. This process was repeated later by the same operator with the same dataset to ascertain whether the results of this method were repeatable.

3.3.4 Point-based design

A group at the German Cancer Research Centre have produced bespoke software and a number of related plugins allowing analysis and modelling of the mitral valve as well as the annulus specifically (Graser *et al.*, 2013; Al-Maisary *et al.*, 2017). Their software uses the application of points onto the annulus in different planes by eye.

Importantly, during the design process, the location of the mitral annulus is more easily deduced when identifying the valve leaflet insertion points compared to when isolating the entire valve. When the primary foundation of the design relies on the exact points of insertion, the uncertainty of height up the 3D model for curve application is removed, which would be a concern if relying only on thresholding.

Following from these publications, replication of a similar point-based method was attempted using Mimics software, and the results of this work are presented in Chapter 4.

The production of a similar method in commercially available software represents the potential for much easier incorporation into patient care.

3.4 Surface finishing for anticoagulation

3.4.1 Sample Production

15 disks of 8mm diameter were produced in Ti6Al4V titanium alloy (LPW Technology, 15-45µm) using laser-based powder bed fusion on a Realizer SLM 50 machine. Process parameters were as laid out in Table 3, using standard optimised parameters developed in-house for this material and machine.

Table 3: Processing parameters used in the Realizer SLM50 to produce Ti6Al4V samples

Parameter	Border scan	Core scan
Exposure time (µs)	40	40
Point distance (µm)	10	30
Laser current (mA)	1600	3300
Hatch distance (mm)	0.09	0.09
Hatch offset (mm)	0.06	0.06
Overlap (mm)	0.2	0.2

These samples were then either bagged immediately for blood testing or were subjected to varying parameters of electrolyte jet machining. All samples were cleaned using a Fischione plasma cleaner and rinsed three times in phosphate-buffered saline prior to interaction with blood.

Electrolyte jet machining was applied to one side of each sample with parameters as set out in Table 4. Two samples were produced in each parameter set. Conventionally manufactured control samples were also included in some experiments as a control for the process. 15 disks of 8mm diameter were cut from Ti6Al4V ELI (medical grade) sheet metal and cleaned using the same methods as the additively manufactured samples. A simplified diagram of an EJM setup is provided in Figure 11.

EDX analysis was undertaken using a Hitachi TM3030 scanning electron microscope. EDX was applied to the surfaces of the additively manufactured and the EJM-processed samples, to confirm the presence or absence of contaminants on the surface of AM parts, or chloride, bromide, or sodium ions on the surface following EJM polishing.

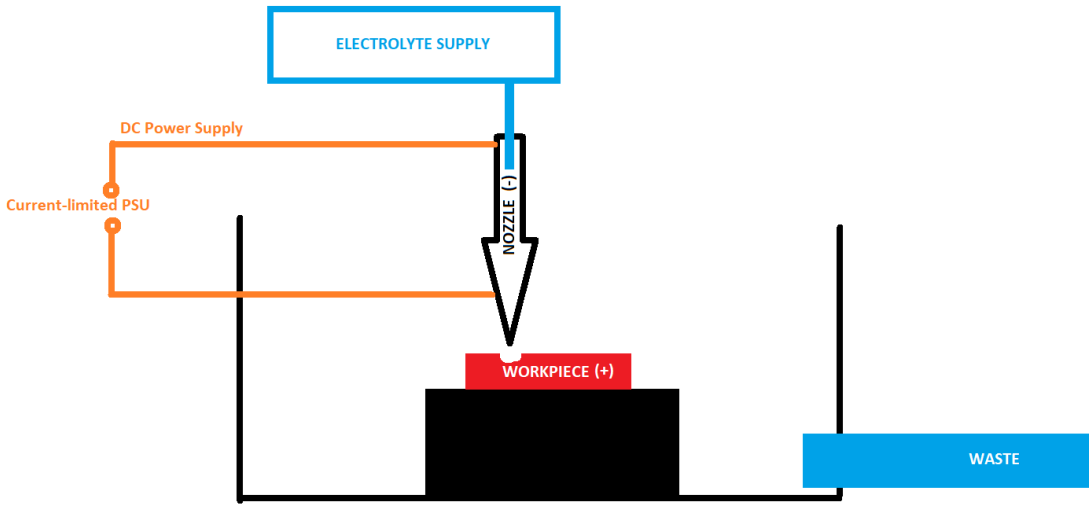

Figure 11: A simplified diagram of EJM equipment, adapted from (Speidel *et al.*, 2016). *The nozzle traverses over the workpiece (Jet speed), applying electrolyte solutions and current (below) to the surface of the workpiece. This can be repeated to remove further material if necessary (Number of passes).*

Table 4: Parameters of Electrolyte Jet Machining applied to AM parts

Sample ID	Current density	Jet speed	Nozzle I.D.	IEG	Nozzle Velocity	Electrolyte Applied	Number of passes
SLM-A	100 A/cm^2	12 m/s	1 m	0.5 mm	0.1 mm/s	3 M NaCl	1
SLM-B	100 A/cm^2	12 m/s	1 m	0.5 mm	0.1 mm/s	3 M NaCl	2: 1st pass @ 0.25mm/s 2nd pass 1mm/s
SLM-C	100 A/cm^2	12 m/s	1 m	0.5 mm	0.1 mm/s	1.5 M NaCl + 0.5 M NaBr	1
SLM-D	100 A/cm^2	12 m/s	1 m	0.5 mm	0.1 mm/s	1.5 M NaCl + 0.5 M NaBr	2: 1st pass @ 0.25mm/s 2nd pass 1mm/s

3.4.2 Blood Incubation

Samples of venous blood were taken voluntarily from healthy human subjects who had not taken any medications or drugs known to interact with platelet activity. Blood was taken using a 21-gauge needle into a plastic syringe and dispensed into 4.5ml sodium citrate-containing tubes (Becton Dickinson), then inverted to mix the contents and placed in a dry bath at 37°C. All experiments were undertaken within 30 minutes of collection.

The titanium samples were placed separately in the bottom of wells in a 48-well culture plate warmed to 37°C on a Bioshake iQ platform. The samples were placed polished side up. 0.5ml

of blood was added to each well. The plate was covered and left for 30 minutes to shake at 37°C and 500rpm.

3.4.3 Flow Cytometry

Flow cytometry was initially employed on a BD FacsCantoII system (using FacsDiVa software). Fixative agents were procured from Platelet Solutions Ltd and fluorescent antibodies were provided by BioRad (CD62P-FITC, CD63-FITC and CD42a-FITC) or Becton Dickinson (CD61-PerCP and IgG-FITC).

The flow cytometry process was performed to evaluate the activity and aggregation profiles of platelets in whole blood after exposure to the material surfaces being investigated. Flow cytometry is a technique used to measure the presence of marker molecules associated with the investigated characteristics. Antibodies specific to certain proteins exhibited on the surface of cells are added to solutions of those cells, and the solution is then injected one cell at a time through the machine, where they are subjected to laser emissions. These emissions are then detected and assessed according to their wavelengths and "scatter", providing quantifiable data on the proteins chosen and the associated characteristics of the cells under investigation.

CD61 is a general marker protein specific to platelets, which can be used to identify the presence of a platelet against other cellular material.

CD62P and CD63 were chosen as marker molecules to check for platelet activation. Both CD62P and CD63 are proteins which are internalised within platelets as they travel through the blood at rest but are externalised to the surface of the platelet when the platelet becomes active. Therefore, the only time that CD62P or CD63 would be recorded in an assay of whole blood would be if the platelets present had been activated. CD62P codes for P-selectin, a cell adhesion molecule which promotes platelet aggregation. CD63 is involved in a number of cellular activities but is accepted as a platelet activation marker for assays.

CD42a was used to assess platelet aggregation. CD42a is a bonding protein on the surface of all platelets. By extension, when platelets aggregate to one another, CD42a becomes less frequently measured as the protein is attached to the other platelets and not exposed for binding to the antibodies being used for assessment.

These antibodies were conjugated directly to the fluorescent molecules FITC (a green-emitting fluorophore) or PerCP (a red-emitting fluorophore) for identification and analysis in the flow cytometer.

A negative control of an empty culture plastic well as well as samples with EDTA chelators to prevent coagulation were included. The clotting agonist ADP was added to sample wells to provide a positive control.

3.4.3.1 Platelet Activation

One well per sample of a 96-well plate was filled with 10µl of solution containing CD61-PerCP antibody in a 1:8 dilution and CD62P-FITC antibody in a 1:20 dilution. One extra well was filled with 10µl of a 1:20 dilution of IgG-FITC antibody as a background control. This plate was covered and stored between 2-8°C until use. Tubes containing the blood samples were inverted repeatedly until cells were suspended, then 5µl of each sample was added to individual wells. The plate was incubated for 20 minutes at 2-8°C in darkness. After incubation, 0.2ml of FACSflow solution was added to each well and the plate was positioned on the flow cytometer stand. 3,000 platelet events were identified by CD61 presence and CD62P activity was quantified as the percentage of cells present within an interval gate set at 3% according to the IgG control. Median fluorescence values for CD62P were also recorded against the whole population of CD61-positive cells present.

CD63 analysis was performed using the same method as CD62P analysis with the replacement of the CD62P-FITC antibody with CD63-FITC. The template used for measurement of CD63 and CD62P is shown in Figure 12.

3.4.4 Preparation of Platelet Solution

Whole blood was collected from non-clinical issue stock provided by NHS Blood and Transplant Sheffield. The whole blood was decanted into sterile flasks and allowed to rest for 24-48 hours until plasma and red blood cells were visibly separated, with translucent platelet-rich plasma at the top of the container. 600µl of platelet-rich plasma was taken from the top of the container and placed into an Eppendorf tube, ensuring no red blood cells were drawn up to contaminate the sample. A 1:1 ratio of Hank's balanced salt solution (with added Prostaglandins at 1µM final concentration) was added to the tube. The tube was then centrifuged for 10 minutes at 1800Xg.

Following centrifugation, a pellet of platelets was formed. Remaining plasma was pipetted out from the top of the Eppendorf tube and discarded, and the pellet was washed gently in 200µl platelet wash buffer. After two washes, the platelet pellet was re-suspended and mixed in 200µl of Tyrode's buffer before counting and seeding on samples.

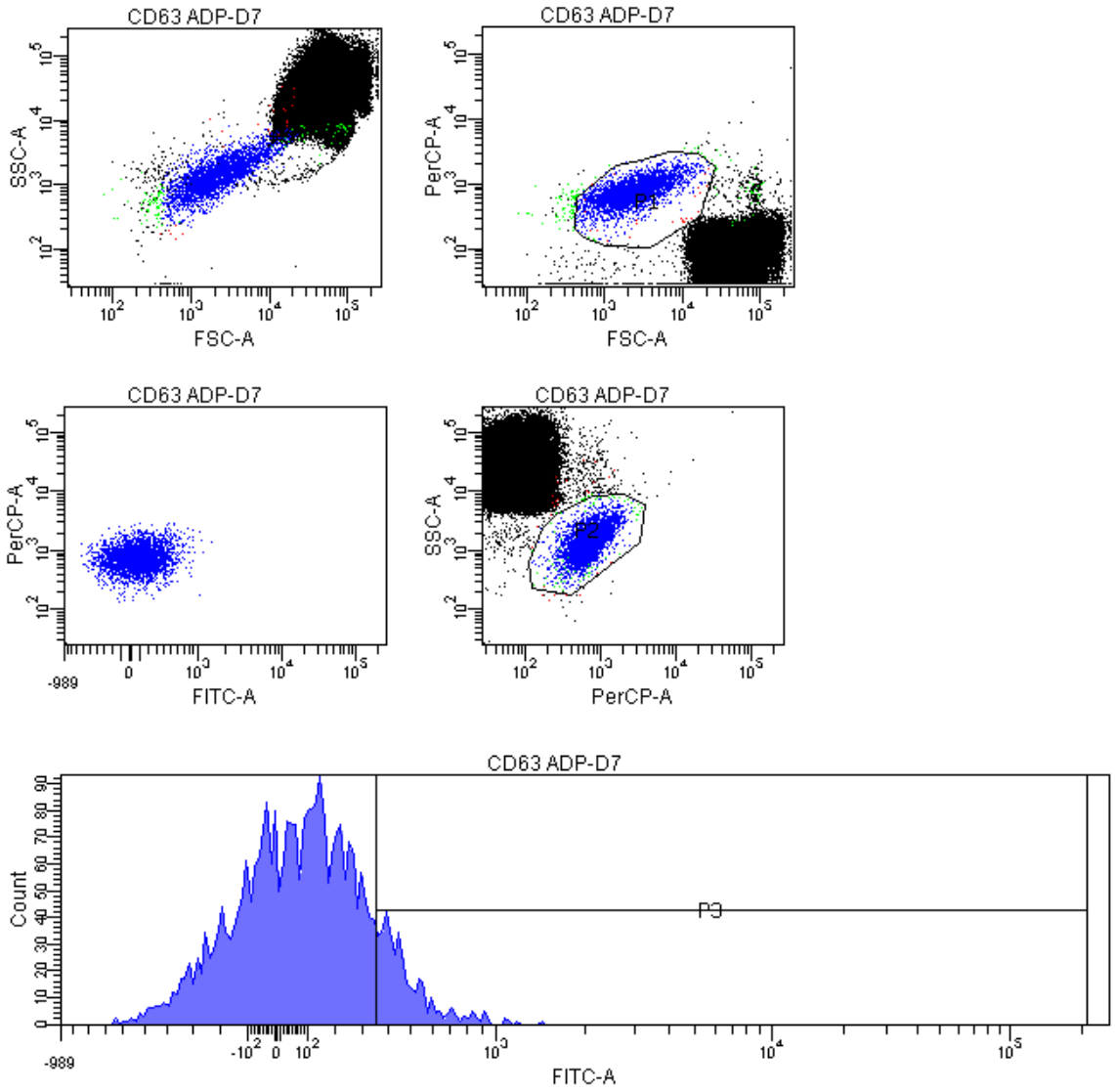

Figure 12: Flow cytometry template setup for platelet activation assay. The initial read of front vs side scatter indicating cell type and presence is shown in the top left graph. Platelets were gated in both P1 (top, right) and P2 (middle, right) in plots of CD63-PerCP against both forward scatter (FSC) and side scatter (SSC) using a CD63-specific antibody. Approximately 3,000 CD63-positive platelet events were recorded. The CD63-positive cells were drawn on a plot of FITC fluorescence against PerCP fluorescence (middle, left). A frequency histogram (bottom) of FITC fluorescence against cell count is used to calculate the percentage of cells from the parent population present in the P3 interval gate. Increased FITC fluorescence will shift this histogram to the right and increase the number of cells present within P3. Gate P3 was set at 1% using the IgG-containing, empty-well control sample and was recorded automatically in the statistics box. Measurement of FITC fluorescence then related directly to expression of CD62P.

3.4.4.1 Platelet Aggregation

A 96-well plate was prepared with 10µl of a CD42a-FITC antibody solution at a 1 in 20 dilution. The plate was covered and stored for up to an hour in a refrigerator at 2-8°C. Samples were inverted to mix and 5µl of each sample added to separate wells with the antibody solution. The plate was incubated for 20 minutes in the dark again at 2-8°C. 0.2ml of FACSflow solution was then added to each well after incubation and the plate was positioned on the sampler of the flow cytometer. The flow cytometry procedure used for identification and quantification of platelets is shown below in Figure 13.

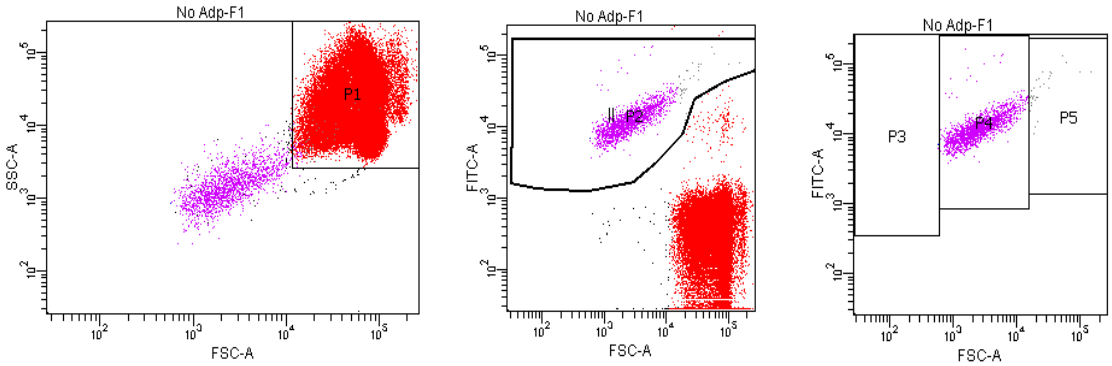

Figure 13: Flow cytometry template setup for individual platelets in whole blood for quantitative aggregation assessment. 50,000 red blood cell (RBC) events were collected in region P1 on a forward scatter/side scatter plot (left). CD42a-FITC fluorescence was plotted against forward scatter and region P2 was selected by drawing a curved line (centre) to include platelets and exclude RBC/platelet coincidences. CD42a-positive platelet events in P2 were then redrawn against forward scatter (right). EDTA-anticoagulated blood was used to set three gates to quantitate microparticles (P3), individual platelets (P4), and microaggregates (P5). These gates were then applied to the plots obtained for all exposed samples of blood, recording individual platelets in P4.

Across the flow cytometry experiments, each sample was only experimented on once due to time and equipment limitations. These experiments were not later reproduced due to the small margins of change, wide variation, and paradoxical responses to known factors, as discussed in Chapter 5. Therefore, few conclusions can be drawn regarding the statistical significance of these differences, however indications were given for the continuation of other work.

3.4.5 SEM Imaging

Following a repeat whole blood incubation for half an hour, the samples produced in Section 3.3.1 were rinsed gently in warm saline and fixed using 3% glutaraldehyde. The samples were held at room temperature under 1ml of glutaraldehyde for one hour without movement to fix any cells which had adhered to the surface. Following this the samples were removed from the glutaraldehyde solution and were left under 0.1M phosphate-cacodylate buffer until processing for microscopy.

Post-fixing was undertaken using 1% osmium tetroxide. 1ml of solution was added to each well and left at room temperature under a fume hood for 30 minutes. The samples were then dehydrated over time using ethanol solutions. Progressive solutions of distilled water, 50%, 70%, and 90% ethanol were applied twice for ten minutes each, followed by a final wash of 1ml 100% ethanol solution for 15 minutes. Samples were stored under 100% ethanol solution overnight. After removal of the ethanol, samples were critical point dried by covering with hexamethyldisilazane twice for five minutes each time and samples were left to air dry. Once dry, the samples were attached to aluminium stubs through carbon tabs and placed in a dessicator. Samples were coated in gold using a Polaron sputter coater prior to SEM analysis. Samples were imaged using a FEI Quanta 200 3D Dual Beam FIB-SEM. Images were acquired at 350, 850 and 1500x magnification to provide a range of views of the sample surface.

3.4.6 Statistical Analysis

SPSS Statistics version 24 was used for all statistical analysis and graphical presentation. Comparison of platelet counts, alamar blue fluorescence and immunofluorescence area was calculated using ANOVA analysis with a post-hoc Tukey test. Significance was set at a minimum expectation of $P<0.05$; where indicated on Figures, $p<0.01$ was achieved.

3.5 Surface finishing for cellular growth

3.5.1 Sample production

Samples of Ti6Al4V were produced in 10mm disks of 3mm depth. Samples were produced from milled titanium sheet in addition to selective laser melting additive manufacturing techniques. Additively manufactured samples were also processed using EJM with bromide and chloride solution, according to SEM results from previous experiments shown in Section 3.4.4. Control samples of non-additively manufactured titanium alloy were produced in the same dimensions from medical grade Ti6Al4V sheet supplied from Unicorn Metals.

Samples polished using EJM were modified using the parameters listed in Table 5.

Table 5: EJM treatment parameters on additively manufactured titanium alloy for cell growth assays

Sample ID	**Current density**	**Jet speed**	**Nozzle I.D.**	**IEG**	**Nozzle Velocity**	**Electrolyte Applied**	**Number of passes**
SLM-C	100 A/cm^2	12 m/s	1 m	0.5 mm	0.1 mm/s	1.5 M NaCl + 0.5 M NaBr	1
SLM-D	100 A/cm^2	12 m/s	1 m	0.5 mm	0.1 mm/s	1.5 M NaCl + 0.5 M NaBr	2: 1st pass @ 0.25mm/s 2nd pass 1mm/s

All samples were washed using acetone, isopropanol, and distilled water on an ultrasonic cleaner and sterilised using UV light for 2 hours prior to cell culturing.

3.5.2 Sample characterisation

Surface chemistry of the samples was compared using X-ray spectroscopy. A VG ESCALab Mark II instrument was used. Samples were imaged using a high-resolution camera and scanning electron microscope (FEI XL-30 SEM) to view the surfaces produced and investigate the surface topography produced with the EJM processing. The surface roughness of samples was measured using a Zeta-20 optical profiler. Surface wettability was investigated using a drop shape analyser (DSA100) to record the contact angle of water droplets for 5 seconds after contact with sample surfaces.

3.5.3 Cell culturing

A 3T3 mouse fibroblast cell line was used for all cell studies, obtained from Sigma-Aldrich. Cells were cultured in DMEM with 10% FBS, 5% antimycotics and 1% NEAA plus ascorbic acid

at 150mg/L. Cells were cultured in flasks at 37°C and 5%CO_2 and were passaged once reaching 80% confluence, as assessed by light microscopy.

3.5.4 Cell proliferation assay

Alamar blue assays were chosen to study cell viability as a non-destructive method of investigating cell activity through metabolic activity.

Cells were counted using a haemocytometer and seeded onto 24-well plates in known concentrations. 1ml of solution was seeded at a concentration of 40,000 cells per ml. The metal samples were seeded onto, along with empty wells containing no sample (direct to the culture plastic) as a negative control for sample surface influence.

Time points of 2 hours and 24 hours were chosen to investigate both initial attachment and growth, and continued viability over longer periods. After 2 or 24 hours, media was removed from wells and the samples were washed 3 times in PBS for 5 minutes. Following rinsing, the samples were covered in 300µl of Alamar Blue solution diluted 1 in 10 using Hank's balanced salt solution. Samples were then shaken for 10 minutes at 150rpm and returned to incubate at 37°C and 5% CO_2 for a further 80 minutes.

100µl of solution was removed and placed into 96-well plates and read using a Bio-Tek FLx800 microplate reader with a standard Alamar Blue protocol.

3.5.5 Cell morphology assay

Scanning electron microscopy (SEM Jeol 6060LV) was used to image cells growing on the surfaces of samples and investigate their morphologies. Again, cells were studied after both 2 and 24 hours of growth.

At the appropriate time point, samples were washed with phosphate-buffered saline (PBS) and fixed with 0.25% glutaraldehyde and 0.1M cacodylate buffer for 30 minutes. The samples were then covered in 7% sucrose in 0.1M cacodylate buffer and stored overnight, after which they were rinsed 3 times in buffer only. Post-fixing was applied using 1% osmium tetroxide solution for 45 minutes, and samples were dehydrated using increasing concentrations of ethanol. Samples were covered using hexamethyldisilazane and left overnight. Prior to imaging, samples were sputter coated with gold.

3.5.6 Statistical Analysis

SPSS Statistics version 24 was used for all statistical analysis and graphical presentation. Comparison of platelet counts, alamar blue fluorescence and immunofluorescence area was

calculated using ANOVA analysis with a post-hoc Tukey test. Significance was set at a minimum expectation of $P<0.05$; other P values are indicated individually in Table 9.

4 Results I: Design of bespoke annuloplasty devices

4.1 Introduction

In this chapter, the natural anatomy of human mitral valves was investigated and compared against commercially available annuloplasty devices. In addition, workflows to produce patient-specific annuloplasty designs were developed using commercially available software and ultrasound scans.

4.2 Assessment of the human mitral valve and commercially available annuloplasty devices

As described in Section 3.2, human cadaveric hearts were categorised and included or excluded from study according to medical history and quality of storage. Of the 27 hearts remaining following exclusion, transverse diameters ranged between 27.5mm and 44.1mm; anteroposterior diameters ranged from 20.5 to 38.4mm.

When plotted graphically (shown in Figure 14) there is little discernible relationship between the diameters. There is generally a trend towards a positive correlation between the values, as would be expected, however it is not a clear linear relationship.

A positive relationship is found when using transverse diameter to predict the anteroposterior diameter (shown in Figure 14). A significant regression equation was found ($F(1, 25) = 21.20$, $p < 0.001$), with an R^2 of 0.459, suggesting that whilst there is a relationship between the measurements overall, individual points are not a close fit to the equation given.

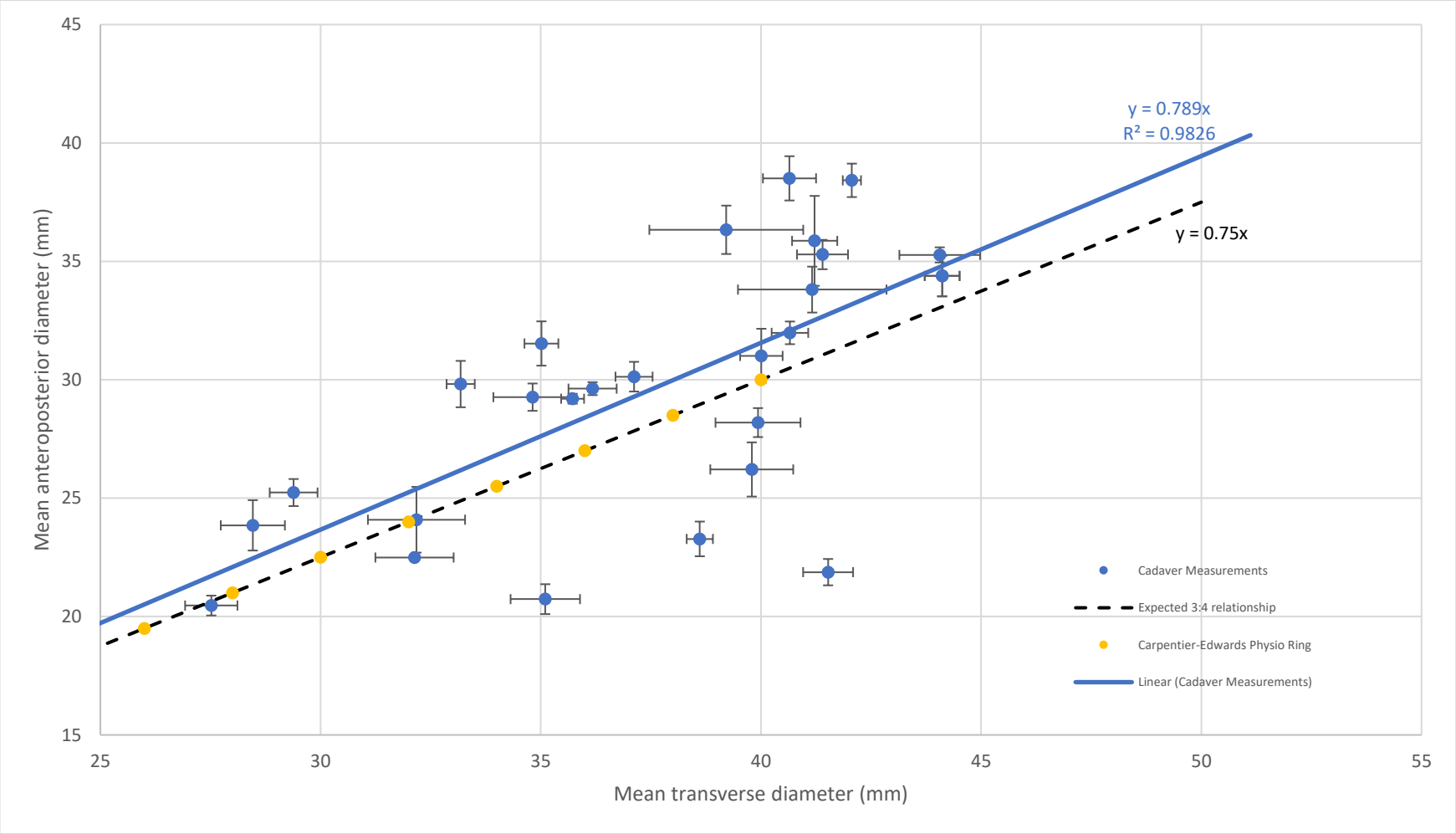

Figure 14: Relationship between the transverse and anteroposterior diameters of mitral valves in 27 samples. The linear relationship between dimensions measured is shown in solid blue (y=0.789x); an expected 3:4 ratio of values (y=0.75x) in dashed black. The existing sizes of a commercially marketed annuloplasty device are shown in yellow.

The expected relationship between transverse and anteroposterior dimensions as per current design methods would be y=0.75x. By comparison, the values found for this relationship ranged between 0.53 and 0.95. This suggests that the anatomy of individual mitral annuli ranged from near-circular to a width twice as large in the transverse direction as in the anteroposterior direction. This variation in shape between individual hearts can be seen comparatively in images of two dissected valves in Figure 15.

The available sizes of a currently marketed, commercially available annuloplasty ring (Carpentier-Edwards Physio) are also marked on Figure 14 in yellow. As shown, the largest available size in transverse diameter is 40mm, which would exclude 8 (30%) of the samples from having an as-sized annuloplasty device.

Figure 15: Photographs of two mitral valves used for analysis showing drastically different overall shapes in the mitral annulus. The left image showed a ratio between anteroposterior and transverse diameters of around 0.5; whereas the annulus of the right-hand image represented a ratio of nearly 1.0.

In addition, even when a size is available near the existing dimensions, the anteroposterior distance available is often far away from those measured. For example, two hearts measured to have a transverse diameter of 32mm had a corresponding anteroposterior distance of 24mm and 22.5mm. If these patients were treated using this model of annuloplasty ring according to the "natural 3:4 ratio", an anteroposterior distance of 24mm would be achieved. In one patient, this would exactly restore their natural anatomy; however, in the second patient it would oversize their mitral valve opening by 1.5mm.

A root mean square calculation was performed for the 0.75 expected relationship and the actual values measured in the study. The RMS across the whole population was equal to 4.41, suggesting that applying the 3:4 ratio assumption across the population gives an average error of over 4mm in the anteroposterior distance compared to that physically measured.

4.3 Device design from patient data

Materialise Mimics is commercially available software designed specifically for the production of three-dimensional CAD files from medical scan data. This software predominantly relies on the thresholding of different areas of scans according to density, as indicated by Hounsfield units and the black to white range of visualisation. In CT, MRI and ultrasound scans, more dense tissues appear lighter and less dense tissue or water appears darker, to allow this distinction.

In the production of skeletal implants, as discussed in Chapter 2, the delineation between hard and soft tissues is clearly visible according to the colour of segments visible. Bones, being much more dense than surrounding muscle and fascia, are clearly separated for design of bespoke surgical guides or implantable devices (Rotaru *et al.*, 2015; Wysocki *et al.*, 2016; Dall'Ava *et al.*, 2019).

In spite of the reduced contrast between heart structures, muscle tissue is still visibly denser than surrounding blood flowing through the heart, and as such scans can be used preoperatively to inform surgery and aid planning. Thus, initially the inbuilt thresholding capabilities of Mimics were used to produce an anatomical representation of the valve shape in line with the annulus.

4.3.1 2D thresholding

Initially, a single layer of the mitral valve anatomy in line with the plane of the annulus was selected and thresholded using Mimics inbuilt thresholding capabilities. The resulting, semi-automated threshold is shown in Figure 16.

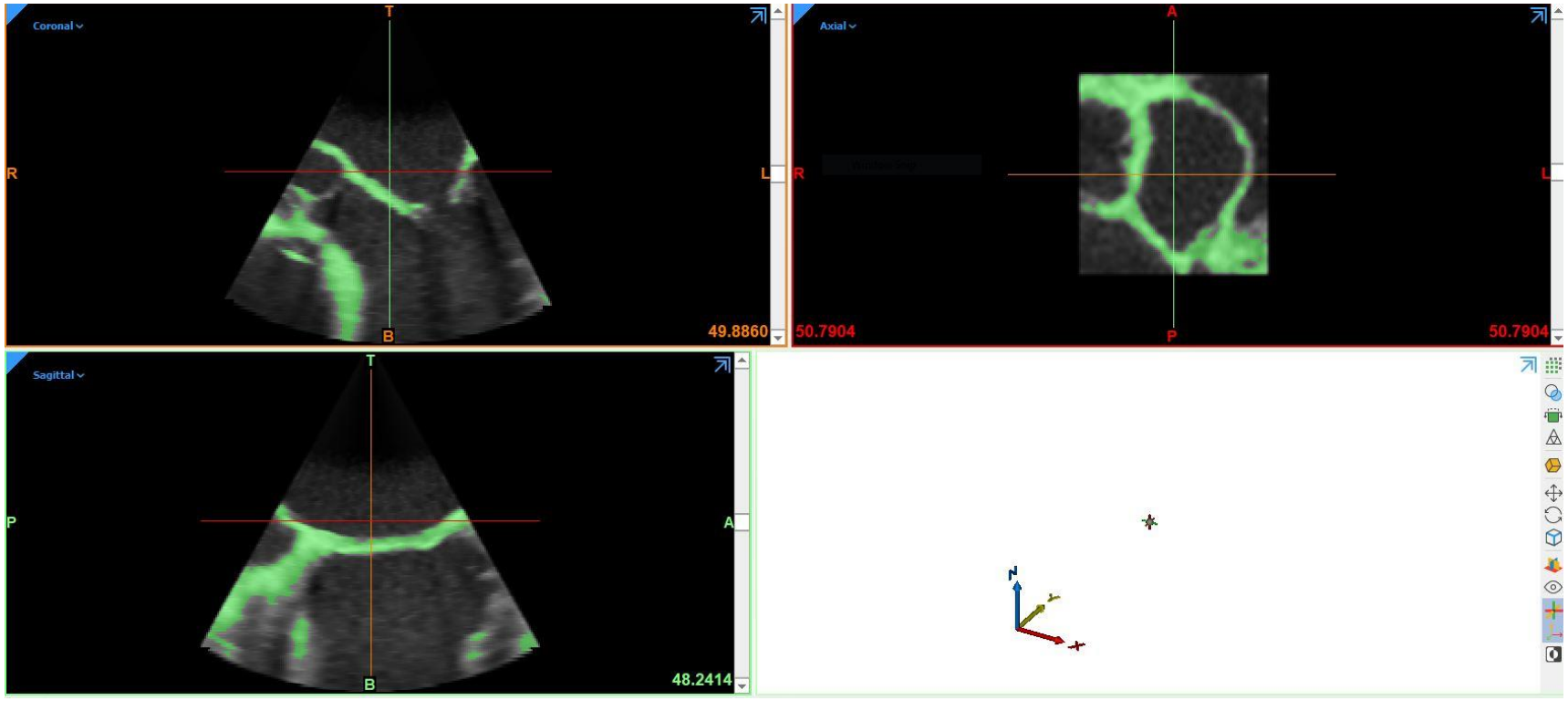

Figure 16: Thresholding of a mitral valve echocardiogram in Mimics software. Thresholded areas selected for inclusion in the design mask are shown in green.

As a balance must be achieved to reduce noise arising from tissues of similar density elsewhere in the heart, some structures of the mitral valve were not included in the original thresholding mask. In order to rectify this, the mask was manually edited, and areas were marked to be included in addition to the previously segmented parts. This decision was made by human input and therefore this method would rely heavily on the knowledge and experience of the person performing the segmentation.

Once segmentation of the valve circumference was completed to a sufficient standard, the 3D object created was exported to 3-Matic, the CAD software associated with MIMICS. On inspection using fixing wizards, it appeared that the model was made up of multiple shells, not one single part. Whilst some noise shells were successfully removed by inbuilt fixing wizards, the remaining shells could not be re-attached. As a result of this, when a curve was drawn on the internal circumference of the valve opening to provide an annular shape, the curve would end at the junction of two shells and could not create a continuous shape for further design (see

Figure 17).

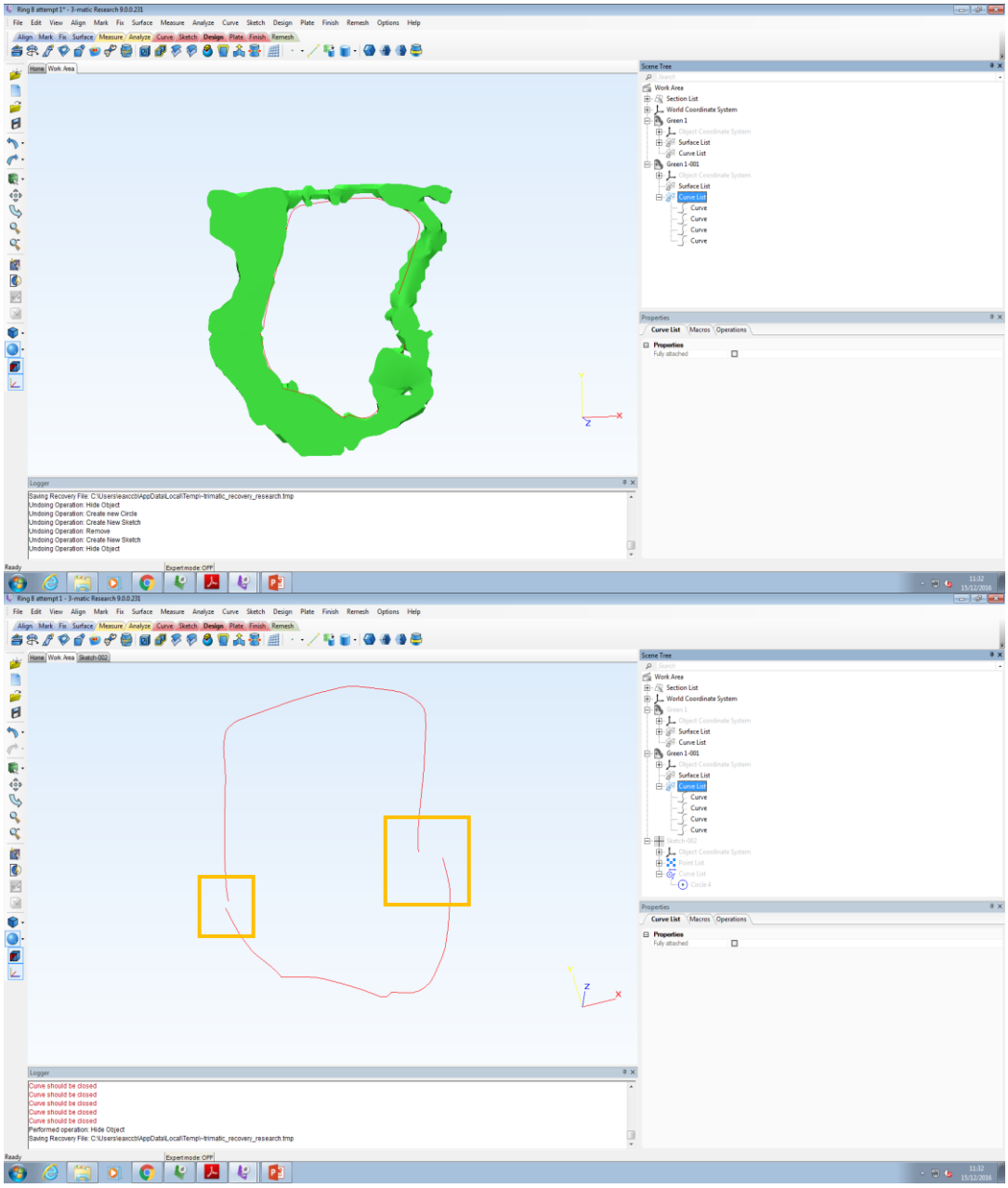

Figure 17: Failure of a continuous curve due to production of a 3D object formed of multiple shells. Highlighted in red are the areas of breakage where the curve could not be connected and therefore a full annulus shape could not be reproduced.

Further iterations of the single-layer data were attempted using less stringent thresholding parameters to reduce the disjoint between different areas. In using less stringent parameters, the risk of including noise in the design not actually associated with dense tissue is raised, however the likelihood of missing segments of the valve geometry is reduced. Figure 18 and Figure 19 show the thresholded anatomy from the scan with these less stringent parameters, alongside the resulting curve and ring geometry produced from the internal face of the thresholded valve scan.

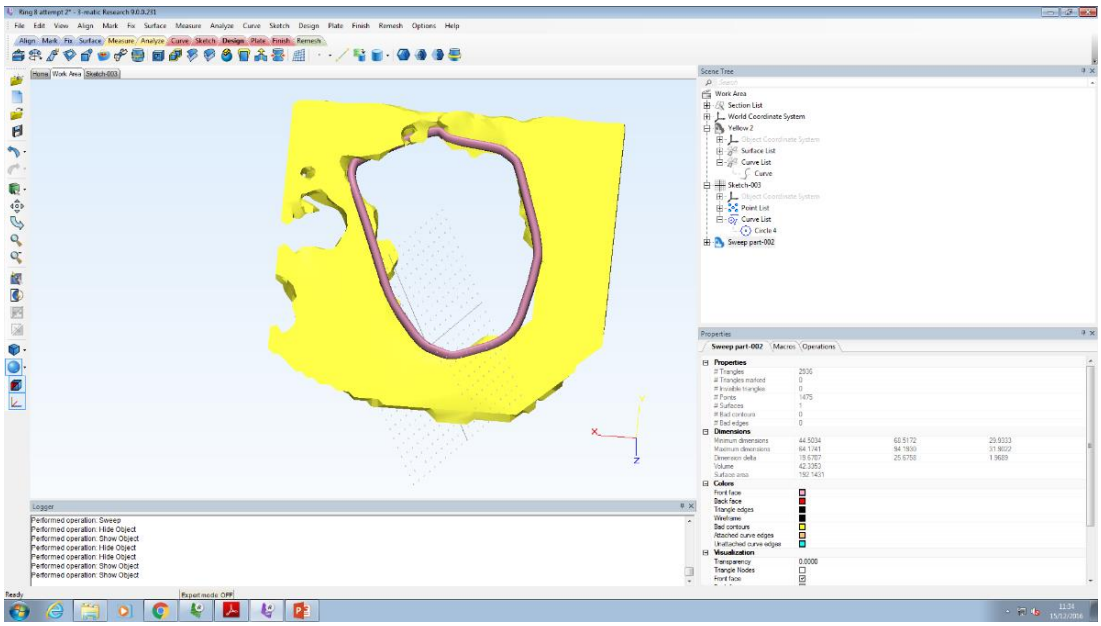

Figure 18: Completed ring shape within the thresholded mitral valve opening

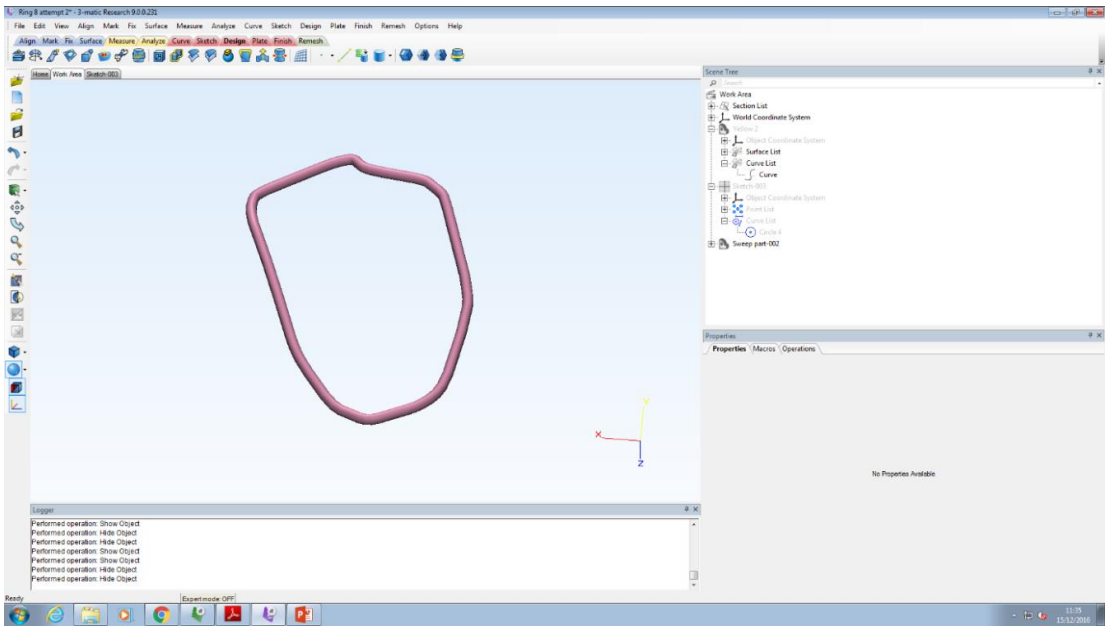

Figure 19: Completed ring shape designed from scan data

4.3.2 *Multi-layer thresholding*

Given that the mitral valve and its annulus are known to be non-planar (Mahmood *et al.*, 2013), the inclusion of only one layer of scan data will not give a full representation of internal annulus geometry. Thus, further iterations of thresholding for design were undertaken, including multiple layers of the valve volume rather than just those in line with the centre plane of the annulus.

This full valve volume is shown in Figure 20. This produced a ring of a similar shape, however incorporated more of the three-dimensional saddle structure seen in a healthy native annulus, shown in Figure 21 with a comparison of the side view of the two rings.

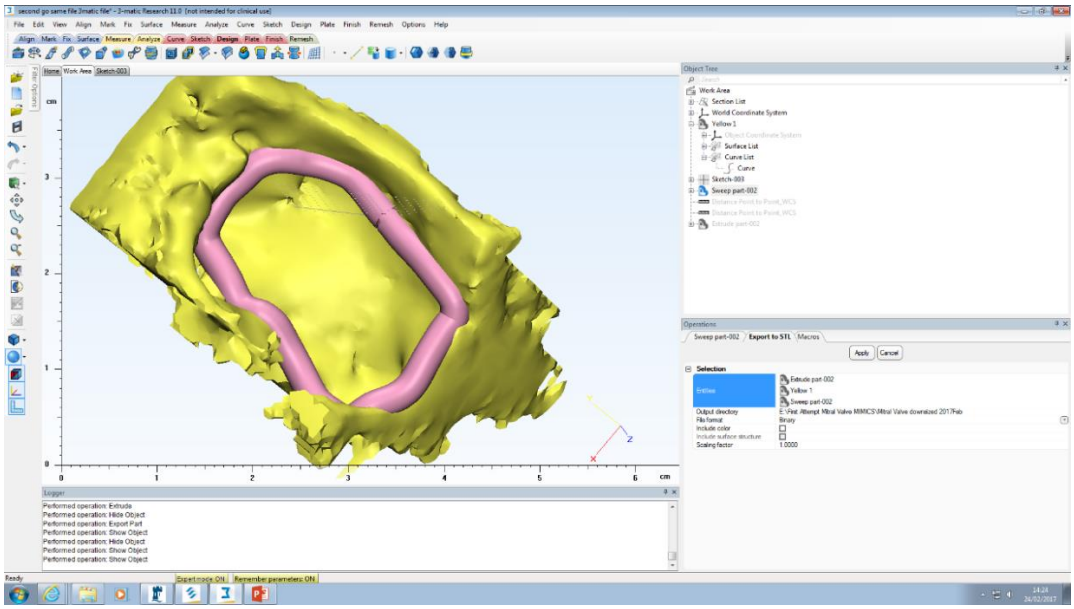

Figure 20: Ring produced using an increased number of layers, in situ within the resolved 3D valve model.

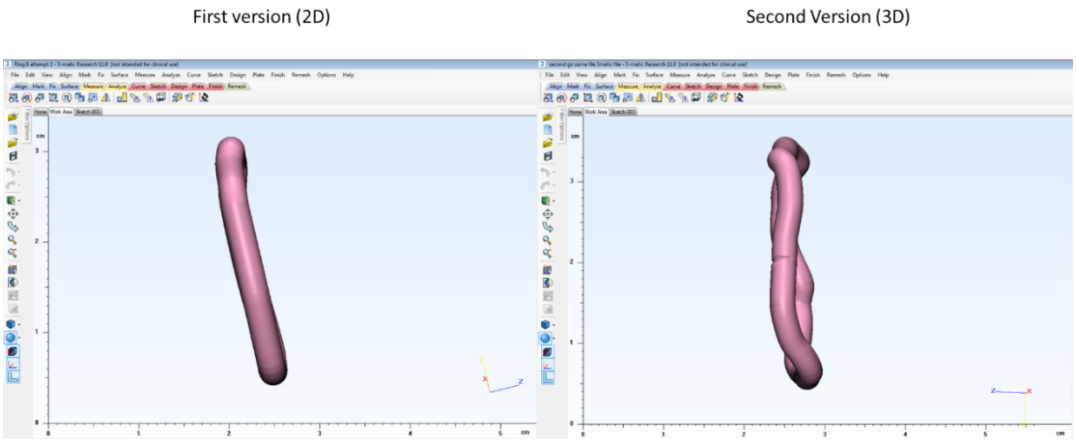

Figure 21: Comparison of the lateral three-dimensional shape of rings produced using single-layer and whole valve shapes.

This process was repeated later to ascertain whether the results of this method were replicable. Although a slightly different shape was produced on the second iteration, the dimensions of the ring were near-identical as can be seen in Figure 22, suggesting that this technique was relatively robust in producing a ring of appropriate size for implantation. Given that the downsizing of the diseased annulus is the primary aim of annuloplasty rings, this method would likely succeed in producing surgically appropriate implants, however the differences in shapes produced could result in different mechanical stresses on the valve and may compromise some longevity if the shape chosen was not the most advantageous option.

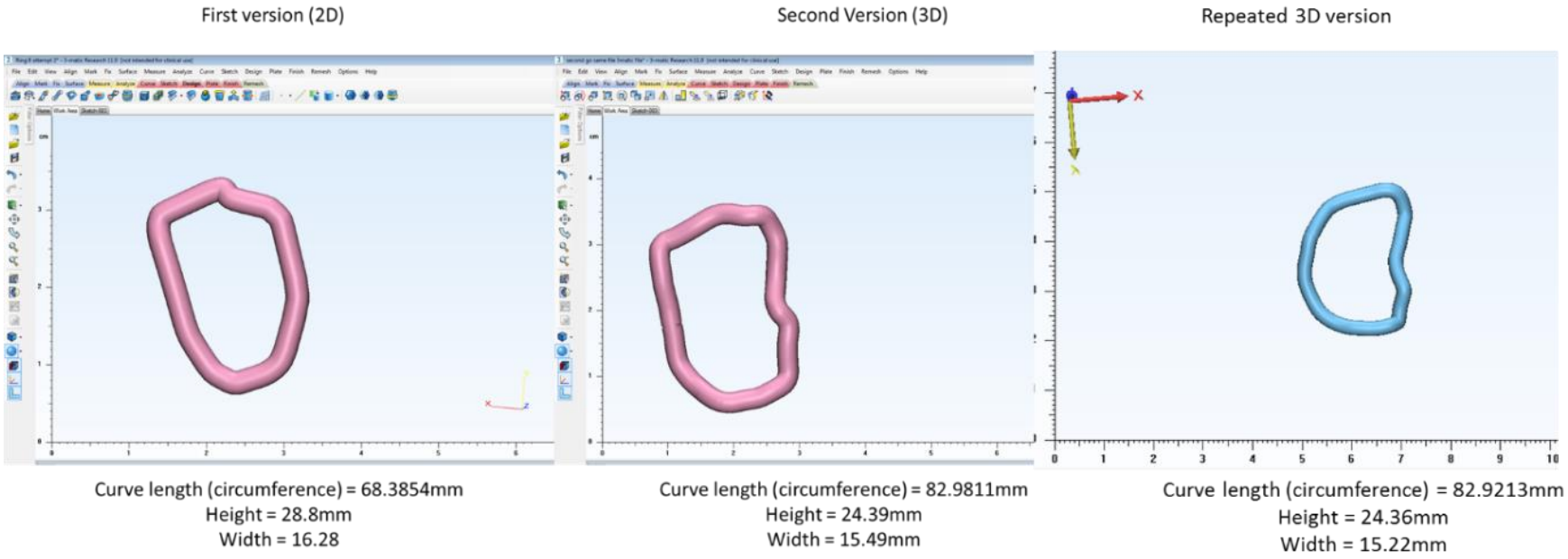

Figure 22: Comparison of three ring designs from the same scan: initial design from single-layer model (left), and two repeats (centre, right) of designs produced through the same method of full valve design.

4.3.3 Point-based design

As ultrasound is also prone to noise, designs produced using thresholding may result in increased, unnecessary complexity in the ring shape which has arisen not from the shape of the patient's anatomy but from an inaccuracy in the imaging technique.

The DKFZ research centre in Germany produced bespoke, in-house programming software for identification of valve leaflet insertion points throughout an ultrasound scan – providing multiple layers of single points which can be joined, in comparison to a single 3D image which must be drawn on internally to produce geometry (Graser *et al.*, 2013, 2014; Al-Maisary *et al.*, 2017). This method therefore accounts somewhat for the potential for noise in scans and reduces its impact on the overall resulting ring design.

This methodology was investigated using the Materialise Mimics software to produce an annulus geometry from a second patient scan. Placement of points at the leaflet insertion was undertaken manually and points exported to 3Matic for completion of a ring design from the joined points. Figure 23 shows the work undertaken on the ultrasound scan and positioning of the points on the imported data.

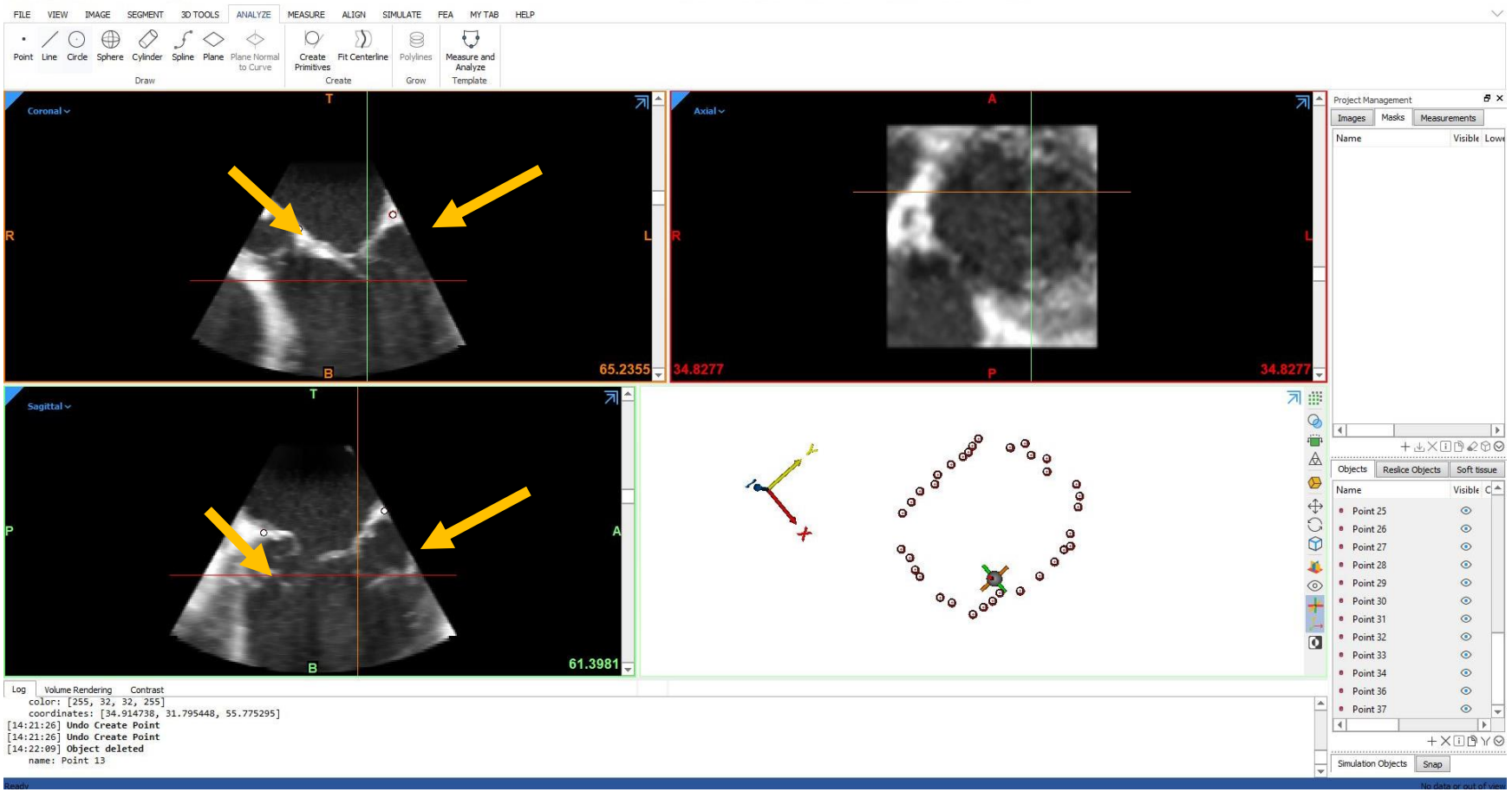

Figure 23: Method of placing points on the leaflet-annulus intersection on individual layers of scans. Blue arrows (left) show the placement of points at leaflet insertion points of the mitral valve on scan images.

Figure 24 shows the imported and averaged points resulting in an annular ring geometry. The saddle-shape of the annulus is clearly visible in Figure 24, and connection of the points using a smoothed curve followed by circular sweeping of the shape produced a shape clearly representative of an appropriate annuloplasty ring design.

This method also proved less labour intensive overall given the reduced number of steps involved in finding the annulus shape on scans. By avoiding thresholding of the image, there was no need to manually add or remove areas after the initial thresholding, and curves did not have to be drawn by hand across the inside surface of the 3D model following exportation.

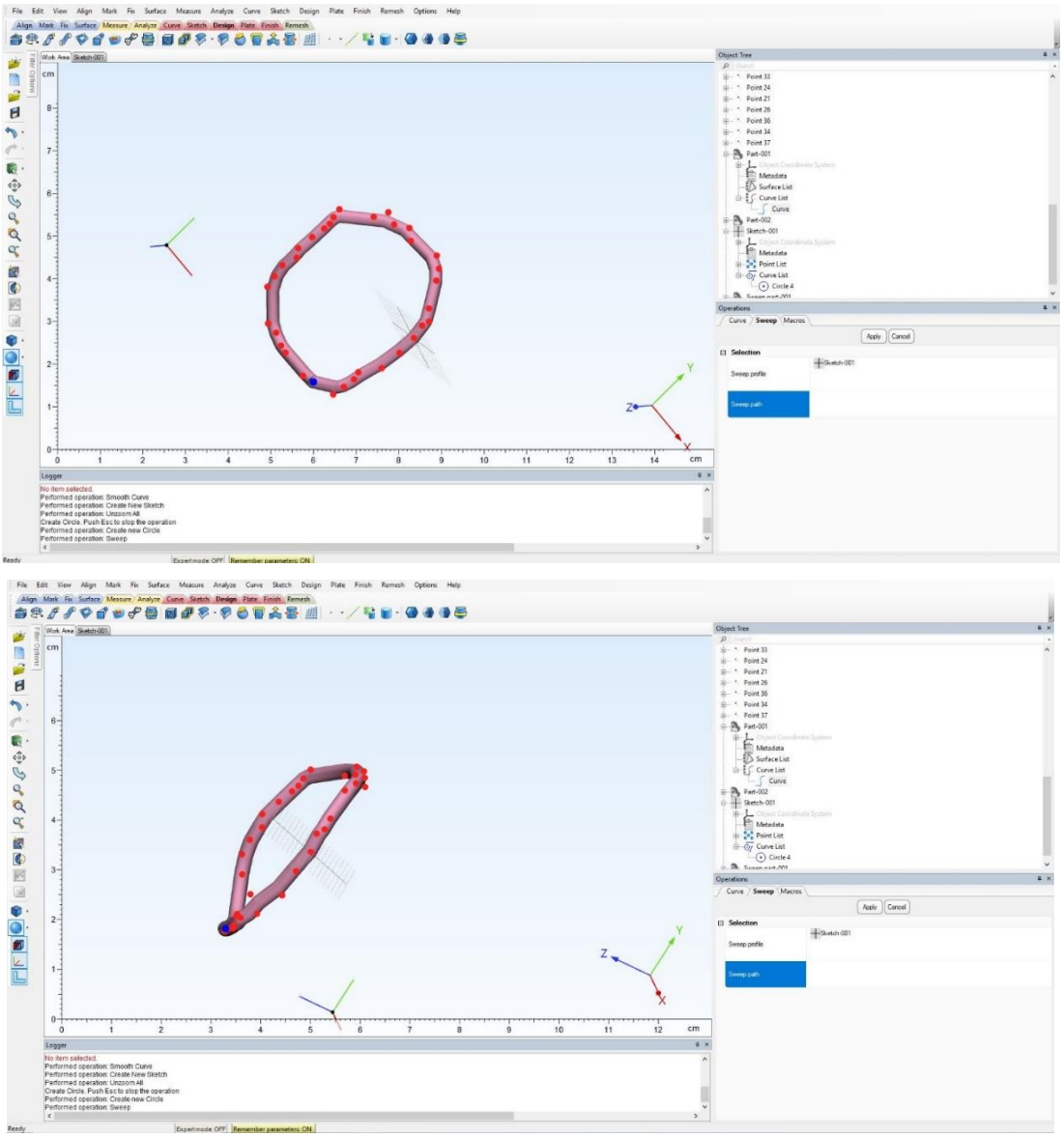

Figure 24: Mitral annuloplasty ring design produced from point-based method

4.4 Conclusions

In these chapter, the design of annuloplasty devices has been considered, particularly focussing on the validation of existing geometrical assumptions and potential workflows for the creation of bespoke designs in place of off-the-shelf sizes and shapes. From this work, the following conclusions have been drawn:

- The mean ratio between transverse and anteroposterior dimensions of the human mitral valve is close to, although not exactly, 3:4; however, human populations vary widely around this average, with an error of 4mm compared to actual measurements.
- Therefore, some patients are not served accurately by existing off-the-shelf annuloplasty device designs.
- Existing commercial software is appropriate for designing cardiovascular devices from patient data – homemade tools are not required.
- Whilst in-built thresholding tools can be used on valve structures and produce reasonably replicable dimensions, placement of points on leaflet insertion positions is a quicker method less reliant on manual editing of valve anatomy by the user.

5 Results II: Prevention of detrimental surface coagulation

5.1 Introduction

In this chapter, the effect of Electrolyte Jet Machining on platelet activation on the surface of SLM-manufactured Ti6Al4V samples. Samples included an as-manufactured Ti6Al4V SLM alloy (SLM-AM), four parameter sets of EJM (SLM-A, SLM-B, SLM-C and SLM-D), and a conventionally manufactured sheet Ti6Al4V material (Ti64-S). Annuloplasty devices reside within the core of the heart, in constant contact with turbulent and high-pressure blood flow towards the body. As-built additively manufactured Ti6Al4V samples, and AM samples processed with various parameter sets of EJM were tested, in addition to conventionally manufactured sheet Ti6Al4V samples.

5.2 Whole-blood Results

5.2.1 Production of Ti6Al4V samples

Titanium disk samples were produced successfully by SLM, according to the CAD files and parameters laid out in Section 3.4.1. Four categories of EJM processing were applied as also described in Section 3.4.1 (Samples SLM A-D), alongside untreated, as-built control samples (SLM-AM).

EDX analysis, shown in Figure 26, confirmed that the majority of surface elements present were Titanium, Carbon and Aluminium. Titanium represented most of the surface, with aluminium expected to have a surface presence according to its inclusion in the medical Ti6Al4V alloy. The carbon found was likely to be an unavoidable environmental contaminant from exposure to air, however it represented the least common element on the surface of all samples investigated.

Importantly, the presence of sodium or halide ions was not found in significant quantities on any polished sample, suggesting that the EJM process does not leave behind residues on the surface of samples. The presence of oxygen was increased on SLM-C, which suggests an increase in the titanium oxide layer found on the outside of most titanium alloy parts, when compared to the other samples.

In addition to producing the disks described for these *in vitro* studies, the parameters described in Section 3.4.1 were also trialled for the manufacture of bespoke annuloplasty device designs produced using the methods of Chapter 4. The resulting build was successful, producing a component faithful to the original CAD and without build failure or errors in the part. The part produced, shown in Figure 25, suggests that SLM manufacturing with these parameters could successfully manufacture appropriate annuloplasty devices in the future, and the disks used for *in vitro* studies would be representative of these parts.

Figure 25: A bespoke annuloplasty device manufactured in Ti6Al4V using SLM, using individual patient scan data to produce CAD models (CAD shown in Figure 24)

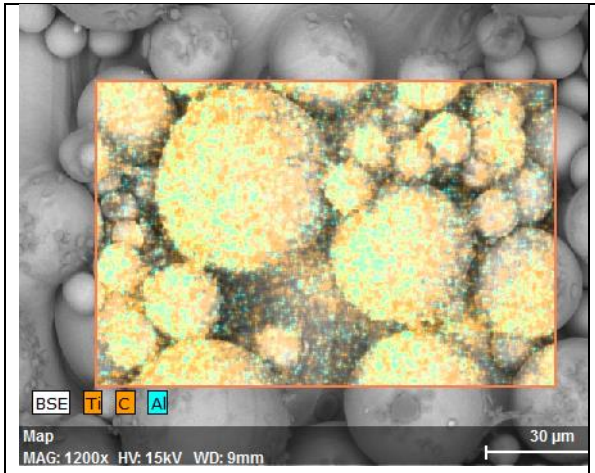

As-built AM sample (SLM-AM)

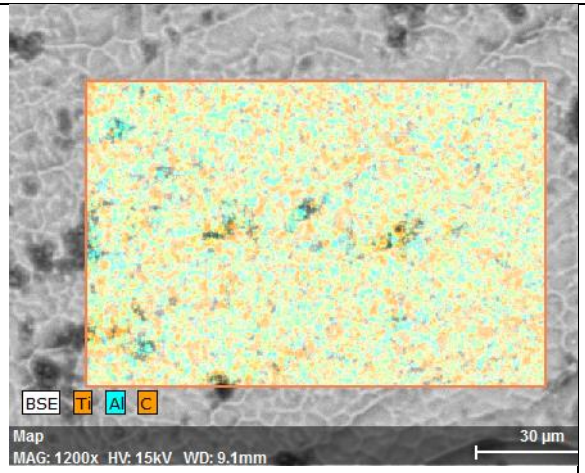

SLM-A

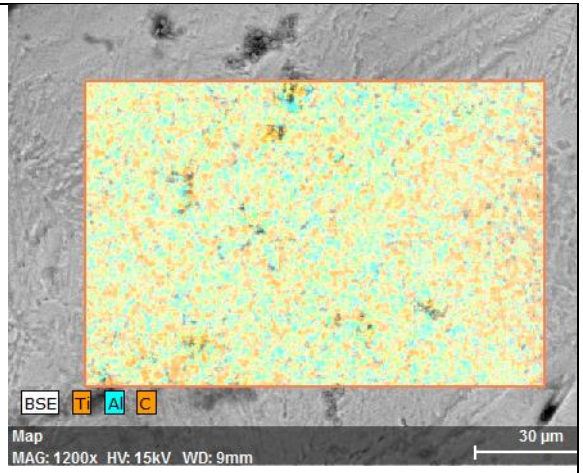

SLM-B

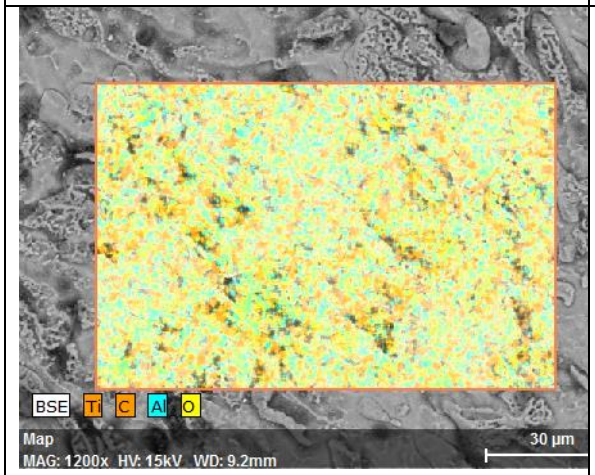

SLM-C

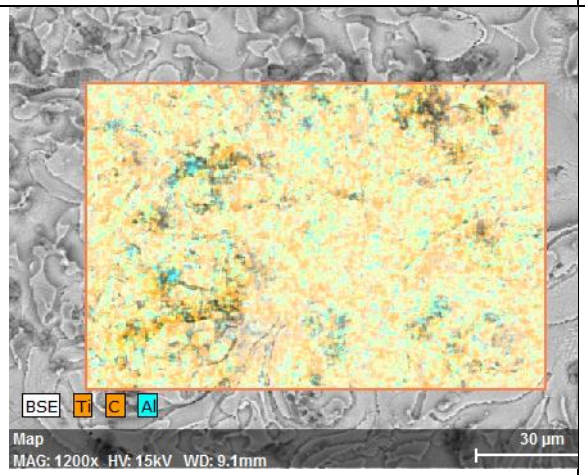

SLM-D

Figure 26: EDX of surfaces before and after EJM processing of a SLM-produced titanium alloy sample.

5.2.2 Flow cytometry

5.2.2.1 Platelet activation

With regards to platelet activation as marked by CD62P externalisation, little difference could be seen between samples with or without ADP activation (Figure 27). The negative control samples which had not contained any titanium disks when shaking did show a lower number of activated platelets compared to other samples with both CD62P and CD63 markers. Aside from this, however, the overall percentage of active CD62P-positive platelets found in solution was very low, with no more than 15% of platelets found even with activation by ADP.

Most of the polished samples, with the exception of SLM-C, appeared to increase the incidence of CD62P-positive platelets in solution after exposure to their surfaces with activating factors. However, without the addition of and activation by ADP, samples B and C both showed a slight reduction in the percentage of active platelets found. The culture plastic wells showed a reduction in active platelets over both environments, with both activated and non-activated blood showing a decrease in active platelets present compared to the AM sample, decreasing by 1.6% without ADP presence and 2.9% with ADP.

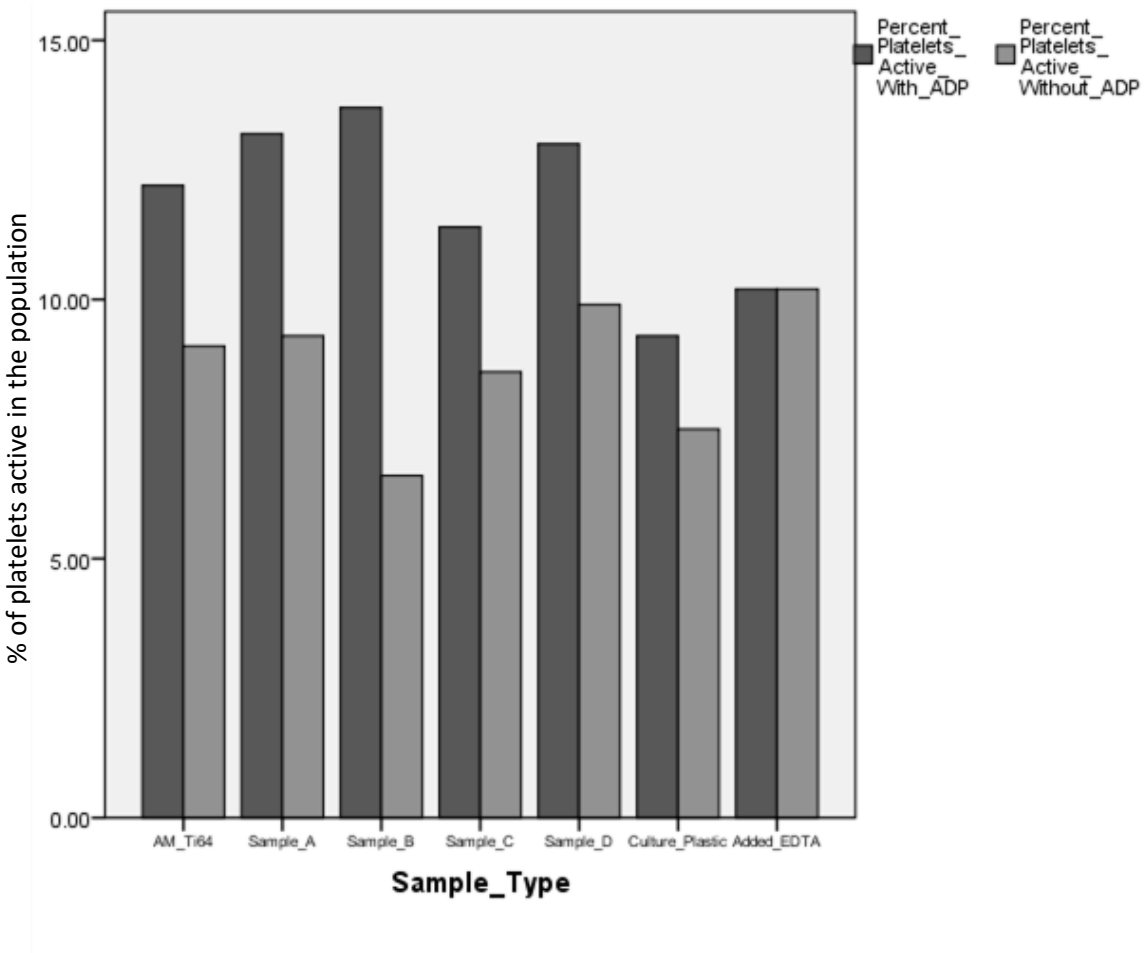

Figure 27: Percentage of CD62P-positive platelets active within the population in solution after exposure to sample surfaces, according to flow cytometric analysis. EDTA anti-coagulant was applied as a negative coagulatory control along with inclusion of wells containing only tissue culture plastic.

In the activity of CD63 markers shown in Figure 28, again only a small difference can be seen in the activity of platelets on the different surfaces. The percentage of active platelets again did not pass 15% even with the addition of activating ADP.

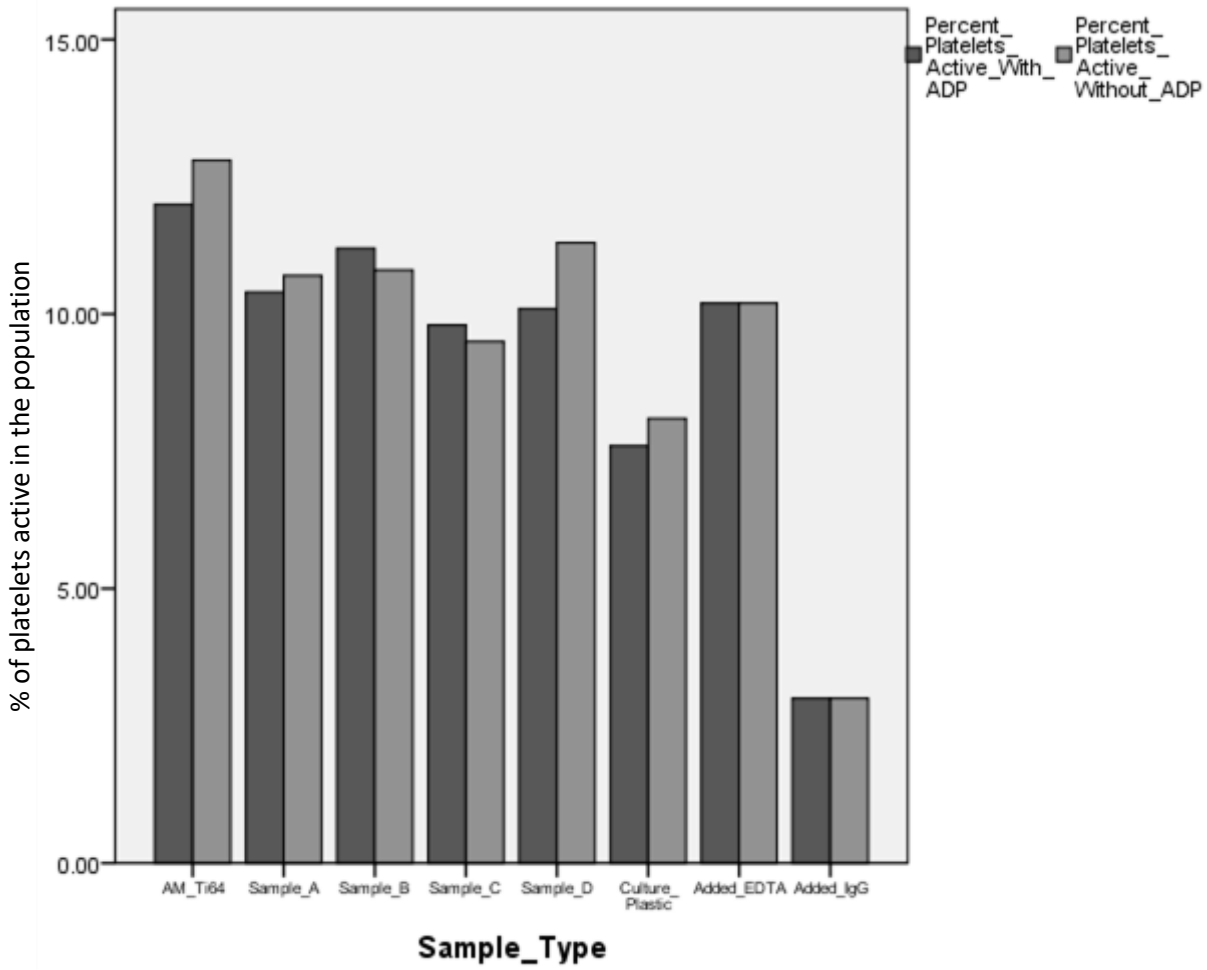

Figure 28: Percentage of CD63-positive platelets active within the population in solution after exposure to sample surfaces, according to flow cytometric analysis. EDTA anti-coagulant was applied as a negative coagulatory control along with inclusion of wells containing only tissue culture plastic.

Despite this, the unpolished surface produced a slightly higher activity of platelets with and without ADP input when compared to the polished samples and the blood with no titanium disk. In particular, SLM-C produced a lower activation than any other sample, with under 10% of platelets activated under both conditions. However, the activation of the platelets was so low in all cases that the difference between samples was still minimal. Further, the addition of ADP to some wells appeared to paradoxically decrease the number of active platelets found in the solution. Again, the tissue culture plastic showed a more marked reduction in the percentage of active platelets found in solution.

The conclusions of these two assays are not in agreement, despite the chosen markers being related in their response on platelet activation. CD62P and CD63 are both markers of platelet activity, with CD63 increasing on platelet surfaces after granule release, and CD62P being externalised on the platelet surface during activation through membrane flipping. Therefore there should be a greater degree of agreement between the results of the flow cytometric analyses; although the exact changes between samples may not be identical due to involvement in different processes, there should be some consensus in which samples produce greater or lesser extents of activation.

5.2.2.2 Platelet Aggregation

After measurement of the number of single platelet events in the fixed samples the percentage of aggregation was calculated for each sample. The number of single platelet events in the EDTA-chelated blood sample was used as a reference point. The formula is given below:

$$\%\, aggregation = 100 \times \frac{[start\ count - sample\ count]}{[start\ count]}$$

$$Start\ count\ =\ number\ of\ platelet\ events\ present\ in\ EDTA\ chelated\ blood\ sample$$

$$Sample\ count\ =\ number\ of\ platelet\ events\ in\ the\ fixed\ test\ samples$$

The differences in aggregation seen across samples had a wide variability, with some results showing different responses relative to the unpolished sample dependent on ADP presence. Shown in Figure 29, SLM-A for example elicits less aggregation without the presence of ADP than the unpolished sample; however it shows increased aggregation compared to the unpolished sample when ADP is added.

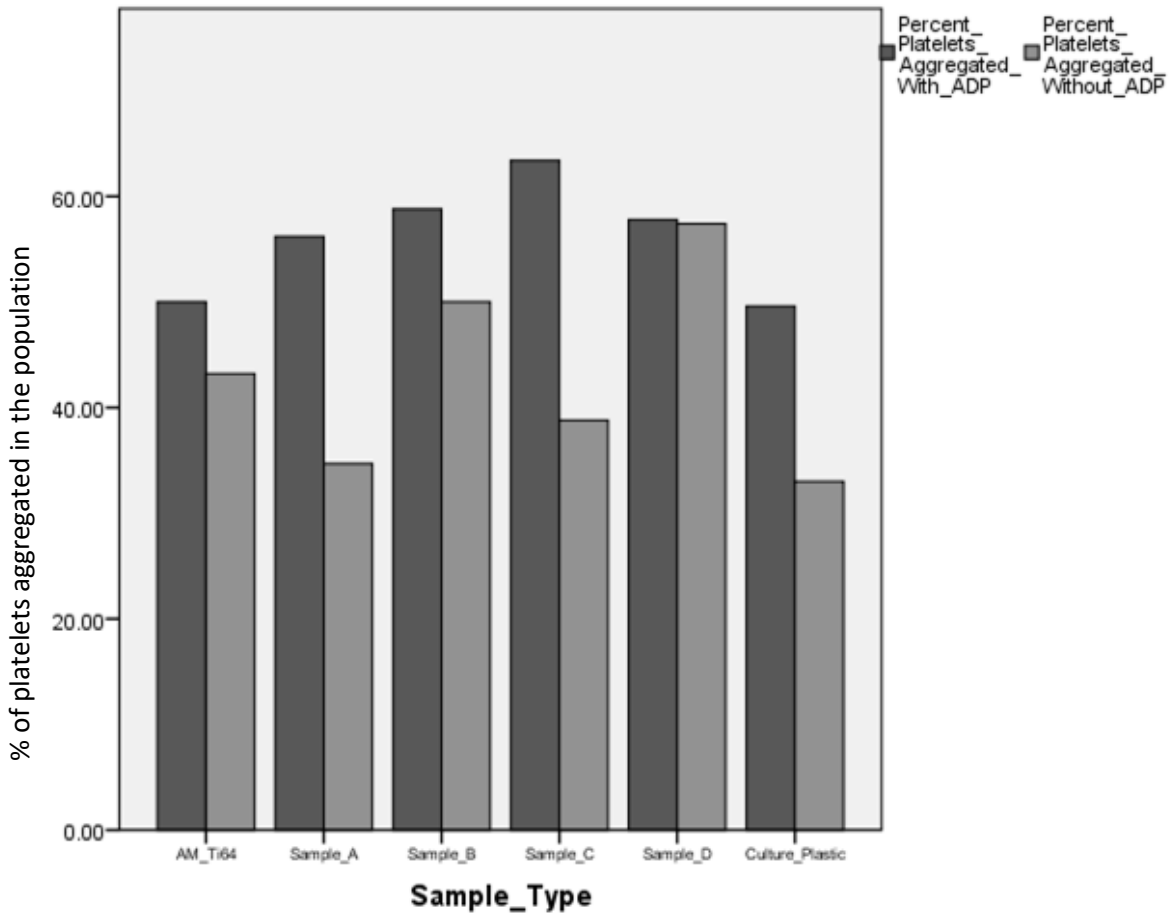

Figure 29: Percentage of aggregated platelets in solution following exposure to sample surfaces.

Overall, SLM-C shows the greatest increase in activated platelet aggregation, with AM samples and culture plastic showing roughly similar responses. However, similarly to the CD63 analysis, experiments with and without ADP involvement did not follow the same pattern of activity. With the inclusion of ADP, SLM-A showed an increase in platelet aggregation in solution compared to the as-built AM sample, however without ADP the opposite is true. As expected, tissue culture plastic showed equal aggregation to the lowest values both with ADP (equal to the AM sample) and without ADP (equal to SLM-A).

5.2.3 SEM Imaging

Following initial investigations, discussions regarding the results shown were had due to the small differences found even between control samples during experimentation. According to previous operator experience, similar flow cytometry investigations into oxygenator fibres had shown minimal difference between differing materials using flow cytometry on this equipment. However, when further investigations were undertaken, imaging techniques showed a significant change in blood contents found on the surface of the materials. According to this, it was decided that surface imaging of the samples themselves would be more appropriate to investigate the cellular response on it. This is especially the case given that where blood constituents including platelets *had* responded to the material surface, they would become attached to the surface itself and would no longer be found in solution, which may have affected results.

Figure 30 shows the surface of an as-built, additively manufactured titanium alloy sample. It clearly shows that the platelet response to these rough, powder-laden surfaces is substantial. There are active platelets spread over the whole surface of visible powder particles, in addition to the presence of red blood cells which appear to be in the process of being recruited to the formation of platelet plugs and further clotting influences. This is further confirmed in Figure 31 wherein a comparison of two surfaces areas, pre- and post- polishing is shown. The process of electrolyte jet machining has been successful in the removal of large, obvious powder particles from the surface of the part, and in response the presence of visible organic material has significantly reduced. This supports the idea that as-fabricated additively manufactured parts are a significant risk when introduced directly into the blood stream.

In particular it should be noted that the platelets appear to rest on the side of powder particles or in crevasses between powder particles and in small holes. It appears that these platelets have become trapped in these niches, resting inside these gaps in large numbers as well as trapping red blood cells in the same spaces. This positioning and the active nature of the platelets suggests that they are passing over the rough surface and activating when becoming caught in these areas.

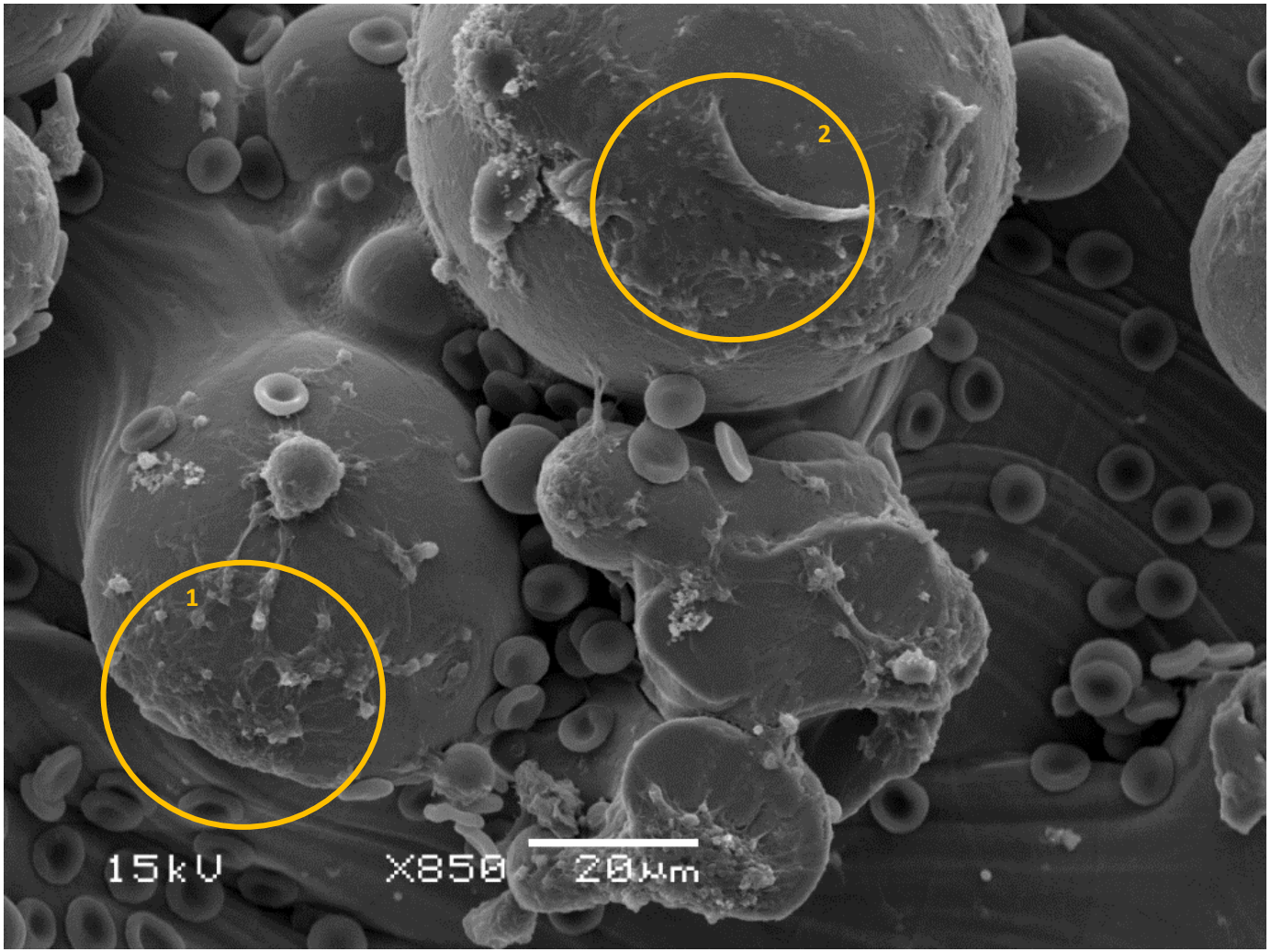

Figure 30: SEM image of an unpolished control sample imaged at 850x magnification after whole blood exposure. The large, spherical titanium powder particles have become covered in highly active platelets. The platelets are visible both through their dendritic projections on the left of the image(1), and as a completely spread hypoplasm towards the top of the image(2). The active platelets have already begun to significantly trap other cells and particles to produce a clot on the surface, as evidenced through the large numbers of red blood cells attached to the surface.

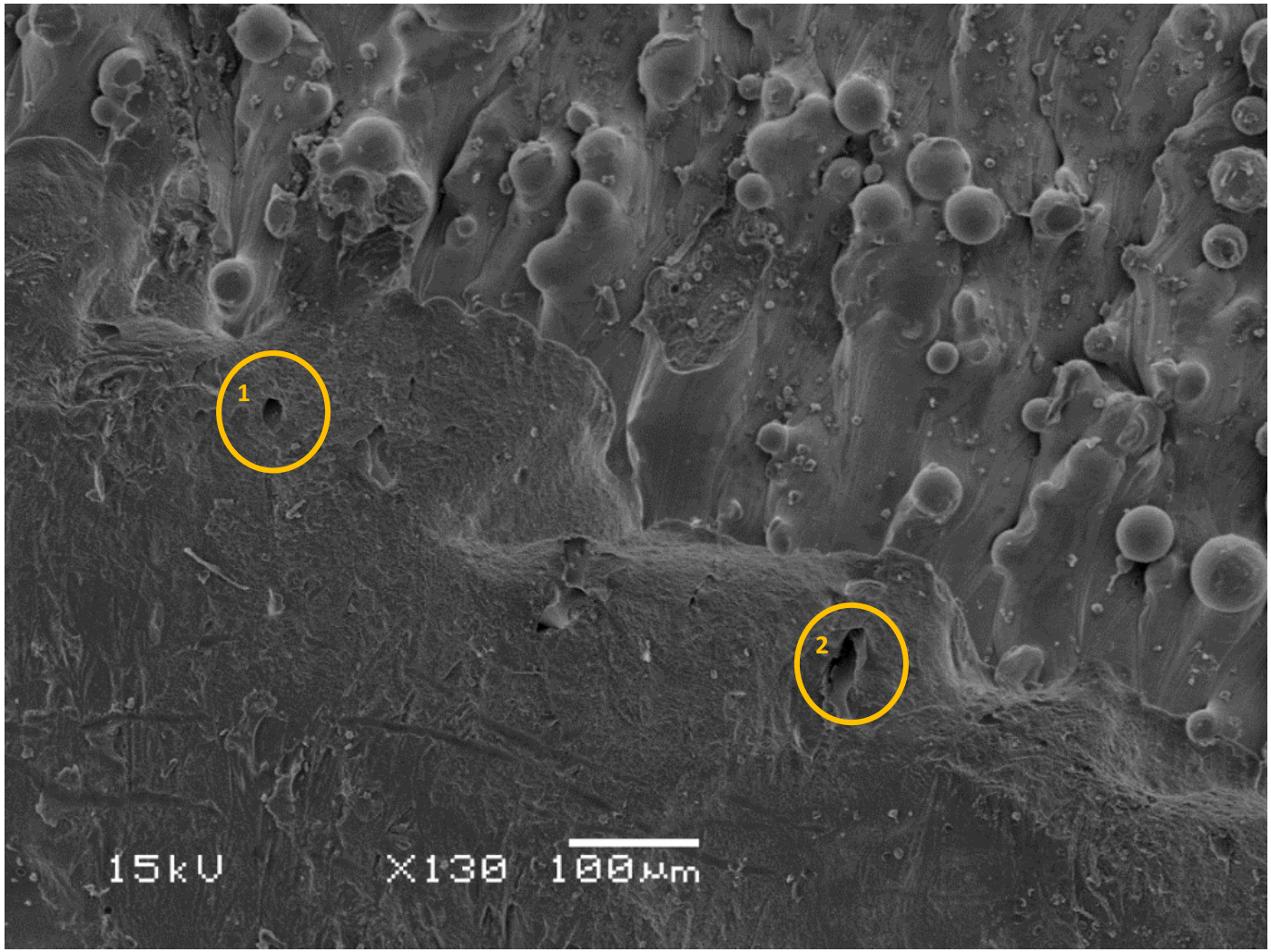

Figure 31: SEM image showing a comparison of the pre- and post-processed surfaces (SLM-A). The lower half of the image has been polished using EJM and as a result the spherical powder particles on the top half of the image have been entirely removed and the surface appears overall more smooth. It is also visible from this low magnification that there is less debris (likely platelets and other organic material) present on the polished area of the surface. Finally, small holes in the surface resulting from removal of material above a process-related void are visible (1 and 2).

Generally, the images of Figure 32 show that electrolyte jet machining did remove the powder particle coated surface and decrease the gross roughness of the sample surface. In addition, the application of two passes over surfaces as compared to one provided a more consistent surface and ensured that more of the surface was as smooth as possible. It is also clearly visible between Figure 30 and Figure 32 that as a surface becomes more uniform and smooth, there tends to be fewer platelets aggregated and blood cells present on the surface of the sample. It is expected that as these platelets decrease in number and in activity, they will pose a significantly smaller risk to patients (Smith, Travers and Morrissey, 2015).

Despite there being some differences in the topography of samples based on their processing parameters, all applications resulted in a field of view with fewer aggregated platelets visible. However, individual small features show the differences in response in samples. Areas of high current density in the centre of the nozzle's target area provide small spaces with the visibly smoothest surface and a complete absence of organic material (shown in the left of Figure 33). This suggests that the application of a high current density across a whole sample would provide the most beneficial surface, however these parameters must be considered within the context of material loss and compensatory design in the size of samples.

On some samples, there were gaps remaining where the nozzle of the EJM had missed areas and powder particles were still visible, particularly between areas of high smoothing success (Figure 33). It appears that the path of the EJM nozzle may be responsible for this, with areas to either side of the main path receiving less effective final results. Biologically speaking this is of great importance as unwanted powder particles may present a risk in coagulation potential by providing even small environments for platelets to become trapped, activate and aggregate, causing a clot.

Further to this, in samples with higher numbers of passes used, holes such as that shown in Figure 31 and Figure 34 were produced in the surface due to the underlying porosity of an additively manufactured part. These holes showed concerning numbers of red blood cells trapped within them, suggesting that a platelet plug had already begun to form within the confines of this hole. This is of equally high concern as the possibility of an external clot, as the potential for dislodging of the plug and movement systemically through the bloodstream could lead to strokes, pulmonary emboli or other ischaemic disease (Aytekin *et al.*, 2011; Smith, Travers and Morrissey, 2015).

It must be considered with this that the propensity of additively manufactured parts for defects and particularly powder bed fusion processes to gain internal voids therefore poses

a significant risk when producing a blood-contacting device (Gibson, Rosen and Stuker, 2013).

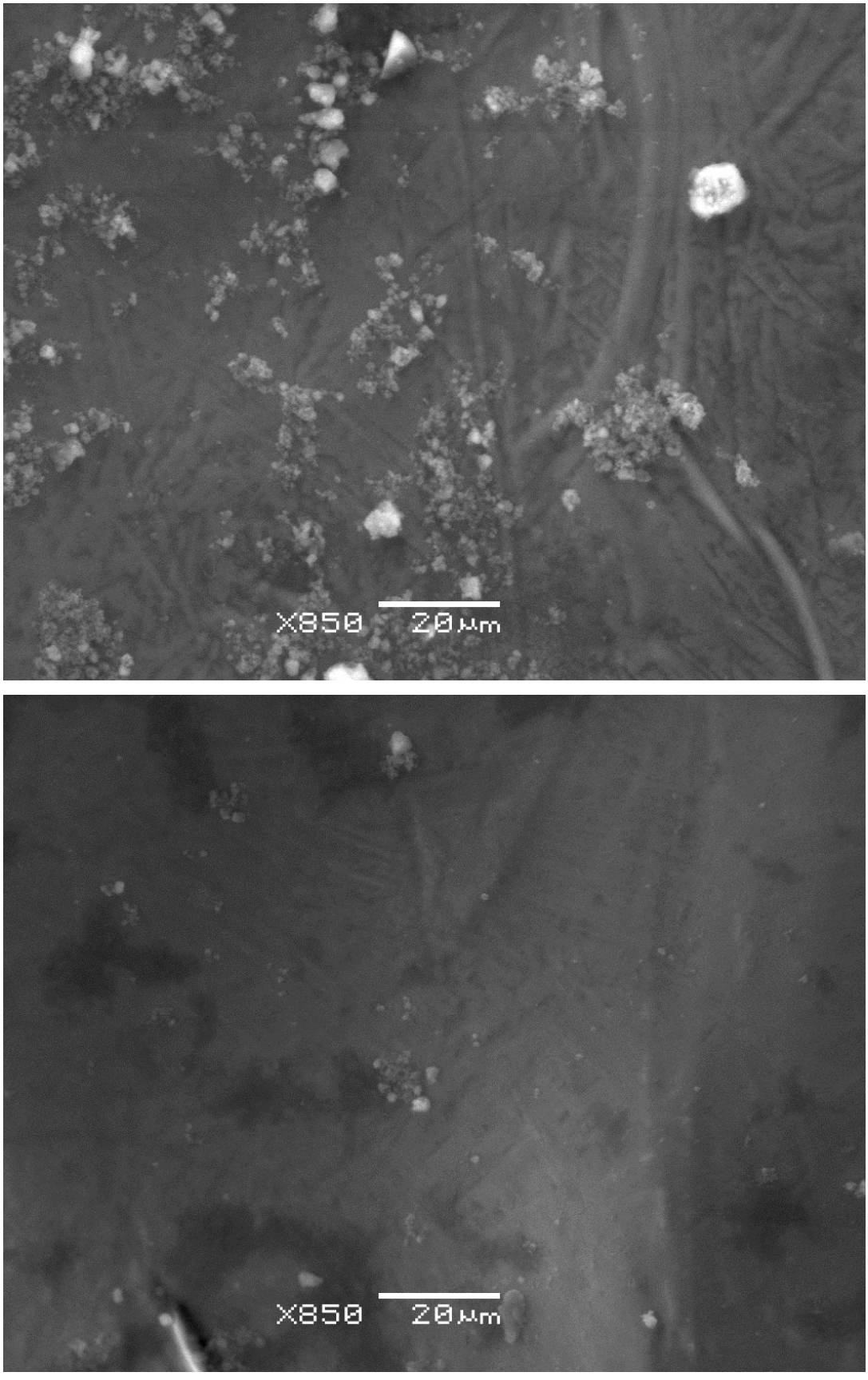

Figure 32: SEM images of Chloride-polished samples with one (above, SLM-A) and two (below, SLM-B) passes used following exposure to whole human blood.

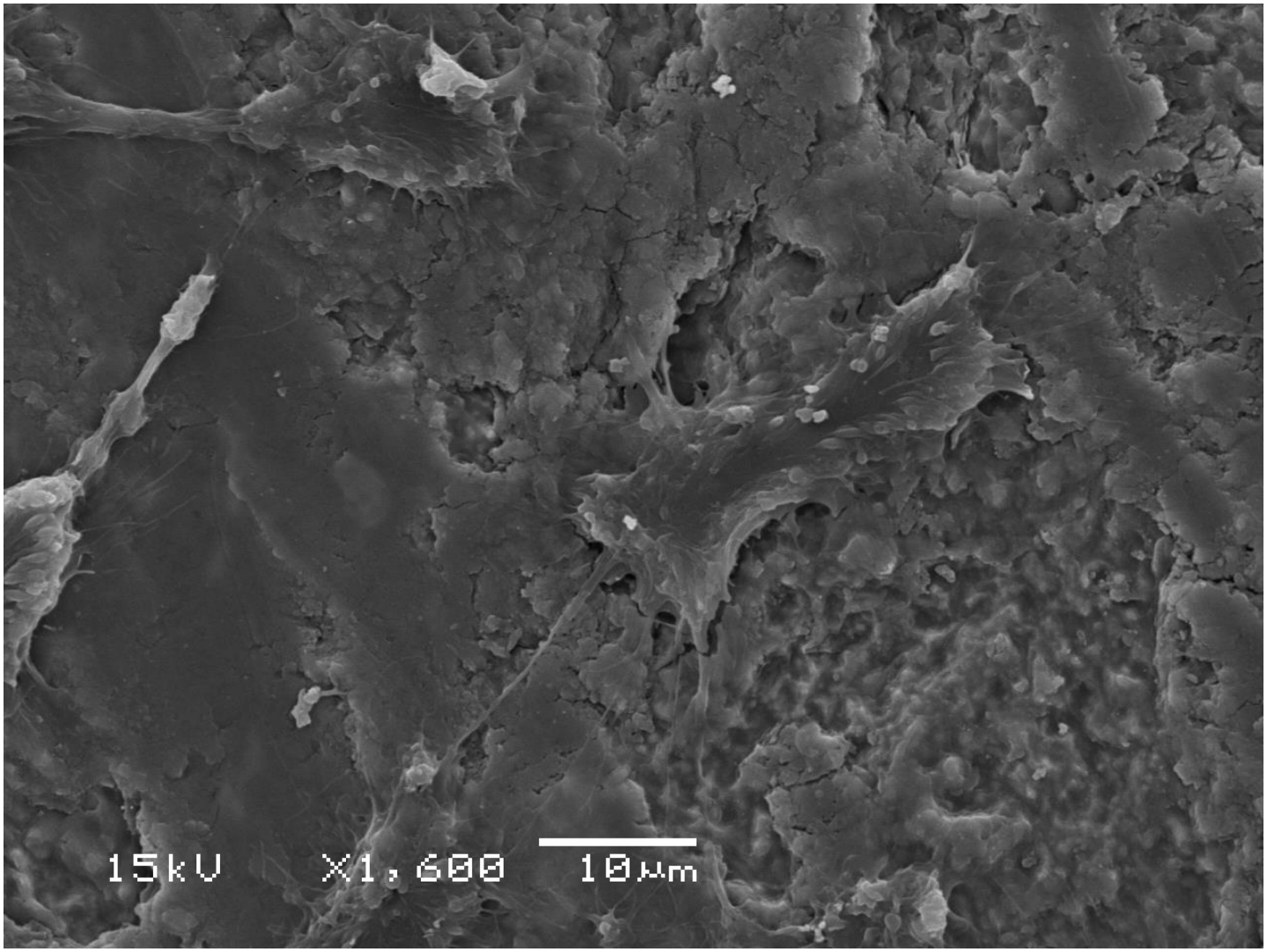

Figure 33: SEM image showing a polished surface exhibiting significant topographical differences between adjacent areas. The smoother surface to the left of the image is nearly clear of all biological material, whereas platelets are present and active to the right of the image where the surface is less smooth.

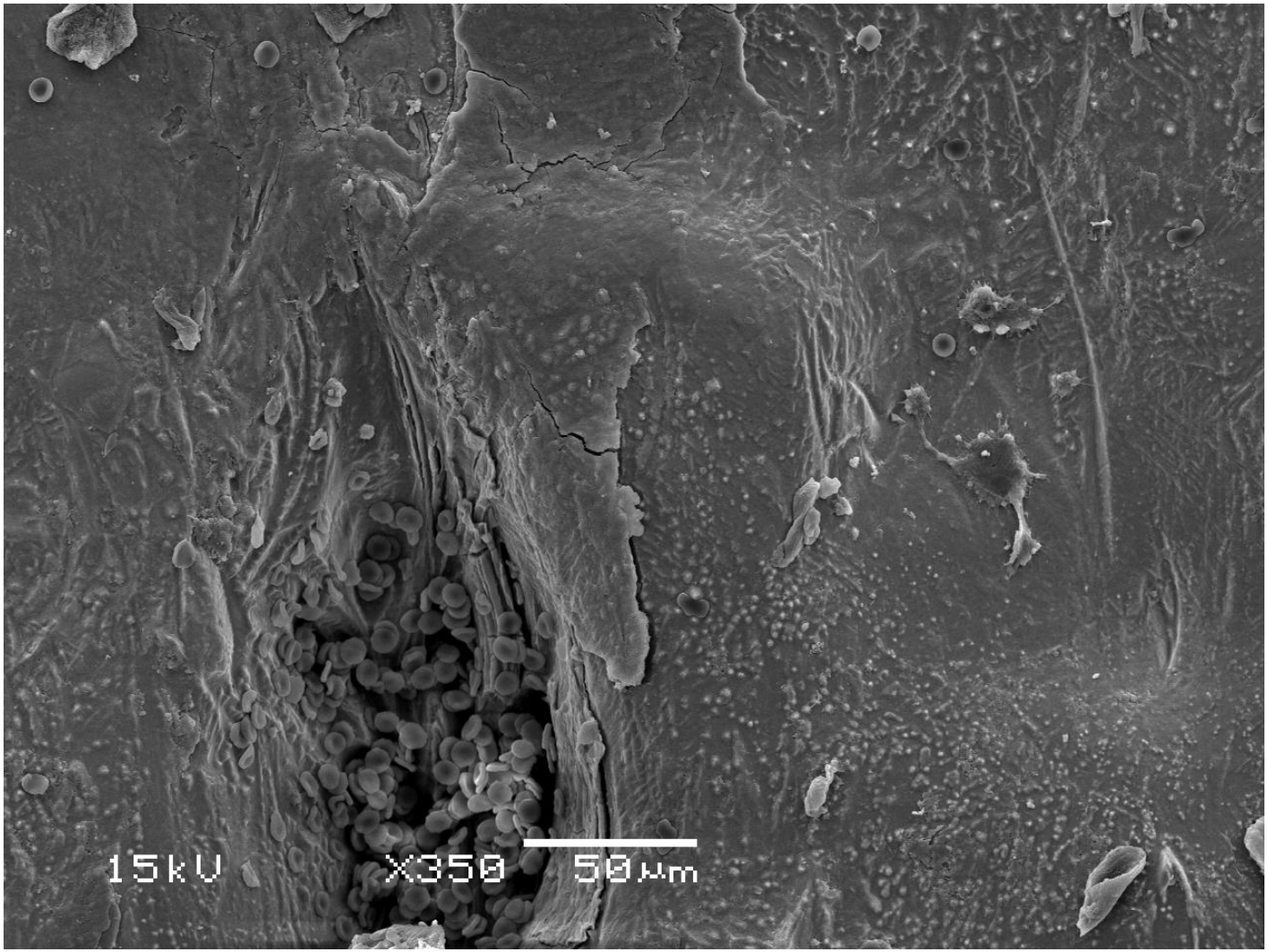

Figure 34: SEM image showing a polished surface containing a large void in which blood has pooled and may cause a significant clot.

Samples C and D, when compared to the processing parameters involving only chloride ions, produced much more pitted and uneven surfaces (shown in Figure 35). These surfaces proved difficult to image using scanning electron microscopy, but where visualisation was achieved, the unevenness of the surface along with the presence of cells and platelets on the surface deemed the inclusion of bromide ions in the polishing inappropriate for this application.

It is likely that the surfaces of the images were not amenable to imaging easily due to the different focal planes produced by such an unpredictable surface texture. As a result of this, the cellular material present on the surface was difficult to visualise also, however some can be seen in the lower-right image of Figure 35, where platelets have aggregated to the uneven surface and onto a powder particle which has become pitted after processing.

Due to these considerations, it was decided that these samples would not be included for further investigation regarding their anticoagulant properties. However, it was noted that they may serve benefit in the promotion of cell growth according to the provision of cellular anchors for fibroblast-type cells. Further work on this is found in Chapter 6 (Integration of Device with Patient).

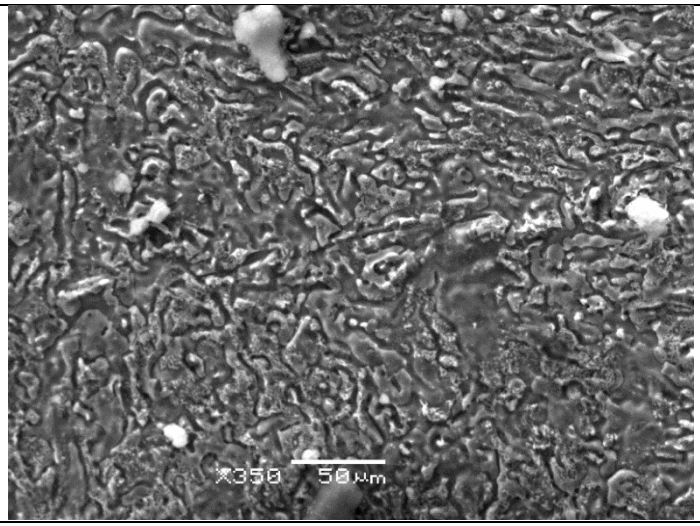

SLM-C

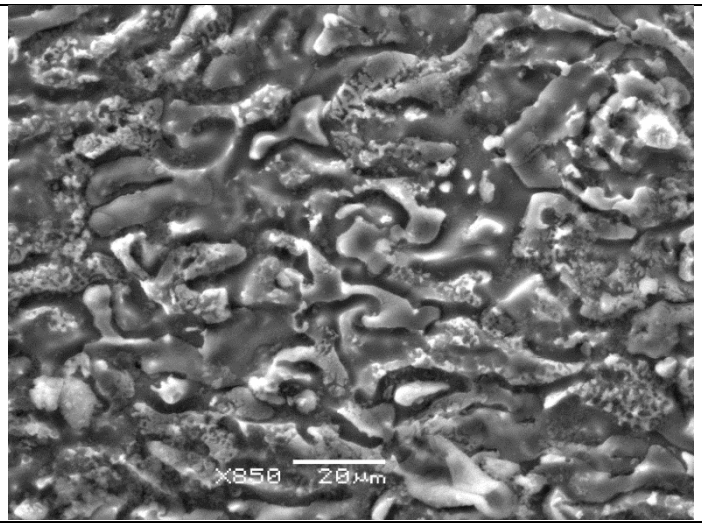

SLM-C

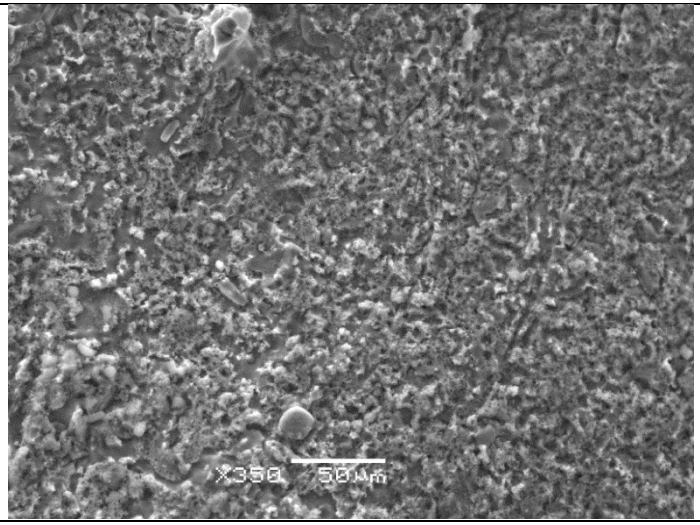

SLM-D

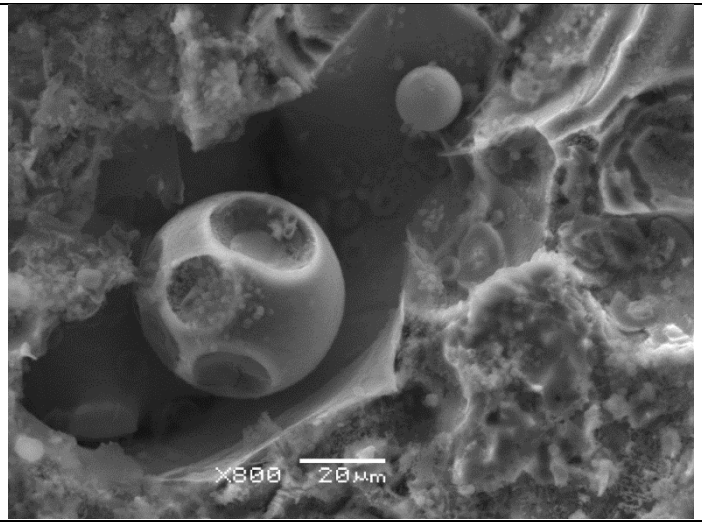

SLM-D

Figure 35: SEM images of samples C and D following contact with whole human blood. Images were taken at 350, 800 and 850X magnification, however acceptable imaging of the surface was difficult. The image on the bottom right shows collections of platelets visible on the surface of the powder particle and attracted to the uneven surface around it also.

5.3 Platelet-solution results

5.3.1 Sample Production

A further 20 SLM samples were produced successfully as in previous experiments (Section 4.2.1). 8 of the unused conventionally manufactured titanium alloy disks from Section 4.2.1 were used as controls for the manufacturing process.

5.3.2 Platelet Extraction

Platelet extraction produced platelet solutions consistently averaging around 50 million platelets/ml. This extraction was generally successful; however, it was found that more success was had working directly from plasma which had naturally separated from red blood cells while resting before use. Through allowing the blood to rest for a few days, fewer red blood cells were erroneously included in the centrifuged solutions leading to less contamination and confounding cellular presence in results.

5.3.3 Platelet Counting

Counting of platelets provides a simple method of assessing the activity of platelets in solution (Claesson, Lindahl and Faxälv, 2016). Known numbers of platelets can be seeded into culture wells and over time, any reduction in the number of individual platelets can be attributed to adherence of platelets elsewhere. In this case, platelets have activated and adhered either to the surface of the well or sample, or to one another, meaning that the number of free and resting platelets in solution goes down.

In Figure 36, it can be seen that all test samples except AM titanium with polishing parameter A produced a reduction in free platelets, suggesting an increase in platelet activity attributable to the samples within the well. This stands in contrast to the flow cytometry results discussed in Section 4.3.2 where the aggregates of platelets were counted only in solution, without accounting for those lost to the sample surface during reaction times.

The as-built AM titanium is shown to have produced a significant ($p<0.05$) reduction in the number of free platelets in solution. The bar titanium is also shown to have reduced the free platelet number significantly compared to the empty well, however there is no significant difference between these samples. Despite the statistical analysis, however, it can still be seen that the bar titanium alloy surface has, on average, left a greater number of platelets free in solution, suggesting that fewer have stuck to the surface due to activation by the material.

SLM-A is shown to have a significantly larger number of platelets free in solution than the as-built AM titanium alloy surface. The same can be said of SLM-B, suggesting that both of these EJM polishing parameters were successful in reducing the number of platelets attracted to and activating and adhering on the sample surface.

The average number of platelets present in SLM-A solutions was higher than those in the wells with no sample. This is likely due to assumptions made in counting platelets manually using haemocytometers. This method, whilst respectably accurate and a standard for manual cell counting, does assume that the sample used is representative across the entire volume of the well, and in some cases, large aggregates may be missed, or some areas may just have fewer cells present due to random chance.

Similarly, the additively manufactured samples proved to be more thrombogenic than the addition of thrombin to tissue culture wells. In this case, this could be rectified with a larger concentration of thrombin included in the well, as there may not have been enough to produce the maximal effect.

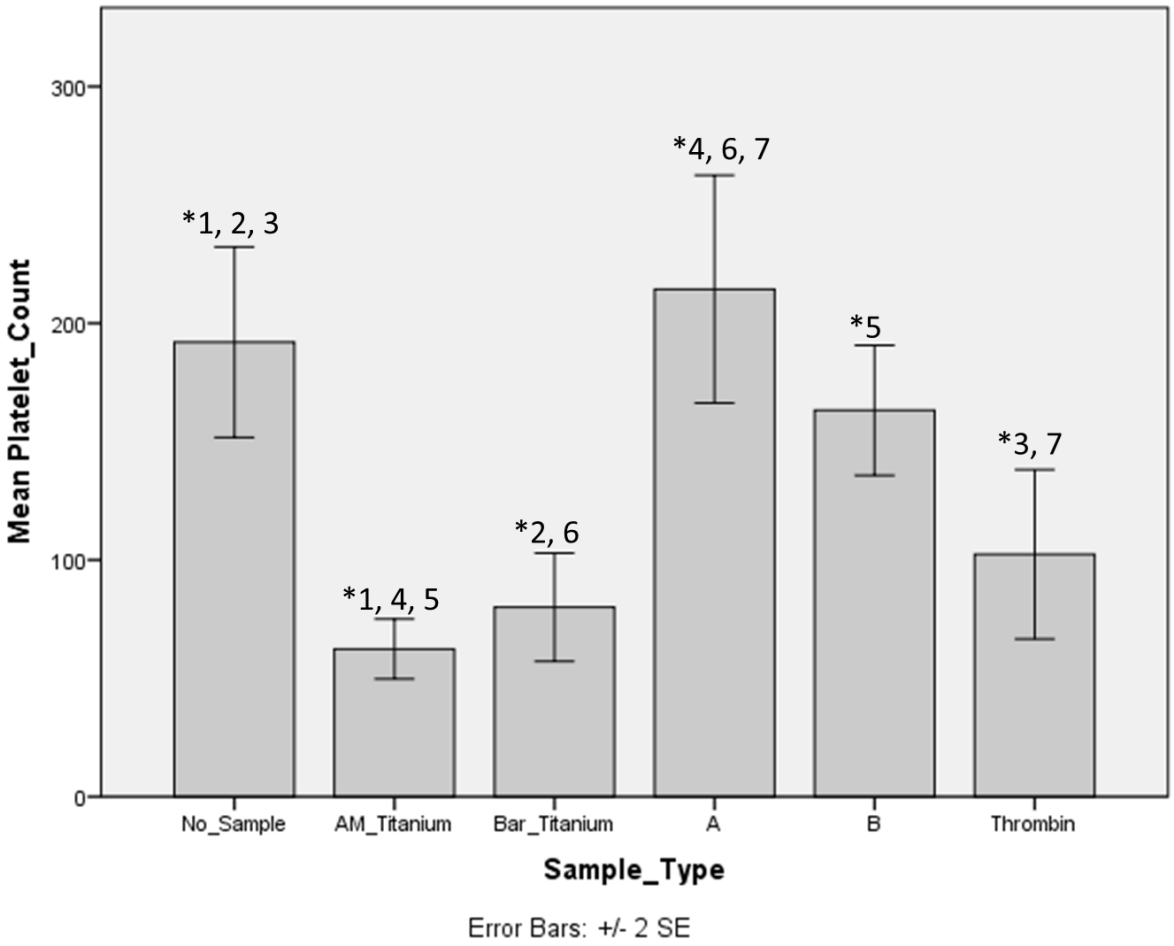

Figure 36: Mean number of platelets present in solution when samples had been incubated for a 2-hour period. A reduction in the number of platelets in solution is assumed to be related to adhesion of platelets to the surface introduced or to each other due to activation associated with the surface. Statistical significance calculated using ANOVA is denoted numerically.

5.3.4 Alamar Blue

Alamar blue studies were performed to assess short-term platelet activity levels after exposure to the surfaces of samples. Figure 37 shows the initial study including the as-built AM titanium samples, and the bar titanium alloy compared against a well of no platelets and a thrombin positive control.

Alamar blue assays show metabolic activity of material inside the wells being investigated. Through a reduction reaction, cell activity transitions the alamar blue solution from blue to a fluorescent red molecule. Thus, increased cell activity leads to an increase in fluorescence in the reading of the plate solutions. In this case an increase in fluorescence suggests an increase in platelet activity, which would be indicative of thrombotic activity.

Initially, experiments were undertaken to compare metabolic activity on titanium alloy surfaces, dependent on the manufacturing process being additive or traditional sheet metal. In Figure 37 it can be seen that additively manufactured titanium has increased metabolic activity, and therefore more active platelets, than the bar titanium samples. Whilst not as active as a thrombin activator, this increase in activity compared to the bar titanium is indicative of an increased thrombotic risk from AM surface material than bar metal. However, this difference is not significant ($p>0.05$), which is likely related to the wide variation found in the bar titanium samples.

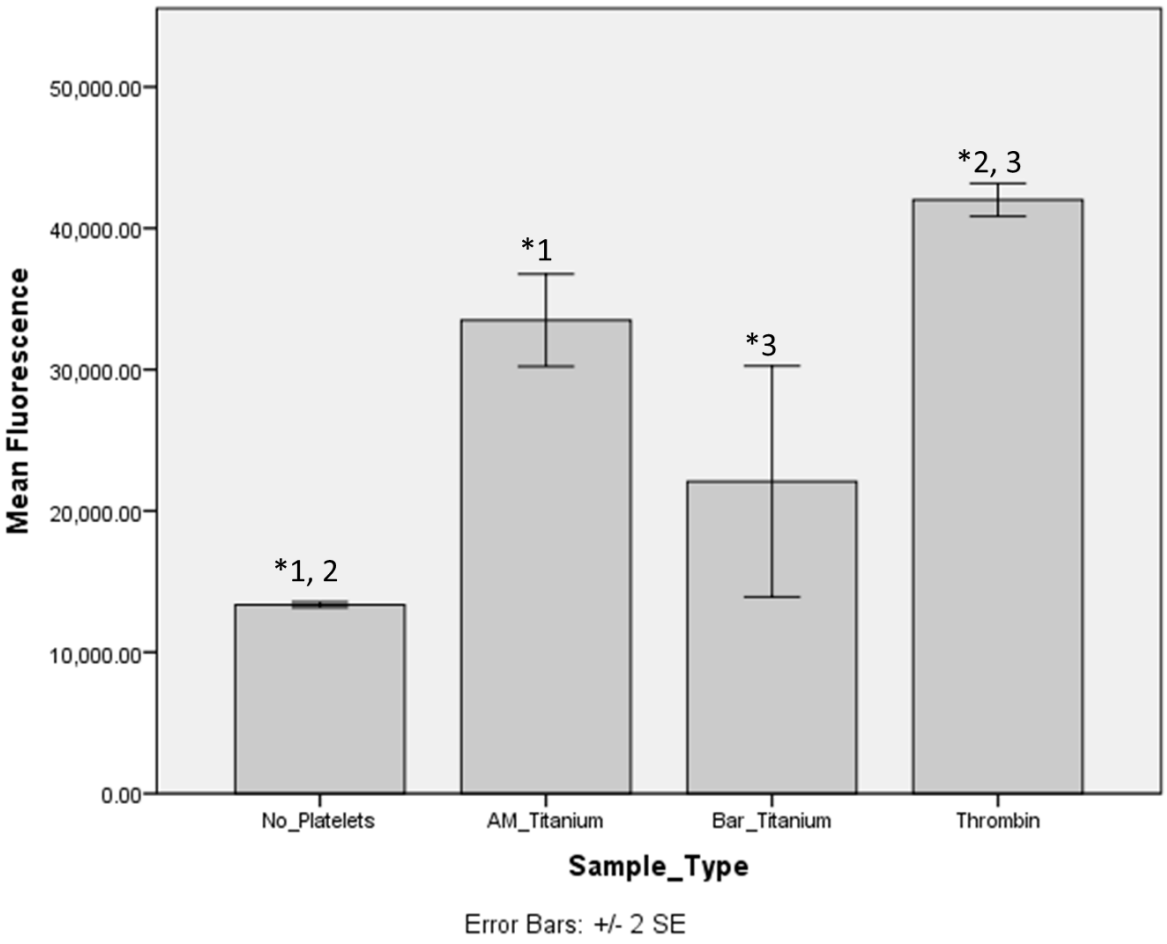

Figure 37: Mean fluorescence of alamar blue assay showing metabolic activity of biological constituents (platelets) in solution while in contact with samples included.

Figure 38 shows a comparison amongst all the additively manufactured samples used, compared to a well containing no sample, no platelets, and a thrombin activator. The well without platelets shows a significant difference from all other samples, indicating that it is only the activity of platelets that have caused the majority of changes in fluorescence.

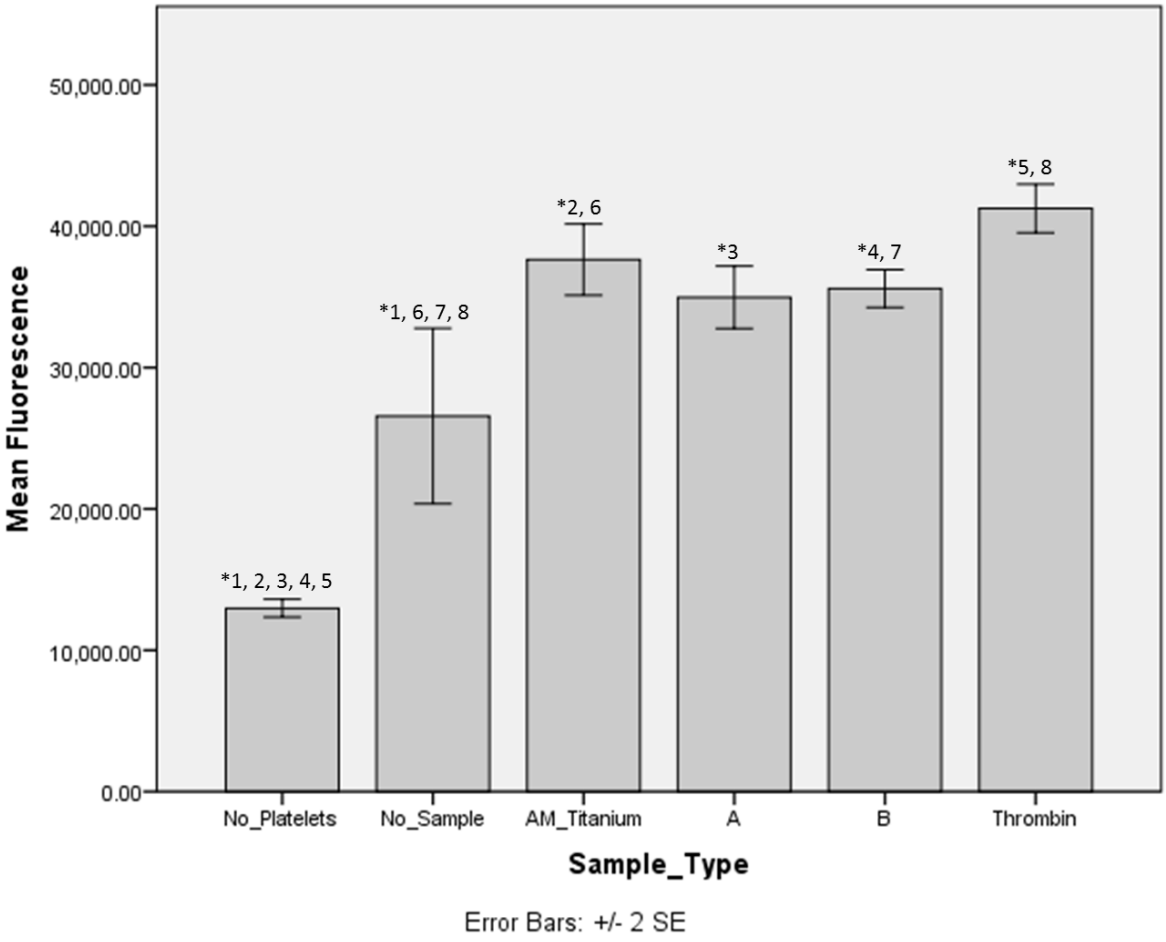

Figure 38: Mean fluorescence of alamar blue assay showing metabolic activity of biological constituents (platelets) in solution while in contact with samples included. A selection of polishing parameters was included along with additively manufactured titanium alloy and negative and positive controls.

The AM titanium sample, batch B polished samples, and thrombin activators all show significantly increased cell activity compared to the wells incubated with no sample present. Whilst there is not a statistically significant difference between the as-built AM sample and the polished sample, it can be seen that on average there is a reduction in cell activity shown by fluorescence in both the polished samples. All the samples are less thrombogenic than the thrombin activator, however the as-built AM sample approaches the values found with thrombin activation, showing that it is a major risk factor in the instigation of erroneous coagulation.

The as-built AM sample and batch B polished samples both show a significant increase in metabolic activity compared to platelet solutions incubated on just tissue culture plastic (No_Sample). Again, this suggests a significant increase in thrombogenic risk produced just from the inclusion of these samples in the well. Contrastingly, whilst SLM-A is not significantly different in its response from the as-built AM titanium surface, nor is it significantly *more* thrombogenic than the empty wells of tissue culture plastic. Again, similarly to the bar titanium discussed previously, tissue culture plastic showed a very wide variation in response amongst the populations.

5.3.5 Immunofluorescence Microscopy

Samples were fluorescently tagged using CD61-FITC antibodies to visualise the location of platelets on the surface of samples (Figures have been re-coloured for clarity). These samples were then imaged using a Leica IRE2 microscope with an excitation wavelength of 488nm.

Initial viewing of the immunofluorescence images shown in Figure 39 shows a dramatic change between the four samples regarding platelet p resence on their surfaces. The bar titanium material is nearly completely void of platelet presence, with only a small number of fluorescent points which do not appear to be in the same shape or formation as platelets found on other samples. By comparison, the additively manufactured sample is covered nearly completely in fluorescently-tagged platelets. SLM-A shows an overall reduction of fluorescence compared to the as-built AM sample, and SLM-B a further reduction, however neither approach the completely clear surface of the bar titanium.

Interestingly, on the additively manufactured sample, the underlying shape of the powder-based material surface can be seen through the fluorescence, with rounded features influencing the pattern of visible fluorescence to show waving patterns across the whole sample surface. With the average size of powder particles around 40µm, the propensity of platelets to stick to the sides of and crevasses between powder particles seen in Section 4.2.4 is again visible. Contrastingly, the EJM-polished samples show much larger spaces free of platelets, with areas surrounding them attracting platelet presence. These clear spaces cannot be explained by the powder material surface, as in the AM surface, given that the voids appear hundreds of microns wide – much larger than even the combined, partially melted powder particles.

In this case, it appears much more likely that this patterning of the surface is attributable to the EJM process itself. In Section 4.2.4 it was noted that some areas of EJM processing produced highly clear “tracks” which were surrounded by less smooth, platelet-attracting areas. It is likely that these images are confirming this lack of surface uniformity and showing the adhesion of platelets in the areas surrounding the successfully polished surface.

Overall, SLM-B, produced with two passes of the EJM nozzle over the surface, again has a reduced platelet fluorescence compared to SLM-A. Earlier work had suggested that the surface produced by two passes of EJM was smoother and had less residue than the SLM-A parameters, however it risked opening internal pores due to the depth of material removal. In the centre of the image showing SLM-B in Figure 39, one larger, bright spot can be seen

(identified as point A), which may be such a case of a large number of co-localised platelets inside a small hole or pore.

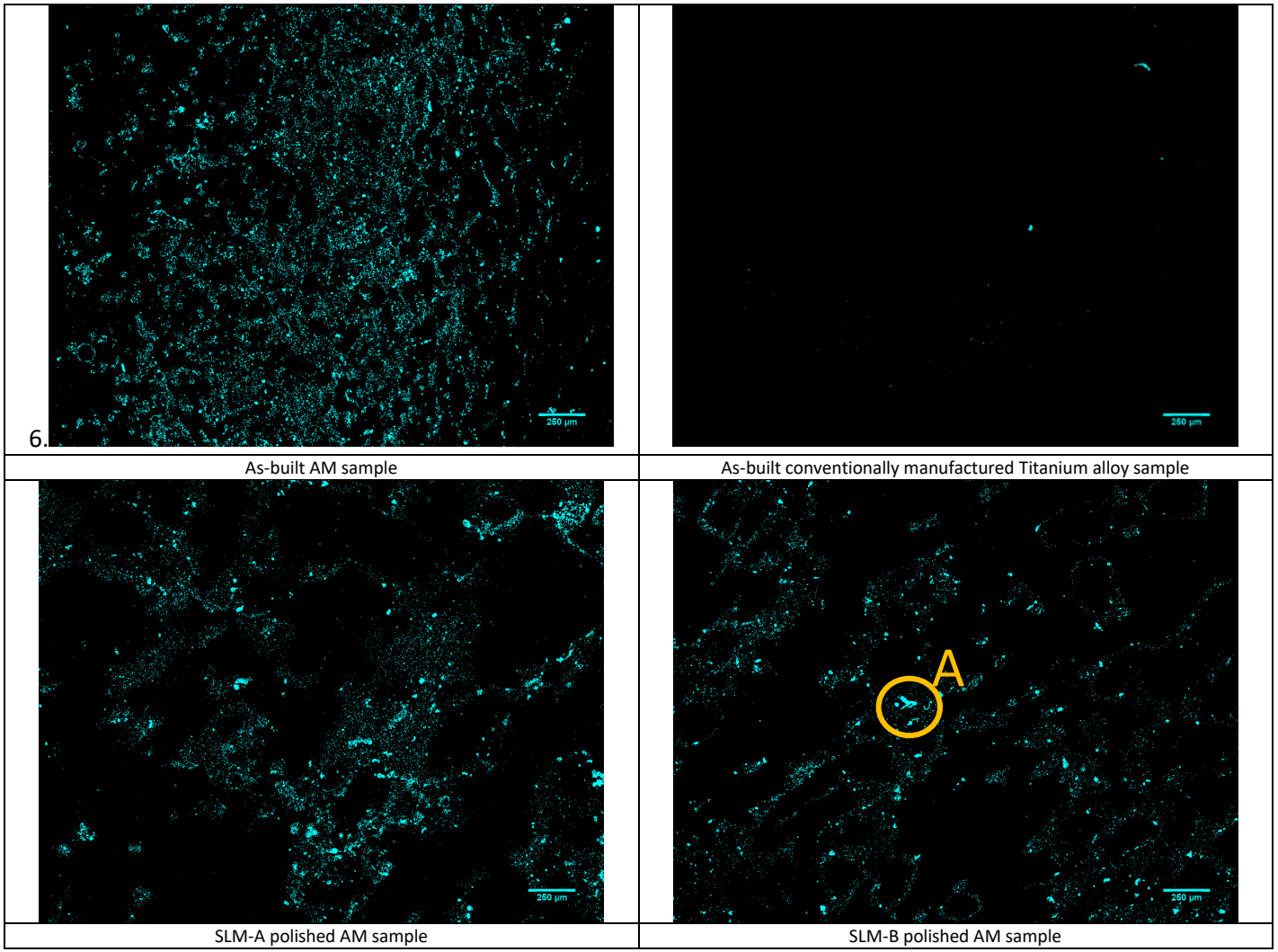

As-built AM sample | As-built conventionally manufactured Titanium alloy sample

SLM-A polished AM sample | SLM-B polished AM sample

Figure 39: Immunofluorescence images taken at 10x magnification on four samples of titanium alloy material following exposure to platelet solution and CD61-conjugated fluorescent antibodies showing a large increase in fluorescence on as-built AM surface (top left), reduced somewhat by polishing (bottom, left and right), and minimised the most in a conventionally manufactured material (top right). The polished samples (bottom) show patterning over the surface likely associated with the movement of the jet nozzle, compared to the whole-surface coating of fluorescence on the as-built surface. "A" shows a point of increased fluorescence, likely due to co-location of large numbers of platelets which may be a result of a pore in the material surface.

Particle analysis of the area of fluorescence across images again shows a dramatic change across the images taken, shown in Figure 40. The AM material was significantly more thrombogenic than all other samples ($p<0.01$). Otherwise, there was limited statistical difference in fluorescence between the bar titanium and two polishing parameters of EJM. However, despite the lack of statistical difference, SLM-B further reduced on average with comparison to SLM-A, again confirming that these parameters of EJM polishing would be preferable in reduction of platelet adhesion to the sample surface.

These results confirm the visual interpretations of Figure 39 and Section 4.3.3, showing that the as-built additively manufactured titanium alloy surface is highly activating towards platelets and would pose a significant thrombogenic risk *in vivo.* This risk is somewhat reduced by both methods of polishing, with SLM-B being most effective in reducing the number of platelets found on the material surface, but with SLM-A still providing a reduction in mean fluorescent surface area by nearly fourfold.

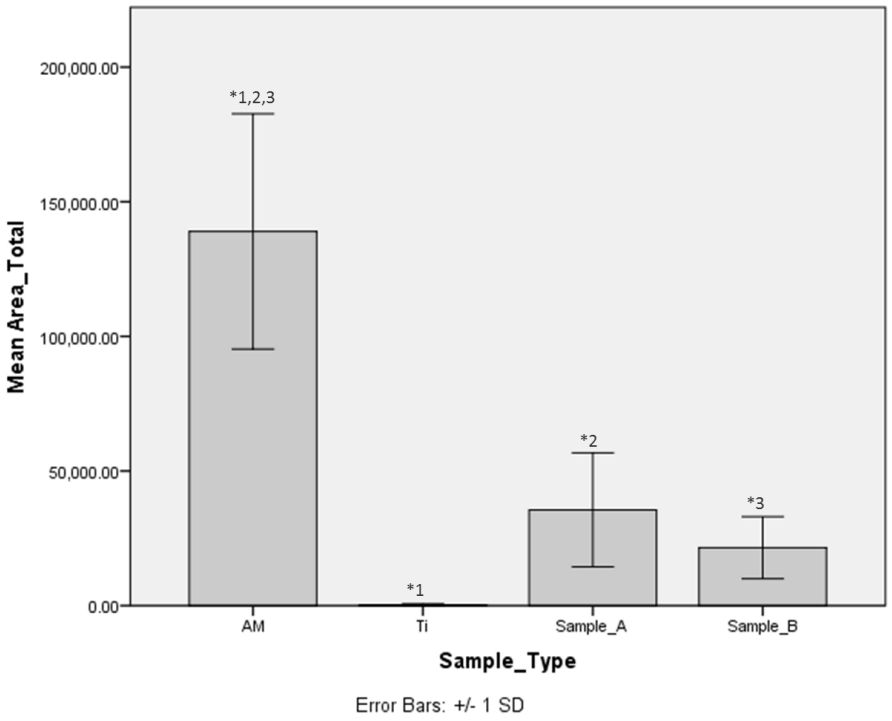

Figure 40: Mean area of fluorescence in pixels across 10 sample spaces on images taken of four titanium alloy surfaces. Statistical significance was calculated using ANOVA analysis and significance pairings at p<0.01 are numbered.

In addition to the total area of fluorescence, the mean number of individual fluorescent events visible per image were calculated and plotted in Figure 41. Again, the number of fluorescent areas was significantly lower ($p<0.01$) in the bar titanium alloy sample surface as well as both EJM-polished surfaces. In this case, however, SLM-A showed a significantly greater number of individual fluorescent particles than the bar titanium surface ($p<0.01$). SLM-B, however, was not significantly higher than the bar titanium sample despite the average number being higher, suggesting again that this polishing method is more successful in reducing the number of platelets found on the AM surfaces than SLM-A.

Whilst the number of individual fluorescent events is not indicative of the number of individual platelets found on the surface of these materials, it is important to note the agreement between the surface area (Figure 40) and the number of individual fluorescent areas (Figure 41). Agreement between these results suggests that the fluorescence is not being produced by background noise or sample contamination, but that the areas of fluorescence are appropriate measurements of individual, fluorescently-tagged material.

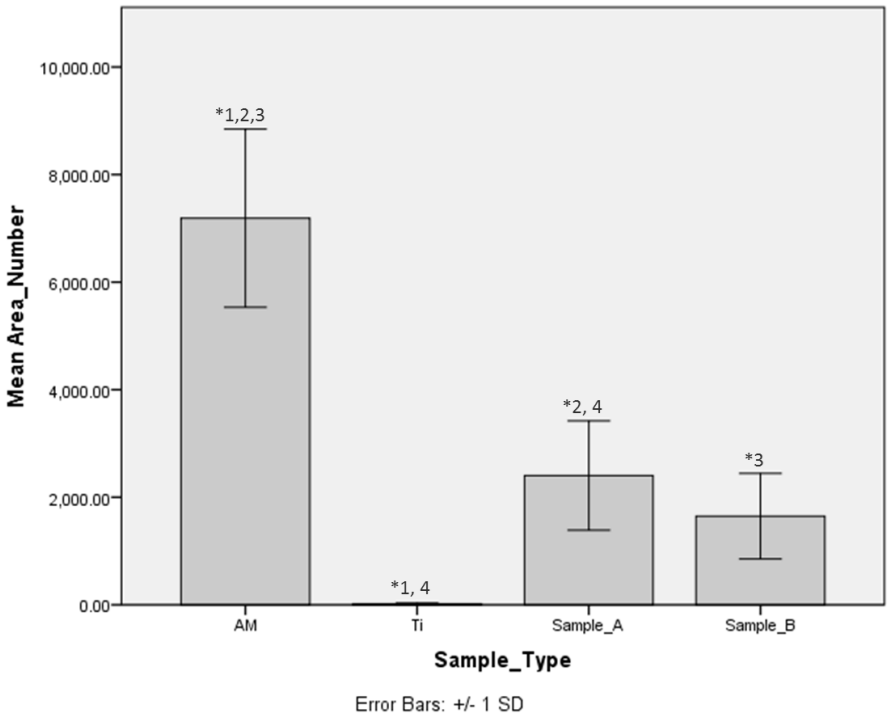

Figure 41: Mean number of fluorescent areas across 10 sample spaces on images taken of four titanium alloy surfaces. Statistical significance was calculated using ANOVA analysis and significance pairings at p<0.01 are numbered.

5.4 Conclusions

This chapter has explored the potential of the novel electrochemical jet machining method for prevention of coagulation on the surfaces of additively manufactured metal components. Annuloplasty rings are high-risk devices for the production of thromboemboli given their presence in direct contact with blood inside the heart. Therefore, prior to the adoption of AM for annuloplasty devices a method of ensuring minimal surface coagulation must be developed.

With these results it has been shown that:

- Flow cytometry is an insufficient method for comparing surface coagulation on AM components, owing to the lack of distinction between positive and negative controls. This is likely related to the inability of flow cytometry to assess platelets adhered to the surface itself.
- SEM and immunofluorescent imaging of sample surfaces give good visual indications of coagulation behaviour.
- EJM surface processing using chloride and bromide solutions showed sub-microscale roughness and no reduction in platelet activity on AM samples.
- EJM surface processing using chloride solution did reduce overall surface unevenness and reduced the coagulation activity on the surface of AM surfaces.
- Second passes of EJM polishing further improved this outcome.

6 Results III: Device integration

6.1 Introduction

In this chapter, the effect of Electrolyte Jet Machining on cell survivability on titanium alloy surfaces was investigated to improve beneficial cell growth on the surface of AM metal components. Annuloplasty devices rely on a layer of endothelial cells covering the surface of the device to provide long-term mechanical support and immune protection. As-built additively manufactured Ti6Al4V samples, and AM samples processed with two parameter sets of EJM were tested, in addition to a sheet Ti6Al4V used as a control.

The work presented in this chapter was undertaken as Master's level research, for which I provided background knowledge, work plans, analysis, and interpretation support. Experimental work was undertaken by Kunj Sachdeva at the University of Nottingham, and results are also presented in the thesis *"To Evaluate the Potentiality to Combine Additive Manufacturing (AM) Technique to Fabricate Customised Implants with Surface Functionalization using Electrolyte Jet Machining (EJM) for the Cardiovascular Application."*.

6.2 Sample production

Ti6Al4V disk samples were again produced successfully by SLM, according to the CAD files and parameters laid out in Section 3.4.1. For SLM-manufactured samples processed using EJM, only parameter sets C and D were repeated to produce samples SLM-C and SLM-D (see Chapter 3 for outline of processing parameters). In addition, untreated SLM samples as manufactured (SLM-AM) and sheet titanium alloy samples (Ti64-S) were again used for comparison of cell behaviour.

Surface chemistry of the samples was investigated using X-ray photoelectron spectroscopy (XPS), with a summary of results shown in Table 6.

Table 6: Results of XPS survey for atomic concentration on the surface of titanium alloy samples.

	Atomic Concentration of Element %					
	Carbon	**Titanium**	**Oxygen**	**Zinc**	**Copper**	**Vanadium**
SLM-AM	39.0	10.2	50.8			
Ti64-S		7.9	79.0	1.2	1.8	10.0
SLM-C	38.9	15.8	45.3			
SLM-D	37.1	16.1	46.7			

All of the samples contained a large proportion of Oxygen (1s) on the surface, indicative of the presence of a metal oxide layer forming over the titanium alloy. O1s peaks can also

overlap peaks created by some metals such as palladium or vanadium on XPS data, however a metal oxide surface is expected on Ti6Al4V material and vanadium is also expected to be present in the sample without causing issue, due to the alloy used (Thermo Scientific, 2013). The highest % of oxide presence was found in Ti64-S samples, with SLM-AM following and the processed SLM-C and SLM-D reduced further.

Carbon (1s) is present on the additively manufactured surfaces (SLM-AM, SLM-C and SLM-D), regardless of processing, which suggests carbon-carbon or carbon-oxygen binding. Most commonly, this is indicative of carbon contamination from exposure to atmosphere before scanning (Thermo Scientific, 2013). This agrees with previous studies and with the shallow depth at which XPS scans were taken, as (Vaithilingam *et al.*, 2016) found that all samples attracted adventitious carbon contamination, and that at greater depth of scanning, carbon content readily reduced to much lower levels. However, these studies did also show the presence of some Ti-C bonds which may also have been available on the samples studied here; this was attributed to manufacturing in an incompletely inert atmosphere during SLM processing, leading to the bonding of some titanium and carbon molecules inside the manufactured samples.

Following carbon and oxygen presence, the most common element on all samples was titanium (2p). The overwhelming majority of material should be titanium (>90% of Grade 5 Ti6Al4V), however owing to the limited depth of analysis provided by XPS this may have resulted in the higher carbon and oxygen readings. The titanium presence however was indicative of titanium oxide presence on the outer surface of all samples, again expected due to the readiness of titanium to form a “passive film” of titanium oxide in air (Jäger *et al.*, 2017).

Vanadium presence on Ti64-S was higher on the surface than in all the additively manufactured samples, which highlights potential for sample toxicity due to its higher concentrations. As stated above, some vanadium presence may be masked in other samples by the high Oxygen (1s) reading (Thermo Scientific, 2013). Aluminium, however, was not present in great enough concentrations to provide XPS readings in any given sample. This is somewhat surprising given the percentage presence of aluminium should be greater than vanadium in Grade 5 Titanium alloy (~6%Al vs ~4%V); however it is important to note that XPS scans are only representative of the outer surface elements and aluminium may have been more prevalent on lower layers of sampled material. In these studies, depth analyses were not undertaken; however previous studies have found differences in the

concentrations of elements at greater depths of study, with reduced vanadium on the surface compared to its internal concentrations (Vaithilingam *et al.*, 2016).

Similarly, there was a lack of vanadium presence on SLM-AM samples and a presence in conventionally manufactured samples (Ti64-S) in these studies, however mechanical polishing of the SLM-AM samples led to an increase in surface vanadium to detectable levels, with both studies therefore suggesting that while vanadium is extremely low in concentration at the surface of AM samples, it is likely still present within the bulk of the manufactured part (Vaithilingam *et al.*, 2016).

Other elements present on the surface included zinc and copper, most likely contaminants during manufacture or processing of Ti64-S. These are not expected alloys to be found within Ti6Al4V alloy, and therefore must have arisen from contamination or overlap with expected alloys on readout.

Importantly however, there was no evidence of sodium, bromide or chloride chemistry found on the surface of the EJM-processed additively manufactured samples (SLM-C and SLM-D). This indicates that residual solutes do not remain on the surface of samples which have been processed using EJM, even when taking into account the pitted surface left after processing. Whilst EJM had not previously been applied to SLM surfaces prior to this study, these pitted surfaces were previously highlighted as an opportunity for osteoblastic or other cell growth due to the high oxide concentration formed when compared against chloride solutions used on SLM-A and SLM-B (Speidel *et al.*, 2016). The consideration of residual halide ions on SLM surfaces had therefore not previously been highlighted and does add credence to the opportunity of EJM to provide surface finishing without risking the chemical benefits of Ti6Al4V surfaces.

6.3 Sample characterisation

6.3.1 Surface topography

The results of a surface topography analysis are shown in Table 7.

The roughness and peak-to-valley height of the SLM-AM sample is clearly much higher than Ti64-S. This is to be expected as additively manufactured parts are known to contain rough surfaces, owing to the powder base from which parts are fabricated. As fresh layers of powder are layered on top of one another, gaps can appear where particles do not spread completely evenly or are not fully melted, producing an uneven surface. The roughness of SLM-C was reduced compared to the SLM-AM; however, it was still higher than the sheet material. Contrastingly, the second pass of electrolyte jet machining used on SLM-D resulted in a higher overall surface roughness than any other treatment.

Whilst Ti64-S was significantly more smooth and regular overall compared to the other samples included in this study, it did still include some small features due to manufacturing defects or contact with other items since manufacture – including scratches and dents in the surface of the samples. However, this is not anywhere near as common as the features found on any of the other samples which are visibly more frequent and larger than those on Ti64-S, as discussed above (and shown in Chapter 5). The SEM images shown in Figure 42 visualise this comparison.

Although the average surface roughness shows an overall trend of high to low roughness in the order *SLM-D, SLM-AM, SLM-C, Ti64-S;* the difference between the greatest peak and valley provide further information on the actual topography of the surface. The Sz value of the samples provides an alternative order of *SLM-AM, SLM-D, SLM-C, Ti64-S.* In this order, it appears that EJM processing on SLM-D has somewhat reduced the greatest variation in topography on AM samples, however SLM-C remains more reduced and Ti64-S is still the least uneven. Whilst it is expected that Ti64-S presents the least variable surface, it is surprising that SLM-D has a reduced Sz compared to SLM-C. The additional second pass of electrolyte machining used SLM-D had previously produced a more even surface with parameter set B than set A (see Chapter 5), however in this case the second pass appears to have not maintained this reduction. It is possible, however, that large existing peaks or valleys produced by SLM manufacturing, were uncovered by the processing – this was seen previously in the opening of internal voids to the surface when two passes of EJM were applied in Chapter 5 (Figure 34).

Figure 42 illustrates in greater visual detail the differences in surface features found between these samples. The Ti64-S sample (top right) showed small, infrequent features including scratches as shown in the figure. These are defects of the surface and may be attributable to either minor manufacturing issues or, more likely, handling. SLM-AM samples (top left) show significantly uneven surfaces with clearly visible round features produced by unmelted powder material. After EJM processing (bottom), these round features are significantly less clear and have been replaced by a more evenly spread, finer roughness which covers the whole visible surface of the sample. Some spheroid-like shapes can be seen amongst the unevenness in SLM-C (bottom left), however this is almost entirely removed with the application of a second EJM pass for SLM-D (bottom right).

Table 7: Surface roughness and associated measurements of the Ti6Al4V samples. All measurements in µm.

Sample	Average Surface Roughness (Sa)	Peak to valley height (Sz)	Depth of deepest valley (sv)	Height of highest peak (sp)	Root mean square height (sq)	Skewness of height distribution n (ssk)	Kurtosis (Sku)
Ti64-S	1.27	7.62	7.64	4.30	1.67	-1.04	4.51
SLM-AM	10.74	52.89	33.49	41.52	13.58	0.33	2.80
SLM-C	4.80	30.06	28.34	25.26	6.19	-0.17	3.60
SLM-D	13.85	51.21	54.90	30.99	17.13	-0.76	2.80

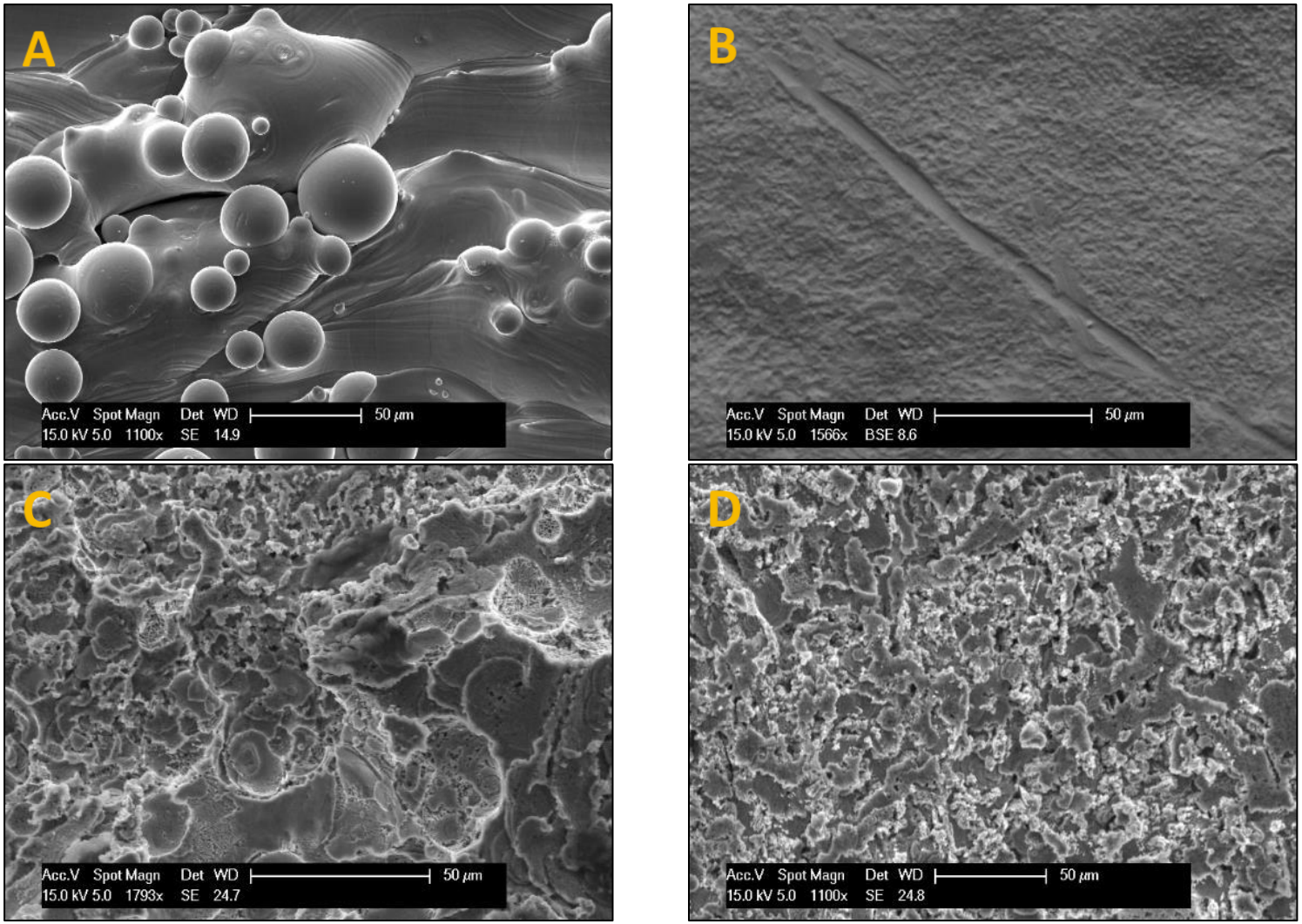

Figure 42: SEM images of the surfaces of Ti6Al4V samples. Left to right: (A) SLM-AM, (B) Ti64-S, (C) SLM-C, (D) SLM-D.

6.3.2 Surface wettability

All the samples except Ti64-S exhibited hydrophobic behaviour (contact angle greater than 90°), with the static contact angles shown in Table 8 and visual comparisons of water droplets shown in Figure 43. The contact angle of Ti64-S and both EJM-processed samples SLM-C and SLM-D remained relatively constant after initial droplet contact. However, in addition to showing overall hydrophilic surface behaviour, SLM-AM samples showed variation over time and between different areas on the sample surface. This would be expected given the unpredictable nature of the SLM surfaces, varying dependent on the amount of unmelted powder present on the external surfaces and the exact packing of the Ti6Al4V powder on the SLM substrate bed. Whereas the Ti64-S samples were mostly uniform with some minor features, the surface area of various points across an SLM-manufactured sample will change according to those variables discussed above.

Regardless, across all sample sites the SLM-AM surface remained hydrophilic in all measurements, and in fact the contact angle reduced over time with AM samples, suggesting greater hydrophilicity than that initially recorded.

Table 8: Average static contact angle of wettability tests on titanium alloy samples

Sample	**Average contact angle (°)**
Ti-64S	104.48
SLM-AM	74.96
SLM-C	114.70
SLM-D	113.65

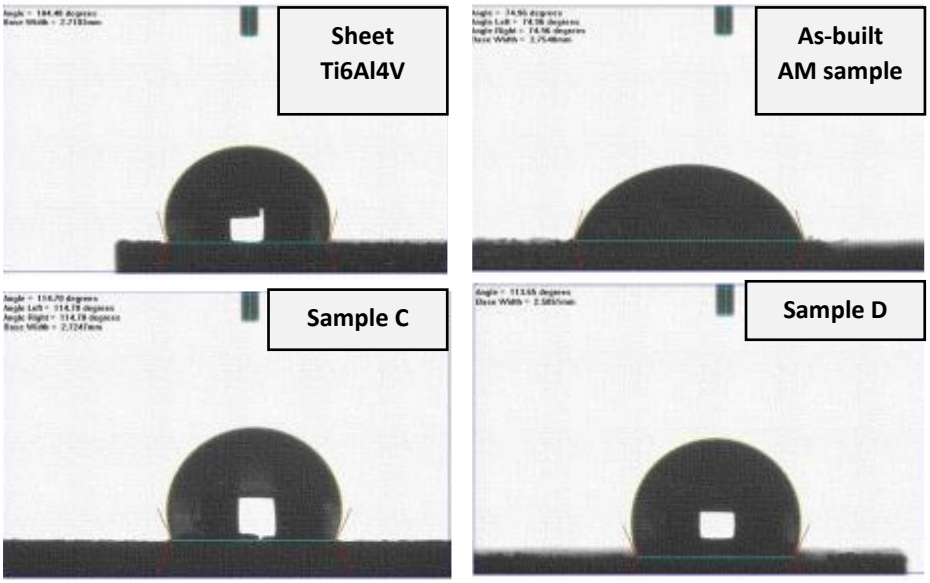

Figure 43: Images taken of static contact angle during wettability testing of titanium alloy samples

Given that hydrophilicity is associated with an increase in cell spreading, attachment and proliferation, these results suggest that the SLM-AM surface will be best suited to cell growth

(Drelich *et al.*, 2011). Following the SLM-AM surface, it would be expected that the Ti64-S surface would be next most successful, with the EJM-processed samples being the most hydrophobic and thus the least appropriate surfaces for cell growth.

6.4 Cell proliferation

As expected, alamar blue assays of cell metabolic activity shown in Figure 44 and Figure 45 showed that SLM-AM samples encourage more growth and activity of the 3T3 cells seeded to the surface. There was no significant difference (statistical test shown in Table 9) in cell activity between the SLM-AM surface and a standard tissue culture plastic, suggesting that the surface is equally at good at encouraging cell growth as the current standard for cell growth in a lab setting. This remained similar across both the 2- and 24-hour time periods, although a wider range in activity was found at the 2-hour period of cell growth on SLM-AM surfaces.

Ti64-S samples were found to have low cellular activity within 2 hours of seeding, with further decrease after 24 hours relative to both 2 hours and the other samples. This suggests that suggesting that growth and integration is low in early stages on Ti64-S surfaces, and even less successful over longer periods of time.

Both EJM-processed samples showed a slight reduction in 2-hour cellular activity, however not a statistically significant reduction when compare to the SLM-AM samples. They were further reduced when compared to culture plate activity, however still significantly more active than cells on Ti64-S.

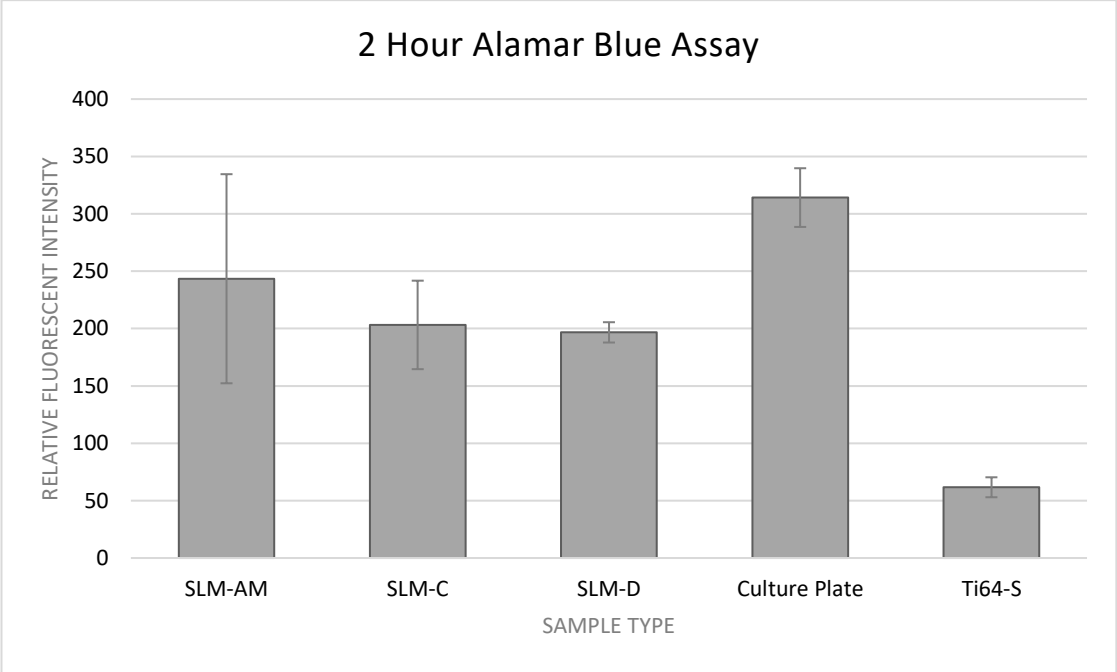

Figure 44: Relative absorptivity of samples in Alamar Blue assay after incubation for 2 hours as an indicator of cell activity.

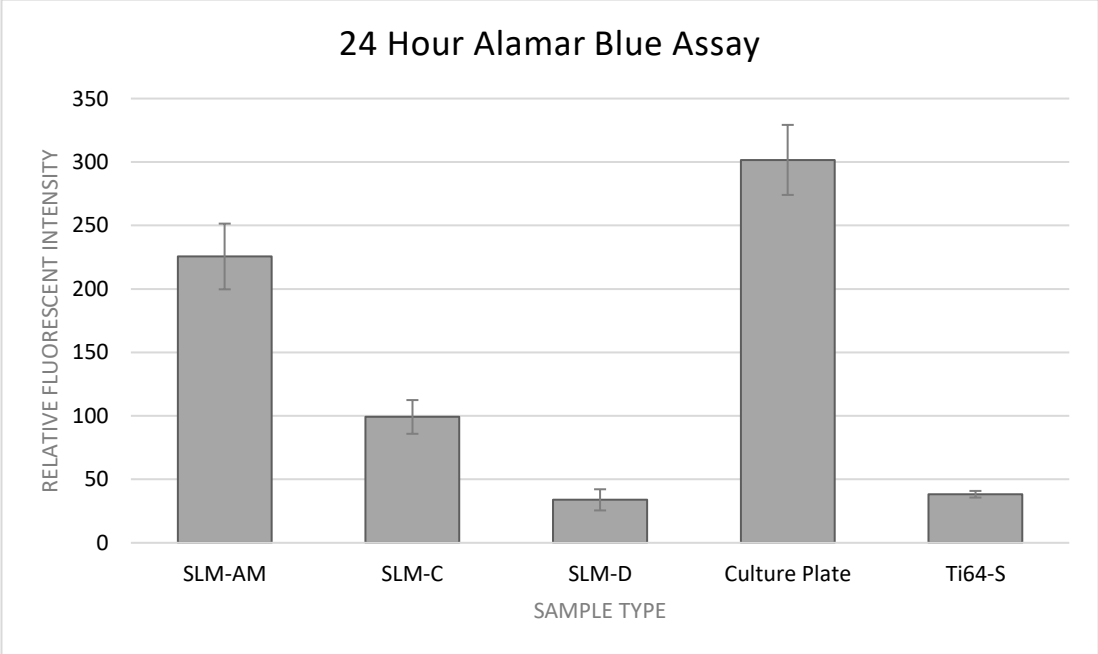

Figure 45: Relative absorptivity of samples in Alamar Blue assay after 24 hours incubation as an indicator of cell activity.

Table 9: Post-hoc Tukey test results for ANOVA analysis of 2 hour and 24-hour Alamar Blue readings. Statistical significance at p<0.05 is indicated with an underlined value, and statistical significance at p<0.001 is indicated with an asterisk in addition.*

Sample Pairing	**P value 2 hours**	**P value 24 hours**
SLM-AM + SLM-C	0.539	0.001*
SLM-AM + SLM-D	0.396	0.001*
SLM-AM + Culture Plate	0.015	0.001*
SLM-AM + Ti64-S	0.001*	0.001*
SLM-C + SLM-D	0.900	0.001*
SLM-C + Culture Plate	0.001*	0.001*
SLM-C + Ti64-S	0.001*	0.001*
SLM-D + Culture Plate	0.001*	0.001*
SLM-D + Ti64-S	0.001*	0.900
Culture Plate + Ti64-S	0.001*	0.001*

However, both EJM polished samples SLM-C and SLM-D showed low cell proliferation over time. Whilst the 2-hour growth was not significantly different between samples or against the control sample, the 24-hour time point shows a significant decrease in cell activity compared to controls and earlier cell proliferation on the same surface.

Both the SLM-AM samples and culture plates maintained high, and similar, cell activity and survivability. The Ti64-S samples had reduced further in cell activity compared to other samples tested after 24 hours.

These results suggest that the inclusion of EJM modified surfaces (SLM-C and SLM-D) significantly reduced the biocompatibility compared to the SLM-AM samples with regards to the specific 3T3 cell line used. Whilst the initial activity at 2 hours was greater in SLM-C and SLM-D samples than Ti64-S, after 24 hours the activity had significantly reduced and the cell activity was roughly equal to or less than the Ti64-S samples, and significantly less so than SLM-AM samples. This is somewhat surprising given that previous studies have shown reasonable survivability of cells on post-EJM treated titanium alloy surfaces (Mitchell-Smith *et al.*, 2018). However, these previous studies only included the sodium-based electrolyte solutions, not the sodium and bromine solution applied to samples SLM-C and SLM-D. The difference in surface response between the inclusion and exclusion of bromine may be responsible for these varying cellular responses, given the difference in topography found in Chapter 5 between SLM-A/SLM-B and SLM-C/SLM-D. These studies also focussed on much longer term survivability, up to 21 days; whilst we only studied early stage attachment and

proliferation, some long-term likely outcomes can be predicted in that if cells are completely non-viable within 24 hours, they will not likely survive to 21 days (Mitchell-Smith *et al.*, 2018).

6.5 Cell morphology

At the same time points as the alamar blue assays (2- and 24-hours post-seeding), SEM images were taken of the surfaces of samples with cells growing on them. A comparison of the SLM-AM and Ti64-S sample morphologies is shown in Figure 46.

The cells growing on the Ti64-S surface appeared primarily flat in morphology and loosely attached to the surface of the samples. By comparison, the SLM-AM samples provided multipolar morphologies, with the beginning of cell bridges and filopodia forming between growing cells, suggesting more meaningful adhesion indicative of cell survivability. The cells growing on the EJM-processed sample surfaces (SLM-C and SLM-D) were extremely challenging to identify against the exigent surface for imaging (see Chapter 5).

On the surface of SLM-AM samples, cells were strongly attracted to the sides of powder particles and the crevasses found between them. The space in between spherical powder particles provided areas for the formation of cell bridges and orientation of the cells towards one another. Where spaces were available on the Ti64-S samples, such as through defects or scratches, these same behaviours are observed: cells form extrusions across the gaps and ridges in the surface to attach to one another.

SLM-AM Sample | **Ti64-S Sample**

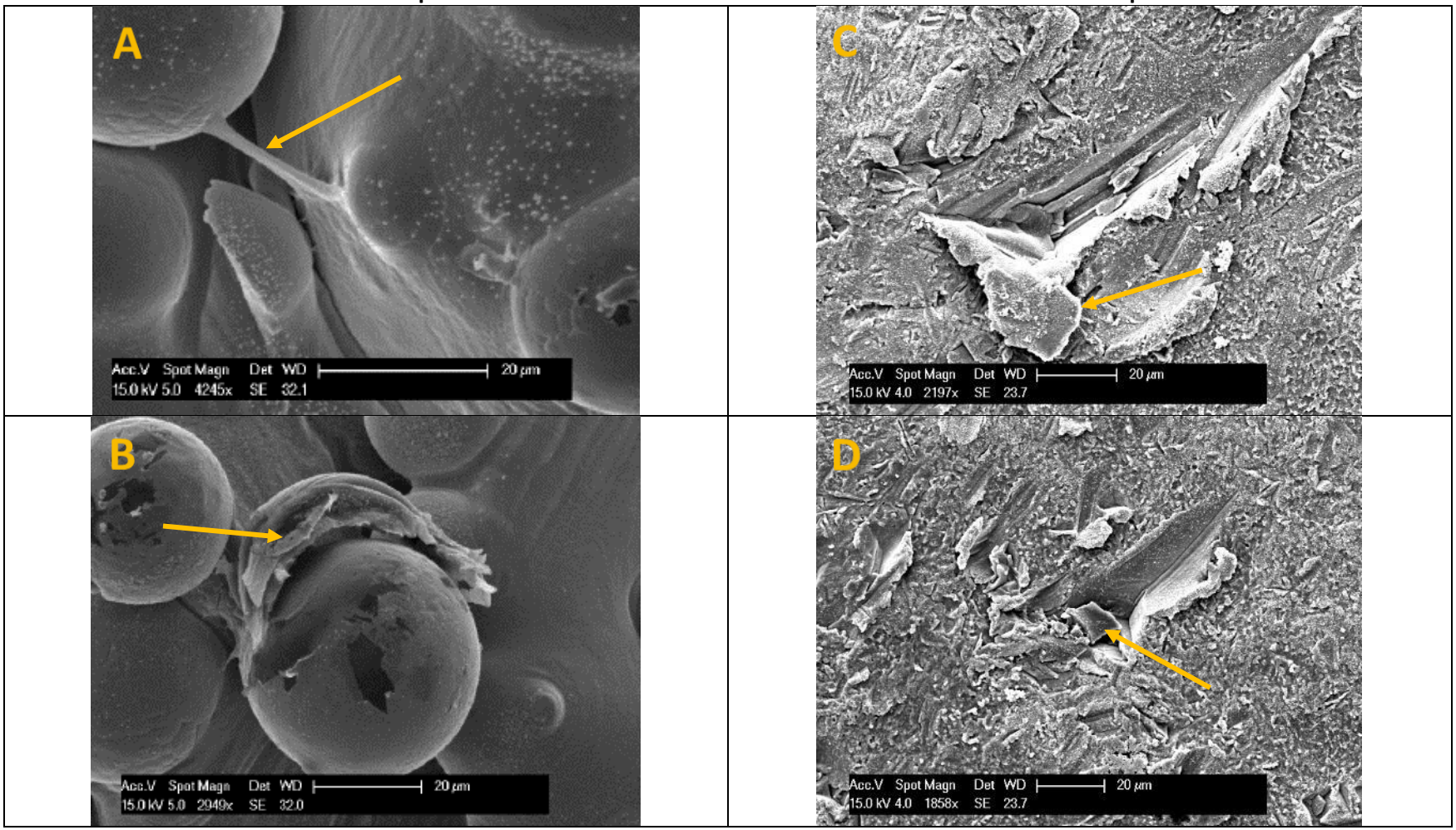

Figure 46: Comparison of cell morphology and adhesion to SLM-AM and Ti64-S samples at 24 hours post-seeding. Cells of interest are highlighted with yellow arrows. In SLM-AM samples, cellular extrusions are visible (A), and the round shape of cells is also seen adhering and aligning to unmelted powder particles (B). By comparison, cells on Ti64-S are flatter, without protrusions adhering to surfaces (C), but do still show a tendency to rest in available crevices (D).

After 24 hours the filopodia of cells on the SLM-AM surfaces became more obvious, agreeing with the alamar blue study results of a continued cell proliferation and an ability to thrive on the surface of these samples. Contrastingly, cells seeded on the Ti64-S samples had lifted from the surface and cell survival and activity had reduced. This again is consistent with the results shown in section 5.4.3, where a slight reduction in cell activity was seen on the conventionally manufactured Ti64-S surface between 2 hours and 24 hours.

The EJM-treated samples SLM-C and SLM-D proved difficult to image and identify cells on, as was found previously in Chapter 5, due to the high number of small features on the sample surface (Figure 47).

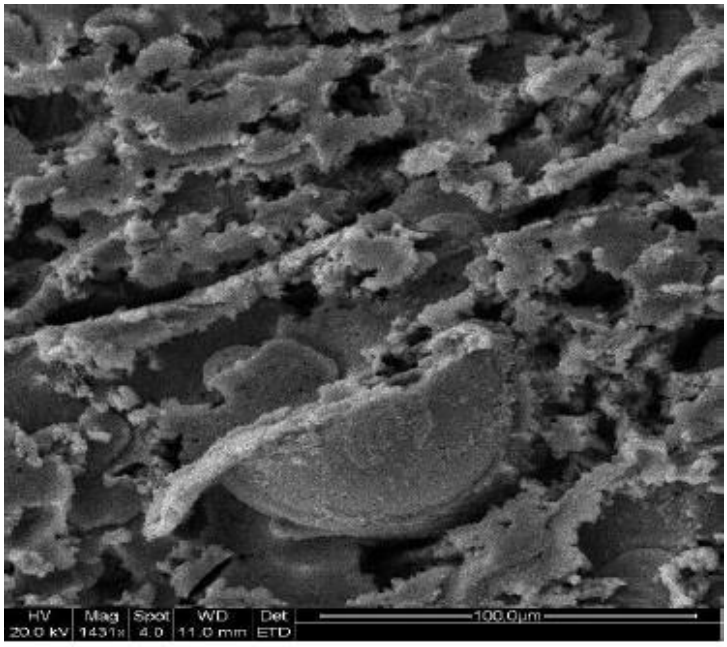

Figure 47: Unclear imaging of SLM-C after cell seeding. Cells are not clearly differentiated from sample surface for investigation.

In spite of the difficulty in imaging the EJM-processed samples SLM-C and SLM-D, some evidence was found of cells shearing away from the sample surface over time, shown in Figure 48. Other cells which could be identified were of an unclear morphology, without obvious extrusions from the cell body. Again, this agrees with the results of the alamar blue assay showing low survivability in the short term, which further reduced in the longer-term 24-hour period. All of these suggest an unviable and growth-averse phenotype, again signifying that the EJM-processed AM surfaces of SLM-C and SLM-D are not sufficiently biocompatible to encourage cell growth on the surface.

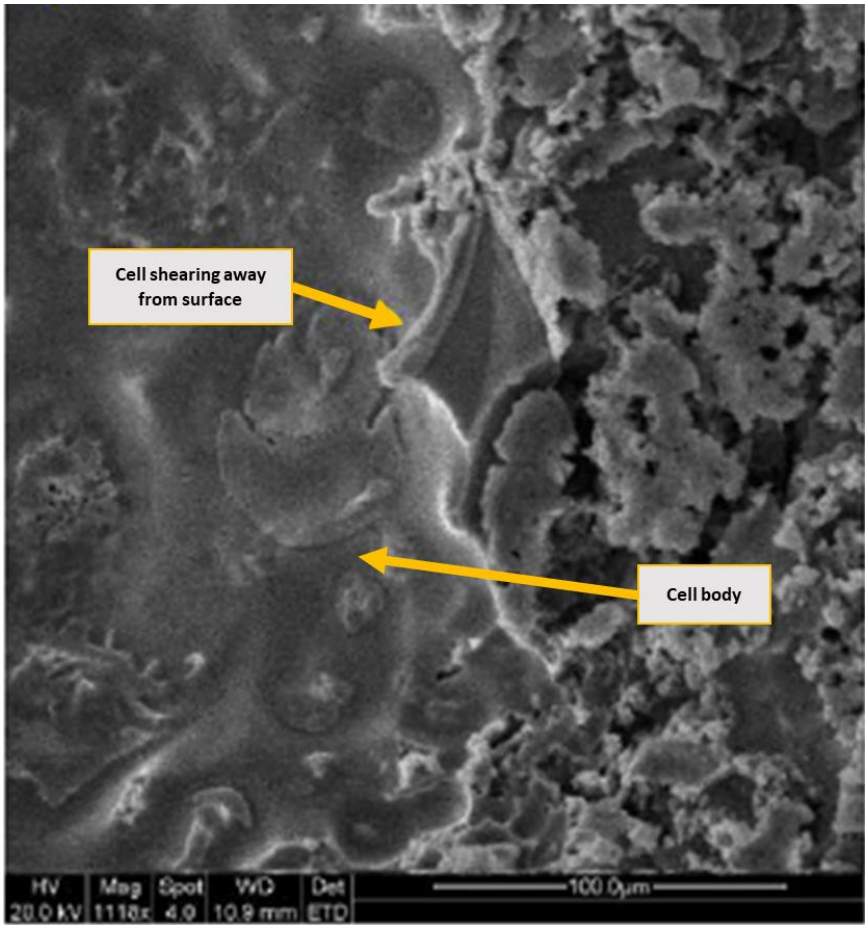

Figure 48: Image of cell adhered to SLM-C surface. The cell is seen detaching and shearing away from the material surface, indicating poor long-term survivability on this surface.

6.6 Conclusions

The results presented in this chapter have shown:

- Conventionally manufactured (Ti64-S) and EJM-processed (SLM-C and SLM-D) Ti6Al4V surfaces exhibited hydrophobic behaviour whilst as-built AM samples (SLM-AM) had hydrophilic surfaces, which are better suited to the promotion of cell survival and proliferation.
- Additively manufactured Ti6Al4V surfaces (SLM-AM) show improved cell activity and survival in both the short term (2 hours) and long term (24 hours) compared to conventionally manufactured sheet Ti6Al4V (Ti64-S) surfaces.
- EJM-treated surfaces (SLM-C and SLM-D) showed improved cell activity and survival at both time points compared against conventionally manufactured (Ti64-S) samples, however, they showed reduced cell activity compared to as-built AM surfaces.
- Cell morphology was highly influenced by the surface topography:
    - Conventionally manufactured surfaces (Ti64-S) permitted cell growth but led to flat morphologies without major adhesion extrusions
    - Additively manufactured surfaces (SLM-AM) promoted round and multipolar cell phenotypes with large numbers of filopodia extrusions
    - EJM-processed surfaces (SLM-C and SLM-D) again proved too unpredictable to image, as highlighted in Chapter 5, however cells appeared poorly adhered to surfaces and shearing away, suggesting low survivability phenotypes.

7 Discussion

7.1 Overview

The results presented in Chapters 4 through 6 of this thesis constitute a foundation of research for the production of bespoke annuloplasty devices using SLM additive manufacturing technology. Whilst additive manufacturing, and particularly powder bed fusion, techniques are becoming popular for investigation in medical applications from preoperative planning through to long-term implantable devices, significant work remains particularly relating to design workflows and post-processing.

Several bodies of work have attempted the provision of bespoke mitral annuloplasty devices, however all are limited in different areas with little cross-over of developments. (Díaz Lantada *et al.*, 2010) and (Owais *et al.*, 2014) were both successful in producing CAD files representative of a patient's mitral annulus, however manufactured samples only in non-biocompatible materials with desktop-range FDM systems, rendering them unusable in clinical settings. By comparison, the work presented in this thesis involved manufacturing in Ti6Al4V titanium alloy using SLM, providing a clearer route to biocompatibility and in vivo testing.

(Sündermann *et al.*, 2013) and (Graser *et al.*, 2013) furthered this work by manufacturing rings in Ti6Al4V titanium alloy using powder bed fusion methods, however the workflows of device design were challenging and relied on bespoke software coded by the research group or manual isolation of the mitral valve in a three-dimensional CT scan. Whilst these could more surgically relevant, it is questionable as to whether there is significant value in such a complex method of design which would require specialised skill sets in hospitals and could raise the cost of manufacturing devices. Comparatively, Chapter 4 of this work showed the use of ultrasound scans and showed good repeatability between designs, suggesting that ultrasound could be an appropriate replacement for CT scans with reduced risk to patients.

In addition, neither of the authors sought to assess the biocompatibility of the devices and thus suitability for surgical implantation. (Graser *et al.*, 2013) did not implant the devices at all, simply noting the successful build and the potential for Ti6Al4V biocompatibility in this application. (Sündermann *et al.*, 2013) did implant the devices into pig models, however no human tissue trials were undertaken, and the pigs were anaesthetised immediately after surgical implantation, providing no insight into the survivability or success of the implanted devices beyond geometry. Chapters 5 and 6 of this thesis show early *in vitro* investigations

into biocompatibility, laying groundwork for further testing and progression into *in vivo* studies.

The surface finishing of implantable medical devices manufactured using SLM is already a significant body of work, however limited studies on novel techniques are available and even conventional surface finishing techniques such as machining or mechanical polishing have been shown to behave differently on SLM-manufactured material (Shunmugavel *et al.*, 2017). In particular, a limitation for medical devices is that many existing techniques involve mass material removal or finishing to a single standard across a component, where selective patterning of the device could be beneficial to its biocompatibility. Chapter 5 addressed the use of a novel, selective polishing method for AM titanium and its application in these biological settings, showing some promise in the control of surface coagulation risk.

Similarly, augmenting the biocompatibility of inorganic materials through either surface finishing or functionalisation is a wide field of research with a range of opportunities available to novel devices. In the field of AM medical devices, however, most work has focussed on osteoblastic proliferation by virtue of most research focussing on skeletal implants (Rotaru *et al.*, 2015; Kwon and Park, 2018; Dall'Ava *et al.*, 2019; Lerebours *et al.*, 2019). Chapter 6 discussed the lack of response shown with EJM finishing for textured titanium alloy surfaces with the application of fibroblastic cells. Historical work has found that surface topography, scaffold size, and other material properties of medical parts can influence differentiation and proliferation of cells according to their tissue niche, suggesting that soft tissue (in this case cardiovascular) cells may require their own investigations to provide the most beneficial device characteristics for success (Murphy and O'Brien, 2011; Zareidoost *et al.*, 2012).

A summary of an expected future patient pathway involving bespoke annuloplasty devices, informed by work presented in this thesis, is shown in Figure 49. The contributions of Chapters 4, 5 and 6 are considered in line with the stage of design that this would be applicable to in clinical practice, including suggestions of further necessary work which is considered in greater depth in Section 8.2.

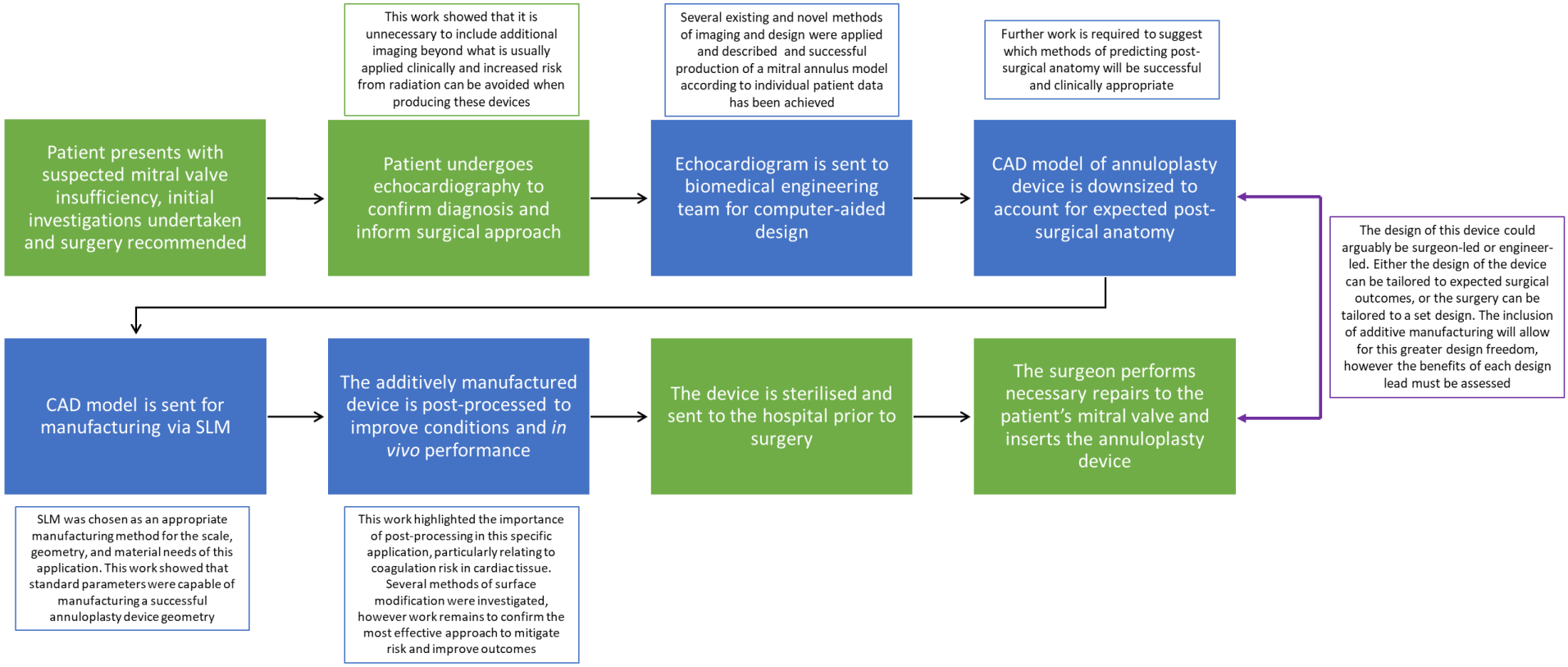

Figure 49: A flow chart exhibiting the patient pathway from symptomatic disease to surgery, with design considerations for the annuloplasty device highlighted. Boxes in green represent existing portions of the pathway; blue boxes represent novel portions of the device creation and application investigated for this work, and specific to additively manufactured devices.

7.2 Design of bespoke annuloplasty devices

The work presented in Chapter 4 introduced the challenges and potential avenues for design of a bespoke cardiovascular device. The initial challenge of cardiovascular device design lies in the nature of the heart itself as an organ: access to clear imaging of an organ within the chest is limited, and isolation of single areas of soft tissues is challenging. Following this, the state of a heart preoperatively is by its nature not the intended outcome of surgical intervention, and therefore methods for design of devices for healthy anatomy must be developed.

With regards to gaining internal imaging of the heart structures, ultrasound presents a promising choice of imaging modality, primarily as it is the current gold standard of imaging valve disease before, during and after surgery (Mahmood *et al.*, 2013). In this work (See Chapter 4), ultrasound scans were found to be sufficient for visualisation of the mitral annulus and design from it. Results of re-designing devices from the same scan showed minimal variation of ring dimensions between two designs, with <0.5mm variance in height, length, and circumference between the two files.

In progressing medical interventions, it is important to weigh the benefits, risks, and comfort of patients at all stages. Particularly when introducing novel technologies, it may be considered necessary to include extra stages in the treatment plan, such as further scans or longer surgeries. In this case it must be considered whether the inclusion of more interventions is outweighed by the benefit of the newer technologies over existing treatment plans. The employment of ultrasound as the primary imaging modality in design of bespoke cardiac devices prevents these further intrusions and provides familiarity in the patient pathway to clinicians and patients alike.

Further importance in this case should also be given to the avoidance of unnecessary radiation exposure in these novel treatments. Several studies have employed CT scans to produce higher resolution images of cardiac structures when investigating bespoke cardiovascular device design (Díaz Lantada *et al.*, 2010; Sündermann *et al.*, 2013). Whilst a CT scan may provide a still and clear image of the heart inside the chest and could prove less reliant on operator experience, it cannot be avoided that this represents the exposure of patients to x-ray radiation in a way that is not currently necessary. This is a particularly important consideration given that studies have found that both CT and ultrasound

modalities equally can fail to pick up fine features such as the chordae tendinae and papillary muscles (Birbara, Otton and Pather, 2019).

Previous studies related to measurement and prediction of the mitral annulus have also been successfully undertaken using ultrasound data (Cooray *et al.*, 2009; Ender *et al.*, 2011). A further study has also succeeded in additively manufacturing a full polymer replica of the entire mitral valve structure using ultrasound scans, although the authors note limitations in the lack of data available on leaflet thickness, which resulted in assumptions being drawn and manual editing of the file produced (Mahmood *et al.*, 2015).

The work of this thesis has shown that it is possible, using an ultrasound scan, to employ commercially available software in the design of personalised annuloplasty designs. Previous work using bespoke software had shown promise in the marking of leaflet insertion points to provide location information on the mitral annulus, however the accessibility of this semi-automated software was of concern (Graser *et al.*, 2013, 2014). Introducing novel, complex software which requires coding knowledge and significant learning is not preferable in a clinical setting. Whilst some localities are introducing specialist Biomedical Engineering roles in the design of AM implants, it would likely be more acceptable to hospitals to give simple and accessible software to existing, trained clinicians. (Owais *et al.*, 2014) showed reasonable success in producing an additively manufactured model of the mitral annulus using commercially available echocardiographic software (TomTec ImageArena®), similarly tracking points along the annulus at the level of valve leaflet insertion.

As a result, a similar method to that described in (Graser *et al.*, 2013) was produced using Materialise Mimics and 3-Matic software, which is available commercially to research institutions and clinical users alike. Materialise Mimics software has traditionally been used in the semi-automatic segmentation of hard skeletal tissues, including long bone and facial reconstruction surgeries, and frequently employed in hip replacement revision surgeries (Rotaru *et al.*, 2015; Lu *et al.*, 2018). However, it has also been used in a previous study investigating the production of models by additive manufacturing for preoperative planning of cardiovascular surgeries (Jacobs *et al.*, 2008).

The method using Materialise Mimics software outlined in Section 3.3.4 of this thesis was successful in replicating an appropriate annular anatomy from a single patient ultrasound (shown in Figures 10 and 11), however it has not yet been compared to patient anatomy or an implanted device. Future validation of this method should include comparison of dimensions of the additively manufactured device against the device used in surgery for that

patient, or in vivo physical comparison of the AM device against the patient's heart in surgery.

Following the acquisition of patient scan data and design of device according to those parameters, next, a method to produce a device appropriate to the size and shape of the mitral valve *after* reconstructive surgery is complete should be developed. Even the concept of pre-surgical sizing for *commercially available* annuloplasty devices remains controversial, wherein a number of potential avenues have previously been investigated for the prediction of sizing choice. Options including leaflet height (Lecuyer *et al.*, 2011), intertrigonal distance (Cooray *et al.*, 2009), and full virtual superimposition of CAD files (Ender *et al.*, 2011) have all been attempted to predict the requirements of patients' valves before surgery begins. If any of these methods proved sufficiently sensitive and accurate, it could be posed that preoperative measurements be used for geometrical design of annuloplasty devices. However, given that even manual intra-operative methods of annuloplasty sizing remain controversial, it may be a steep challenge to provide a simple, single method of predictive design which doesn't involve full valve modelling (Bothe, Miller and Doenst, 2013).

Whilst devices that are designed around an entire population may provide an acceptable repair to the majority of individuals, it can risk a minority of patients' surgeries when their anatomy varies from the average. Outside of this average also, some patients may be rejected for surgery or switched to valve replacement instead of repair, if an appropriate device cannot be found. Given that poor choice of annuloplasty device can lead to mid-term or long-term failure of mitral repairs (Anyanwu and Adams, 2009), ensuring appropriate fit of the device is of great importance.

In addition, whilst the pool of devices available to clinicians in mitral valve surgery is widening, it appears that they are not being used to their full potential. As manufacturers produce annuloplasty devices with a range of material properties, shapes and applications, the market appears to be too large for surgeons and hospitals to properly introduce each of these to the patients who need them. Were, for example, a hospital to hold stock of every possible annuloplasty device in every size to allow complete and free choice by the surgeon of which was most appropriate, the majority of stock would likely become unusable before the appropriate patient was admitted. This issue has previously been highlighted in the presence of "surgeon's preference" being the primary leading attribute towards the device decision making (Wan *et al.*, 2015).

By production of individual devices on-demand according to the patient admitted, this issue can be avoided whilst still allowing for variation between devices to provide the best repair to each patient. In future, provision of bespoke mitral annuloplasty devices therefore could present an improvement in current treatment plans, both in terms of supply chain and manufacturing needs, and patient experience and outcome.

As a simple method of surgical prediction, the ratio of mitral annular dimensions is an attractive option. The human mitral annulus is commonly referred to as having a 3:4 planar ratio in its dimensions, and as a result several commercially available devices adhere to this ratio in their design (Raffoul *et al.*, 1998; Carpentier, Adams and Filsoufi, 2010). If this were the case, the prediction of shape could be achieved by measuring the reasonably constant transverse width (held in place more strongly by more structural tissues found in the intertrigonal space) and calculating the anteroposterior dimensions required.

The studies discussed in this thesis showed that current assumptions of mitral annular shape and size leading the design of existing devices on the market appear to hold true for a general population, but do not account for individual variation in patients' anatomy. Significant variation was found around the average, up to almost two commercial sizes' difference (Figure 14). As discussed above, these misfits can lead to failure of repair and need for further surgical intervention (Flameng, Herijgers and Bogaerts, 2003; Anyanwu and Adams, 2009; Petrus *et al.*, 2019). Therefore, the employment of this ratio assumption would not be sufficient to provide an improved accuracy of device design compared to existing commercial devices. Further investigation will now be required into other methods of predicting the healthy valve pre-operatively.

One potential area for investigation would be the application of the cardiac cycle and constant movement of the heart, which may be of benefit to surgical prediction. Throughout the cycle, the valve annulus moves along with the heart tissue. As systole occurs and the valve shuts, the annulus moves along with the leaflets and encourages the shutting of the valve to prevent backflow. If the movement of a patient's annulus were tracked throughout the cardiac cycle, an extrapolation and prediction of the shape necessary to shut the valve completely could be made from the existing shape of the annulus during systole.

In practice, it may be simpler rather than relying on prediction, to model the repair surgery itself and dictate surgeons' actions to ensure that the entire surgery is planned to an individual patient and will conclude with a device that fits perfectly to the final valve anatomy. Such modelling could include analysis of the stresses placed on the heart tissue

and the annuloplasty device itself, providing information on where sutures are best placed to ensure equal distribution of the forces around the new device and reduce the risk of dehiscence.

7.3 Prevention of detrimental surface coagulation

The risk of implanting a new medical device in human patients is always significant, and even more so when new and untested processes or mechanisms are involved. In Canada, the UK and the USA, the altering of manufacturing method – regardless of material use prior – requires complete revalidation of an implantable device(Health Canada, 2011). Thus, it is appropriate that the impact of variations between traditionally and additively manufactured should be thoroughly investigated. In Chapter 5, the novel Electrolyte Jet Machining (EJM) process was employed to reduce the surface unevenness found on SLM-manufactured titanium alloy components and mitigate the risk posed by these components to device-surface blood clotting.

Whilst some controlled coagulation on the surface of the implant can be beneficial to its integration into the surrounding tissue(Hong *et al.*, 1999), uncontrolled clotting can lead to significant health concerns and potentially patient death. Powder bed fusion techniques of additive manufacturing are known to produce poor surface finish on parts compared to conventional manufacturing methods, including issues of stepping between layers and unmelted or semi-molten powder particles adhering to the outer surfaces of builds (Polishetty *et al.*, 2017). Due to the variability of SLM manufacturing between builds, a great deal of variation has also been found in the amount and effect of unmelted or partially melted powder particles on the surface of components, even across different areas of the same sample (Lerebours *et al.*, 2019). Post-processing relating to surface finish is common with additively manufactured components, and material has previously been found to behave differently from conventionally manufactured samples of the same metal alloy (Polishetty *et al.*, 2017). As a result, controlling this resulting roughness in a predictable manner is of great importance for ensuring predictable interactions between the human body and the implant.

The powder particles used for SLM have an average diameter of around 50µm(Rafi *et al.*, 2013). Given the average diameter of arterioles in the human body is 30µm, the risk of blockages from loose particles alone is also significant. Indeed, partially sintered particles in larger groups or particles surrounded with clotting materials could be capable of blocking larger major arteries.

Initial investigations presented in Chapter 5 concluded that the application of flow cytometry for examining the activity of blood constituents wherein activation will lead to aggregation and adsorption to a material surface was not appropriate. The use of solutions from which

the materials have been removed after exposure does not take into account the loss of material to the surfaces involved, and as such cannot account for the majority of activated platelets from the original blood sample. In this work, it was shown that the same experiment applied to flow cytometry and electron microscopy resulted in vastly different depictions of the surface cellular activity. In addition to this, there was little to no agreement between two similar marker proteins for platelet activity, nor an agreement of ADP-related activation of the blood involved.

An argument could be made for the removal of cellular material from the sample surface, returning it to the blood prior to flow cytometry application. However, in this case it would not be known whether the application of solutes for this purpose may interfere with the results produced. It has long been known that even the application of sample fixation can induce platelet activation through calcium-dependent mechanisms, resulting in erroneous flow cytometric analysis of solutions (Cahill, Macey and Newland, 1993).

Based on previous experience and the interest specifically in the surface of the materials investigated, it was therefore decided to investigate further using scanning electron microscopy. Whilst quantitative data would be beneficial to show numerical comparison of clotting risk between samples, qualitative data is also valuable given the ability to view patterns amongst the processing technique used, and to identify morphologies indicative of cell behaviour.

These images showed a definitive improvement in both the surface texture of the samples generally, but also in the presence of blood cells attached to the surface. This was not entirely confirmed with further assays as the majority of differences in platelet response were found to be non-significant, however trends pointed in agreement with the SEM images taken, with a general improvement in platelet response found with EJM-processed samples compared to AM-built titanium surfaces.

The surface texture of materials used within blood-contacting products is important as it is known to influence cellular activity in cell growth, cell migration, and thrombogenic activation. Previous investigations into roughness on the surface of other blood-contacting materials including plastics have shown that increased surface roughness can result in an increased propensity for thrombus formation and adhesion to the material surface (Hecker and Edwards, 1981; Hecker and Scandrett, 1985). With regards specifically to additively manufactured titanium alloys, previous work in powder bed AM showed that there was a significant increase in thrombogenic properties across the board when compared against

machined samples (Klingvall Ek *et al.*, 2017). Although this work was approached using electron beam manufacturing, EBM presents similar issues with surface finish (stepping, powder) as those seen in SLM given that they are both metal-based powder bed fusion methods of manufacturing.

Importantly, in this work, as-built additively manufactured titanium alloy surfaces were also found to be a significantly higher thrombogenic risk to whole blood and platelet-only solutions than bar titanium alloy. Titanium is already known to be a "highly thrombogenic biomaterial" (Hong *et al.*, 1999), so an increase in thrombogenesis over this is noteworthy given the increasing use of additive manufacturing of titanium alloys in medical implants.

During the lifetime of an additively manufactured cardiovascular device, the implant will remain high risk if thrombogenesis were to occur. Any clotting on the surface of a stent could lead to re-blockage of the artery and a secondary myocardial infarction. Clots forming on annuloplasty devices could lead to stenosis of the valve or could dislodge from its primary position. Should a clot become loose within the cardiovascular system, either through dislodging of the clot itself or through attachment to a loose powder particle, this could travel around the body to cause wider damage. Significant risks in this case would include DVT, strokes and pulmonary embolisms, all of which can be life-altering or fatal events. Previous cases have been reported where prosthetic valve rings specifically have been held responsible for the production of thrombi resulting in acute pulmonary oedema, acute atrial fibrillation, and dyspnea in three patients (Aytekin *et al.*, 2011).

There was wide variation found in some samples, which may be related to some chemical contamination found in the bar titanium material (see Chapter 5), or may be indicative of small variations in platelet numbers between wells, or the number of platelets which had contacted the surface whilst in solution. Equally, only one face of the cylindrical samples had been processed using EJM, which could have contributed to the small differences found between samples despite the polished surface appearing different in texture from as-built samples. Whilst the bottom surface of samples was never in contact with platelet solutions or blood, the sides of the cylindrical samples may have contributed to an increase in contact with non-polished AM material in polished samples.

However, in the SEM images taken, clear patterning involving tracks of smooth and rough material was found. The smoothed surfaces were mostly clean of biological material, showing few to no active platelets or trapped blood cells, however the surrounding area showed greater numbers of active platelets attached to the rougher surface. It therefore

could be argued that the lack of significant difference across the *whole* sample is attributable to this inconsistency in surface texture. Areas of material which remain rough contribute to the activation of platelets in spite of the clearer areas preventing thrombogenesis in these spaces.

This was then confirmed in the confocal imaging of immunofluorescent tagged platelets, shown in Section 4.4.5, with some areas across the sample surface being completely clear, yet surrounded by platelets around those spaces. As discussed, the spaces shown clear of platelets across the EJM-polished samples could not be explained by the powder particles of a usual SLM-produced sample, as the clear spaces were several hundred microns wide, compared to average SLM powder particle size being 50µm (Rafi *et al.*, 2013).

Comparatively over the whole space of the fluorescent images, there were fewer platelets visible on the polished surface of EJM-processed AM material than the as-built material. There were fewer still on the bar titanium sample, which suggests that this polishing is not yet effective enough in reducing platelet attraction to the surface to make it equal to conventionally manufactured metal surfaces.

This immunofluorescence work focussed solely on the *presence* of platelets on these surfaces, not their activity related to the surface they are on. Due to the microscopy methods applied, the images could not be taken at a magnification higher than 10x so the morphology of the fluorescently tagged platelets cannot be verified. However, the SEM images of Section 4.3.3 showed differences in morphology that showed significant increases in platelet activity on the as-built AM samples compared to the EJM-processed samples.

Due to this, however, it would be beneficial to repeat the immunofluorescence imaging studies including co-localisation of platelet activity markers such as CD62P or CD63 to investigate the activity of the platelets on the surfaces. It can be reasonably assumed that adherent platelets on the surface which have not been dislodged during repeated rinsing of the samples are at least somewhat active, however the co-imaging of CD61 and CD63/CD62P markers could differentiate between platelets which are resting or incidentally present, and those which have activated and would pose thrombogenic risk in an *in vivo* environment.

Concerns about the surface chemistry of samples after exposure to sodium chloride and sodium bromide solutions were found to be unnecessary. Following basic washing of the samples, no trace of chloride, bromide or sodium was found on the surface of EJM-polished samples. This is important as the introduction of further chemicals from the surface of the

material could prove cytotoxic, which would increase the risk of *in vivo* implantation, and hamper the beneficial cell growth discussed in Chapter 5. Further, this suggests that the presence or absence of EJM-related chemicals cannot be responsible for the reduction in platelet adherence to the AM surfaces after processing; rather the change in surface texture from the process is more likely to be the cause.

As discussed, in addition to the risk of loose clots produced on the surface of an implant, the size of individual or partially melted powder particles is comparable to that of arterioles in the body. This in itself produces concern that the unmelted powder particles on the surface of the implant may be capable of dislodging and becoming free in the cardiovascular system, leading to the same outcomes.

The results in this thesis show promise for the use of electrolyte jet machining in the processing of additively manufactured parts for medical applications, however there is still room to improve the process before achieving a fully appropriate surface for biointegration. Whilst the specificity of nozzle-based polishing could have excellent applications in the potential for patterning surfaces or selectively polishing to differing parameters, it currently does not succeed in providing an overall surface finish which acts in an anti-thrombogenic manner. As previous work has shown (Mitchell-Smith *et al.*, 2018), the patterning achievable by EJM is of use to biomedical applications, however existing work has focussed on the less risk-inducing skeletal applications, where thrombogenesis is a less critical consideration.

Further investigation into the process for blood-contacting applications would be of great benefit. Primarily, the repeatability and consistency of the process across a whole surface and multiples of that surface must be ensured. Following this, confirmation that the axes of this process can appropriately polish an annuloplasty ring-like shape must be undertaken, given that these initial experiments were performed on flat surfaces appropriate for tissue culture. Finally, the success of and benefit to patterning surfaces selectively should be investigated, particularly in cases like annuloplasty rings or stents where varying cell responses are desired.

As additive manufacturing ventures further into the field of medicine, it will provide an avenue for development of personalised implants within numerous organ systems. For each of these systems and applications, different considerations must be taken for the environment in which the implant will be residing. This work has provided a foundation for further development related to cardiovascular devices, particularly given their high risk for

coagulation, in addition to advancing knowledge in the post-processing of SLM Ti6Al4V for medical device applications.

7.4 Device integration

7.4.1 Cell growth on EJM surfaces

Overall, the work shown in Chapter 6 concluded that the EJM-processed surfaces (SLM-C and SLM-D) did not encourage cell growth on their surface compared to the as-built additively manufactured Ti6Al4V samples (SLM-AM). Previous studies have shown that additively manufactured titanium alloy structures can benefit cell growth when compared to conventional manufacturing techniques. Whilst research in this field has largely focussed on the design freedoms afforded by additive manufacturing allowing for the introduction of pores and cells within a component, arguably the surface features of samples is of equal importance (Matena *et al.*, 2015; Xiong *et al.*, 2020). Previous work has shown that additively manufactured samples show hydrophilic surface behaviour, which is thought to promote biological interactions with inorganic surfaces, in addition to the presence of formation of titanium oxide promoting cell growth and reducing corrosion risk (Tejero, Anitua and Orive, 2014; Vaithilingam *et al.*, 2016).

However, the variability between and within builds of surface finish discussed above is cause for concern if implantable parts are left untreated and surgically placed as they were built (Lerebours *et al.*, 2019). It would be challenging to predict the behaviour of each individual implant compared to the next if the device surface were not controlled in some way. In addition, the benefits of EJM previously discussed in selective patterning would allow for preferential surfaces to each area of the device (internal faces treated to minimise blood clotting; external faces treated to accelerate fibroblastic growth and integration). Thus, the application of EJM surface finishing would have represented a method of providing a more controlled surface finish, with high oxide content and with the potential to maintain a micro-roughened surface finish, which are thought to contribute to the hydrophilicity and beneficial cell growth found on SLM surfaces (Wang *et al.*, 2016; Mitchell-Smith *et al.*, 2018).

Surface chemistry analysis showed that all the samples had a significant titanium oxide layer on the outside of the samples. This layer is important in the provision of biocompatibility, providing protection from liberation of vanadium or aluminium into the body and improving wettability (Ding *et al.*, 2013). In addition, it is hypothesised that this TiO_2 layer is directly related to the improvement of wettability and the interaction with cell surface proteins promoting integration between titanium parts and the human body (Wang *et al.*, 2016). It was previously highlighted by (Speidel *et al.*, 2016; Mitchell-Smith *et al.*, 2018) that the inclusion of bromide solutions, used in SLM-C and SLM-D but not SLM-A or SLM-B, produced a greater concentration of TiO_2 after processing than that found with chloride-only solutions.

In turn, however, bromide solutions had a reduced material removal compared to chloride solutions; thus, a balance must be struck in the surface chemistry and the surface topography which are required (Speidel *et al.*, 2016).

As mentioned previously, the absence of sodium, bromide, or chloride chemistry on the surface of EJM-processed samples is of great importance biologically. NaBr and NaCl could be cytotoxic if found on the surface of the samples and would strongly discourage healthy cell proliferation. The absence of these chemicals suggests that the EJM process successfully avoids leaving residual solute on the surface after polishing, and from this angle is safe for use on medically intended parts.

On the conventionally manufactured Ti64-S samples, contaminants including zinc and copper were found. These may account for the cytotoxic findings in cell culture (section 5.4.3), as zinc and copper are both known to induce cytotoxic responses in cells *in vitro*. As a result of this, the cell viability of bar titanium alloy may be lower than expected, however this contamination was not found on the additively manufactured or EJM-processed samples, thus these remain unaffected by these contaminants.

However, in addition to the chemical contaminants, the bar titanium samples showed a hydrophobic wettability profile. Regardless of the presence of chemical contaminants, this hydrophobic nature suggests that the surface of the bar titanium samples will not actively benefit cell growth. Hydrophilicity is strongly influenced by surface topography, which is further discussed separately below. However, hydrophilicity alone has been shown to be a strong predictor of implant success associated with cell adhesion and proliferation (Kwon and Park, 2018). In osteogenic applications, surface modifications such as chemical treatment to induce greater hydrophilicity which, in turn, actively encourages recruitment of stem cells to integrate implants into the host body (Kwon and Park, 2018).

The surface topography of the samples is of significant interest and importance in cell proliferation promotion. The bar titanium was predominantly flat, with some small defects and scratches being the only source of roughness or unevenness. Additively manufactured samples, by comparison, are very rough and the powder-based production method leaves large numbers of spherical powder particles on the outer surfaces of parts, providing crevasses and sides for cells to grow into and over. It is known that roughness at the interface between a tissue and an implant promotes cell growth through the provision of anchoring points for cells and biomolecules (Tejero, Anitua and Orive, 2014).

It was hypothesised at the outset of this work that the pitted nature of Bromide-EJM-processed surfaces would produce such anchoring points across the surface of a sample. Previous studies (Chapter 4) had indicated that these surfaces were not successful in *repelling* biological material, and as such had encouraged the activation and presence of platelets on their surface. However, the results shown in this chapter suggest that these surfaces were also not beneficial in promoting the growth of fibroblast cells.

According to the XPS results, there were no cytotoxic contaminants on the surface of EJM-processed samples, however the wettability profile of the samples was poor. This suggests that the surface of the sample is averse to cell growth, as discussed above. It could be suggested that the features of the EJM-processed surface, significantly smaller than those produced by the powder particles of an as-built additively manufactured titanium alloy part, were simply too small for the purposes of cell growth. Given that the powder particles are roughly 40µm in diameter on average, the features produced are within the 10s-100s of micrometre range. Comparatively, the SEM images in section 5.4.1 show that the pitting features produced from the Bromide EJM polishing are in the order of single micrometres. Previous studies have shown beneficial cell growth from pores and features in scaffolds with an extremely wide range of sizes (from 20µm to 1500µm (Murphy and O'Brien, 2011)), however the majority of studies concerning metal alloys and cell growth maintain pore sizes within 100s of micrometres diameter (Wysocki *et al.*, 2016; Dall'Ava *et al.*, 2019).

If it were found to be the case that the surface topography of these samples was the primary reason for failure of cell attachment and thus proliferation, it could be posited that these surfaces may be alternatively applied in an antibacterial function. Significant research is currently focussed on non-pharmaceutical methods of preventing bacterial proliferation in hospital, home and public settings (Dunne *et al.*, 2020; Florea *et al.*, 2020). Existing methods include utilization of copper or silver alloys when manufacturing door handles and surgical instruments due to their natural cytotoxic properties, however EJM processing of existing materials may also be investigated for this purpose (Dunne *et al.*, 2020).

8 Conclusions and Outlook

8.1 Conclusion

Overall, the work outlined in this thesis has laid groundwork for significant future investigation into the application of additive manufacturing for annuloplasty devices, cardiovascular devices, and implantable medical devices in a wider sphere. Surface finishing and modification of components for medical applications remains a large field of work with differing approaches according to the specific organ or system for which the device is designed.

The outset of this work aimed to **investigate the use of additive manufacturing to develop bespoke annuloplasty devices for improved patient care**. In order to achieve this, three aims were identified which were addressed throughout the work of this thesis.

Objective 4. Develop a design protocol for design of personalised annuloplasty devices

To address this objective, work was initially undertaken to assess the suitability of existing, mass manufactured annuloplasty devices and their geometries with regards to the range of human anatomy. It was found that whilst assumptions made about geometry of the human mitral valve were correct on average across a population, a variation of up to two commercial annuloplasty device sizes (2.5mm) was present, and average error of the ratio was found to be 4mm. Thus, some communities may be underserved by the currently available commercial annuloplasty devices.

Following this, methods of designing bespoke annuloplasty devices according to individual patient anatomy were investigated. The commercial software Materialise Mimics was found to be suitable for importing and designing on patient scan data; however, the in-built thresholding technique was found to be insufficient for use in discerning different structures within a single organ. Alternative bespoke software packages were considered to overcome this limitation; however, Materialise Mimics was found to be capable of replicating the methodology of these bespoke packages in a user-friendly and more accessible manner.

The work completed to achieve this objective highlighted the need for improvement of existing annuloplasty devices and provided recommendations for the most promising methods of designing improved, patient-specific devices in the future.

Objective 5. Ensure the safety of annuloplasty devices produced using additive manufacturing

To address this objective, whole blood and platelet assays were undertaken on additively manufactured and conventionally manufactured titanium alloy material. In addition, a novel method of surface finishing, electrolyte jet machining, was employed and the biological behaviour of the resulting surface was compared against the two as-manufactured surfaces.

Additively manufactured parts were found to be more thrombogenic than conventionally manufactured Ti6Al4V surfaces using platelet counting, immunofluorescence, and alamar blue assays. Qualitative data showed noteworthy changes in platelet morphology indicating active phenotypes on the as-built SLM surface. Electrolyte jet machining (EJM) was found to have some limited success in the mitigation of clotting risk when in contact with human platelets: cell metabolic activity assays and immunofluorescence both suggested a reduction in platelet activity when compared to as-built SLM parts. With regards to the specific parameters, a chloride-only solution was found to produce smoother surfaces more conducive to reducing thrombogenic risk than a combination of bromide and chloride. Finally, two passes of EJM finishing produced a more beneficial surface when attempting to reduce thrombogenic activity than the single pass alone.

In addition, it was found that whilst a quantitative method of measuring thrombogenic risk on these samples would have been preferred, flow cytometry was not an appropriate method to assess surface coagulation. Therefore, a greater number of visual methods such as immunofluorescence were employed, alongside some semi-quantitative assays such as Alamar Blue assays.

The work undertaken to address this objective highlighted the additional risk that additively manufactured parts and materials will likely pose to a cardiovascular environment such as for annuloplasty devices. It was also shown that the novel surface finishing method of electrolyte jet machining, more finely controllable than mass-material removal processes, is a potentially useful way of mitigating the thrombogenic activity of SLM-manufactured Ti6Al4V.Hhowever, further investigations are recommended, with more detail provided in Section 8.2.

Objective 6. Provide biological integration between the annuloplasty device and patient for repair longevity

To address this objective, the electrolyte jet machining process investigated for Aim 2 was repeated. The results of Aim 2, presented in Chapter 5, suggested that the chloride-bromide solution was a poor choice for reduction of platelet activity on the surface of samples.

However, SEM images of the samples showed a highly textured and featured surface, which was therefore brought forward for trials with endothelial cell growth.

Ultimately, the EJM-processed samples proved a poor surface treatment for the encouragement of fibroblast cell growth. Fibroblast cells were found to survive and attach more successfully to the EJM-processed surfaces than conventionally manufactured Ti6Al4V material, however this was reduced compared to an as-built SLM sample, which was most encouraging to cell growth. This aligned with the results of a surface wettability assay, which showed a much smaller average contact angle (74.96°) indicating hydrophilic behaviour for as-built SLM surfaces than conventionally manufactured surface (104.48°) or either EJM-processed surface (114.70° and 113.65°). It was hypothesised that the features produced by EJM treatment were on too small a scale to encourage the formation of cell protrusions and adherence required for long-term successful growth.

Whilst time did not allow for assessment of biological surface molecules in the encouragement of beneficial cell growth and integration with the body, this would be the next avenue for investigation in this arm of work. Samples of additively and conventionally manufactured titanium alloy and other biocompatible materials including nylon have been selected for trials using “function-spacer-lipid” biotinylation molecules.

The work described in Chapter 6 to achieve this objective provided further understanding of the benefits and downfalls of EJM as a surface finishing method for SLM-manufactured Ti6Al4V in a biological setting. It was ruled out as a method for improving the integration potential of annuloplasty devices with the human body.

8.2 Future work

It is clear that significant work remains both across the technologies addressed in this thesis and within the wider scope of additively manufactured medical implants.

For the design of annuloplasty devices, this thesis has outlined a method of achieving the geometry of a patient's existing mitral valve, however a robust method for providing a beneficial, supportive ring geometry has not yet been formulated. Given that an assumed 3:4 ratio is not appropriate for all patients across a population; could an extended range of shapes within existing size ranges provide improved devices for patients; or should modelling methods be employed to predict the most beneficial shape for each individual patient?

Electrolyte jet machining proved somewhat successful in its prevention of thrombosis on titanium alloy surfaces. With further refinement, and given its success in conventionally manufactured surface finishing, this could prove a finely controllable method of patterning and selectively polishing surfaces to control biological responses to implants. However, the work undertaken in this thesis only assessed processing done in the XY orientation and did not attempt EJM polishing on a Z-plane. Therefore, further study must be undertaken to understand the potential of EJM for processing a full, three-dimensional geometry, and doing so in a selective manner.

When attempting to encourage cell growth, EJM proved less successful, and as-built SLM surfaces provided the most encouragement to fibroblast adhesion and survivability in the short term (2-24 hours). Significant work is already underway on larger scale methods of improving AM fibroblast growth (such as internal lattice structures); however the majority of these studies involve osteoblastic cell types and do not consider the effect of different geometries on differentiation of cell lines, or how this could adjust the needs of an implant based on the organ and application for which it is designed.

A further investigation which could not be completed due to time constraints was to implement the use of surface modification in conjunction with as-built SLM titanium surfaces to further improve cell integration. The results shown in Chapter 6 (discussed in 7.3.1) showed that as-manufactured SLM Ti6Al4V surfaces (SLM-AM) presented the most hospitable surfaces to fibroblastic cell growth amongst those tested. However, concerns about the variability of surfaces within and between builds are still present, and thus an overarching method of encouraging cell growth in addition to the component having some inherent cellular attraction would provide further security of integration.

Whilst surface modification in terms of physical and chemical material characteristics of the component itself has been popular for study (Zhang *et al.*, 2020), addition of materials to the external surface of parts is also a promising method of promoting cell growth into metal structures (Florea *et al.*, 2020). These surface additions have included both chemical and biological molecules known to promote various stages and types of cell growth, including ceramics such as hydroxyapatite or polymers including biopolymers such as collagen to mimic extracellular matrices and other factors known to be instrumental in tissue growth and regulation (Müller *et al.*, 2005; Wei *et al.*, 2015).

Combinations of these methods have proven fruitful, with research taking on both physical characteristics and chemical addition to modify cell behaviour and promote growth for implants (Zareidoost *et al.*, 2012). Thus, a combined effort of as-built SLM surfaces, shown in this thesis to be beneficial for cell growth alone, with the addition of biomolecules for promotion of tissue formation, could equally prove successful. Previous studies have shown success in the attachment of exogenous molecules to the surface of SLM titanium alloy looking towards pharmaceutical functionalisation (Vaithilingam *et al.*, 2015), suggesting that the SLM process would not render surfaces or samples averse to functionalisation for tissue growth purposes.

Biofunctionalisation traditionally requires several steps of processing to provide a reliable, total coating of material surfaces. In addition, these steps are highly variable according to the material being coated and the application needs of the coating *in vivo*. Glycosylation in particular is an area of interest for allowing inorganic surfaces to mimic the surface protein and carbohydrate profiles of cells and tissues, promoting interactions between these surfaces (Williams *et al.*, 2016). A novel method of rapid, single-step glycosylation using "function-spacer-lipid" constructs was developed and tested on polymer, metal and glass surfaces previously and found to provide reasonably robust surface attachment in the short term, withstanding several standard laboratory procedures (Williams *et al.*, 2016; Henry *et al.*, 2018). These constructs have now been tested in a range of experimental and diagnostic settings, however their potential for *in vivo* application remains unexplored despite the possibility of functionalising inorganic materials to improve biocompatibility (Williams *et al.*, 2016; Lim and Kang, 2017; Henry *et al.*, 2018). This remains an area of work which would benefit from investigation.

Outside of the work addressed in this thesis, other questions remain in the field which did not fit the scope of work presented here. The decision of whether to repair or replace a mitral

valve remains subjective and often informed by cardiologist or surgeon experience, rather than data-based decision making. A disease or risk model for assessing mitral regurgitation and assigning repair/replacement surgeries accordingly would likely benefit long-term outcomes for patients with mitral insufficiency. Further to this, such a range of materials are available to manufacture the core of annuloplasty devices with, and many commercially available devices claim a number of benefits with their particular material. The scope of this thesis assesses only titanium alloy cores; however, a comparison of available materials and potential benefits would complement the development of novel manufacturing technologies. Finally, the insertion of any long-term medical device is a high-risk endeavour for introduction of infection. Whilst this thesis addressed the encouragement of beneficial cell growth on the surface of implanted devices, it is often considered a "race to the surface" between beneficial and pathogenic agents within the body. Particularly with the insertion of annuloplasty devices inside the heart, prevention of endocarditis should be a major theme going forwards and the employment of novel technologies in that goal should be considered.

8.3 Final remarks

The outset of this work was envisioned by clinicians as a means to improve patient outcomes during a common but often life-changing surgery. The research described in this thesis has shown the possibility of employing additive manufacturing technologies in the provision of mitral annuloplasty but has also highlighted the complex work necessary to achieve an all-around solution to the challenges posed by cardiovascular devices. In whole, this thesis provides a framework for further development and refinement towards the goal of an annuloplasty device produced using advanced manufacturing technologies.

Additive manufacturing is often viewed as a panacea for bespoke implants, printing organs and manufacturing novel devices to save lives. However, the reality of both medical device development, and of additive manufacturing technologies, is that significant refining is required before full-scale adoption and mass manufacturing become commonplace. To this end, the continued efforts of multidisciplinary teams and collaborative ventures will be vital to the progress of novel technologies in improving clinical results and patient experience.

9 References

Akuffu, A. M. *et al.* (2018) 'Prosthesis-patient mismatch after mitral valve replacement: A single-centered retrospective analysis in East China', *Journal of Cardiothoracic Surgery*. BioMed Central Ltd., 13(1), pp. 1–9. doi: 10.1186/s13019-018-0788-4.

Al-Maisary, S. *et al.* (2017) 'Computer-based comparison of different methods for selecting mitral annuloplasty ring size.', *Journal of cardiothoracic surgery*. BioMed Central, 12(1), p. 8. doi: 10.1186/s13019-017-0571-y.

Alkadhi, H. *et al.* (2007) 'Aortic Regurgitation: Assessment with 64-Section CT', *Radiology*. Radiological Society of North America, 245(1), pp. 111–121. doi: 10.1148/radiol.2451061523.

Alonzo, M. *et al.* (2019) '3D Bioprinting of cardiac tissue and cardiac stem cell therapy', *Translational Research*. Mosby. doi: 10.1016/J.TRSL.2019.04.004.

Anyanwu, A. C. and Adams, D. H. (2009) 'Why Do Mitral Valve Repairs Fail?', *Journal of the American Society of Echocardiography*, 22(11), pp. 1265–1268. doi: 10.1016/j.echo.2009.09.024.

Arabnejad, S. *et al.* (2017) 'Fully Porous 3D Printed Titanium Femoral Stem to Reduce Stress-Shielding Following Total Hip Arthroplasty', *J Orthop Res*, 35, pp. 1774–1783. doi: 10.1002/jor.23445.

Arora, A. and Anyanwu, A. C. (2015) 'Prosthetic Ring Choice in Secondary Mitral Regurgitation', in *Secondary Mitral Valve Regurgitation*. London: Springer London, pp. 97–103. doi: 10.1007/978-1-4471-6488-3_10.

Asopa, S., Patel, A. and Dunning, J. (2006) 'Is short-term anticoagulation necessary after mitral valve repair?', *Interactive CardioVascular and Thoracic Surgery*. Oxford University Press, 5(6), pp. 761–765. doi: 10.1510/icvts.2006.143099.

Aytekin, S. *et al.* (2011) 'Prosthetic Heart Valve Ring Thrombosis', *JACC: Cardiovascular Imaging*. JACC: Cardiovascular Imaging, 4(10), pp. 1141–1143. doi: 10.1016/j.jcmg.2011.03.021.

Bhatnagar, P. *et al.* (2016) 'Trends in the epidemiology of cardiovascular disease in the UK.', *Heart (British Cardiac Society)*. BMJ Publishing Group Ltd and British Cardiovascular Society, 102(24), pp. 1945–1952. doi: 10.1136/heartjnl-2016-309573.

BHF (2019) 'Heart and Circulatory Disease Statistics 2019', *2019 Statistics Compendium (tables)*, (April), pp. 94–96. Available at: https://www.bhf.org.uk/what-we-do/our-research/heart-statistics/heart-statistics-publications/cardiovascular-disease-statistics-2019.

Birbara, N. S., Otton, J. M. and Pather, N. (2019) '3D Modelling and Printing Technology to Produce Patient-Specific 3D Models', *Heart, Lung and Circulation*. Elsevier, 28(2), pp. 302–313. doi: 10.1016/J.HLC.2017.10.017.

Birks, E. J. *et al.* (2006) 'Left Ventricular Assist Device and Drug Therapy for the Reversal of Heart Failure', *New England Journal of Medicine*. Massachusetts Medical Society , 355(18), pp. 1873–1884. doi: 10.1056/NEJMoa053063.

De Bonis, M. *et al.* (2016) 'Surgical and interventional management of mitral valve regurgitation: A position statement from the European society of cardiology working groups on cardiovascular surgery and valvular heart disease', *European Heart Journal*.

Oxford University Press, pp. 133–139. doi: 10.1093/eurheartj/ehv322.

Bothe, W. *et al.* (2010) 'How do annuloplasty rings affect mitral leaflet dynamic motion?', *European journal of cardio-thoracic surgery : official journal of the European Association for Cardio-thoracic Surgery*. NIH Public Access, 38(3), pp. 340–9. doi: 10.1016/j.ejcts.2010.02.011.

Bothe, W., Miller, D. C. and Doenst, T. (2013) 'Sizing for Mitral Annuloplasty: Where Does Science Stop and Voodoo Begin?', *ATS*, 95, pp. 1475–1483. doi: 10.1016/j.athoracsur.2012.10.023.

Bourell, D. L. (2016) 'Perspectives on Additive Manufacturing', *Annual Review of Materials Research*. Annual Reviews , 46(1), pp. 1–18. doi: 10.1146/annurev-matsci-070115-031606.

Cahill, M. R., Macey, M. G. and Newland, A. C. (1993) 'Fixation with formaldehyde induces expression of activation dependent platelet membrane glycoproteins, P selectin (CD62) and GP53 (CD63)', *British Journal of Haematology*. John Wiley & Sons, Ltd (10.1111), 84(3), pp. 527–529. doi: 10.1111/j.1365-2141.1993.tb03112.x.

Carpentier, A., Adams, D. H. and Filsoufi, F. (2010) *Carpentier's reconstructive valve surgery : from valve analysis to valve reconstruction*. Saunders/Elsevier.

Cawley, P. J., Maki, J. H. and Otto, C. M. (2009) 'Cardiovascular Magnetic Resonance Imaging for Valvular Heart Disease', *Circulation*. Lippincott Williams & Wilkins, 119(3), pp. 468–478. doi: 10.1161/CIRCULATIONAHA.107.742486.

Cheng, A. *et al.* (2014) 'Additively manufactured 3D porous Ti-6Al-4V constructs mimic trabecular bone structure and regulate osteoblast proliferation, differentiation and local factor production in a porosity and surface roughness dependent manner', *Biofabrication*. IOP Publishing, 6(4), p. 045007. doi: 10.1088/1758-5082/6/4/045007.

Cikirikcioglu, M., Cherian, S. and Kalangos, A. (2012) 'Mitral annuloplasty using an intra-annular ring.', *Multimedia manual of cardiothoracic surgery : MMCTS*. Oxford University Press, 2012, p. mms019. doi: 10.1093/mmcts/mms019.

Claesson, K., Lindahl, T. and Faxälv, L. (2016) 'Counting the platelets: a robust and sensitive quantification method for thrombus formation', *Thrombosis and Haemostasis*, 115(06), pp. 1178–1190. doi: 10.1160/TH15-10-0799.

Cohen, A. *et al.* (2009) *Mandibular reconstruction using stereolithographic 3-dimensional printing modeling technology*, *Oral Surgery, Oral Medicine, Oral Pathology, Oral Radiology, and Endodontology*. doi: 10.1016/j.tripleo.2009.05.023.

Cohn, L. H. *et al.* (1997) 'Minimally invasive cardiac valve surgery improves patient satisfaction while reducing costs of cardiac valve replacement and repair.', *Annals of surgery*. Lippincott, Williams, and Wilkins, 226(4), pp. 421–6; discussion 427-8. Available at: http://www.ncbi.nlm.nih.gov/pubmed/9351710 (Accessed: 17 November 2016).

Cooray, S. D. *et al.* (2009) 'Echocardiographic measurement of mitral intertrigonal distance is an adjunct to annuloplasty ring sizing.', *The Journal of heart valve disease*, 18(1), pp. 106–10. Available at: http://www.ncbi.nlm.nih.gov/pubmed/19301561 (Accessed: 10 November 2016).

da Costa, F. D. A. *et al.* (2018) 'Long-term results of mitral valve repair', *Brazilian Journal of Cardiovascular Surgery*. Sociedade Brasileira de Cirurgia Cardiovascular, 33(1), pp. 23–31. doi: 10.21470/1678-9741-2017-0145.

D'Souza, S. *et al.* (2008) 'Biodegradable Stents – A New Era?', *European Cardiology Review*, 4(2), p. 82. doi: 10.15420/ecr.2008.4.2.82.

Dal-Bianco, J. P. and Levine, R. A. (2013) 'Anatomy of the mitral valve apparatus: role of 2D and 3D echocardiography.', *Cardiology clinics*. NIH Public Access, 31(2), pp. 151–64. doi: 10.1016/j.ccl.2013.03.001.

Dall'Ava, L. *et al.* (2019) '3D printed acetabular cups for total hip arthroplasty: A review article', *Metals*. MDPI AG, p. 729. doi: 10.3390/met9070729.

Dankowski, R. *et al.* (2014) '3D heart model printing for preparation of percutaneous structural interventions: description of the technology and case report', *Kardiologia Polska (Polish Heart Journal)*, 72(6), pp. 546–551. doi: 10.5603/KP.2014.0119.

Davie, E. W., Fujikawa, K. and Kisiel, W. (1991) 'The Coagulation Cascade: Initiation, Maintenance, and Regulation', *Perspectives in Biochemistry*, 30(43), pp. 10363–10370. Available at: https://pubs.acs.org/doi/pdf/10.1021/bi00107a001 (Accessed: 16 May 2018).

Delling, F. N. and Vasan, R. S. (2014) 'Epidemiology and Pathophysiology of Mitral Valve Prolapse', *Circulation*, 129(21).

Demir, A. G. and Previtali, B. (2017) 'Additive manufacturing of cardiovascular CoCr stents by selective laser melting', *Materials & Design*. Elsevier, 119, pp. 338–350. doi: 10.1016/J.MATDES.2017.01.091.

Díaz Lantada, A. *et al.* (2010) 'Development of Personalized Annuloplasty Rings: Combination of CT Images and CAD-CAM Tools', *Annals of Biomedical Engineering*. Springer US, 38(2), pp. 280–290. doi: 10.1007/s10439-009-9805-z.

Ding, Y. *et al.* (2013) 'Effects of microtopographic patterns on platelet adhesion and activation on titanium oxide surfaces', *Journal of Biomedical Materials Research Part A*. Wiley-Blackwell, 101A(3), pp. 622–632. doi: 10.1002/jbm.a.34361.

Drelich, J. *et al.* (2011) 'Hydrophilic and superhydrophilic surfaces and materials', *Soft Matter*, pp. 9804–9828. doi: 10.1039/c1sm05849e.

Dumont, E. *et al.* (2007) 'Reoperation After Mitral Valve Repair for Degenerative Disease', *The Annals of Thoracic Surgery*, 84(2), pp. 444–450. doi: 10.1016/j.athoracsur.2007.03.078.

Dunne, C. P. *et al.* (2020) 'Antimicrobial coating innovations to prevent infectious disease: a consensus view from the AMiCl COST Action', *Journal of Hospital Infection*. W.B. Saunders Ltd, pp. 116–118. doi: 10.1016/j.jhin.2020.04.006.

Edwards Lifesciences LLC (2010) *Heart Valve Therapy Products*. Irvine, CA. Available at: http://market360online.com/sqlimages/1246/125029.pdf (Accessed: 28 November 2016).

Elahinia, M. *et al.* (2016) 'Fabrication of NiTi through additive manufacturing: A review', *Progress in Materials Science*, 83, pp. 630–663. doi: 10.1016/j.pmatsci.2016.08.001.

Ender, J. *et al.* (2008) 'Value of Augmented Reality-Enhanced Transesophageal Echocardiography (TEE) for Determining Optimal Annuloplasty Ring Size During Mitral Valve Repair', *The Annals of Thoracic Surgery*, 86(5), pp. 1473–1478. doi: 10.1016/j.athoracsur.2008.07.073.

Ender, J. *et al.* (2011) 'Prediction of the annuloplasty ring size in patients undergoing mitral valve repair using real-time three-dimensional transoesophageal echocardiography.', *European journal of echocardiography : the journal of the Working Group on Echocardiography of the European Society of Cardiology*. Oxford University Press, 12(6), pp.

445–53. doi: 10.1093/ejechocard/jer042.

Enriquez-Sarano, M., Akins, C. W. and Vahanian, A. (2009) 'Mitral regurgitation', *The Lancet*, 373(9672), pp. 1382–1394. doi: 10.1016/S0140-6736(09)60692-9.

Ferket, B. S. *et al.* (2018) 'Cost-Effectiveness of Mitral Valve Repair Versus Replacement for Severe Ischemic Mitral Regurgitation: A Randomized Clinical Trial From the Cardiothoracic Surgical Trials Network', *Circulation. Cardiovascular quality and outcomes*. NLM (Medline), 11(11), p. e004466. doi: 10.1161/CIRCOUTCOMES.117.004466.

Flameng, W., Herijgers, P. and Bogaerts, K. (2003) 'Recurrence of Mitral Valve Regurgitation After Mitral Valve Repair in Degenerative Valve Disease', *Circulation*, 107(12), pp. 1609–1613. doi: 10.1161/01.CIR.0000058703.26715.9D.

Florea, D. A. *et al.* (2020) 'Surface modification – A step forward to overcome the current challenges in orthopedic industry and to obtain an improved osseointegration and antimicrobial properties', *Materials Chemistry and Physics*. Elsevier Ltd, p. 122579. doi: 10.1016/j.matchemphys.2019.122579.

Gammie, J. S. *et al.* (2009) 'Trends in mitral valve surgery in the United States: results from the Society of Thoracic Surgeons Adult Cardiac Surgery Database.', *The Annals of thoracic surgery*, 87(5), pp. 1431–7; discussion 1437-9. doi: 10.1016/j.athoracsur.2009.01.064.

Gibson, I., Rosen, D. and Stuker, B. (2013) *Additive Manufacturing Technologies: 3D Printing, Rapid Prototyping, and Direct Digital Manufacturing.*, *Rapid Manufacturing Association*. doi: 10.1520/F2792-12A.2.

Gillinov, A. M. *et al.* (1997) 'Reoperation for failure of mitral valve repair', *The Journal of Thoracic and Cardiovascular Surgery*, 113(3), pp. 467–475. doi: 10.1016/S0022-5223(97)70359-3.

Ginty, O. *et al.* (2017) 'Patient-specific indirectly 3D printed mitral valves for pre-operative surgical modelling', in Webster, R. J. and Fei, B. (eds). International Society for Optics and Photonics, p. 1013517. doi: 10.1117/12.2255567.

Goodson, A. M. *et al.* (2019) 'Patient-specific, printed titanium implants for reconstruction of mandibular continuity defects: A systematic review of the evidence', *Journal of Cranio-Maxillofacial Surgery*. Churchill Livingstone, 47(6), pp. 968–976. doi: 10.1016/J.JCMS.2019.02.010.

Grabow, N. and Schmitz, K.-P. (2018) 'Progress and challenges in the development of novel implant concepts for cardiovascular, ophthalmologic and otolaryngologic applications', *Current Directions in Biomedical Engineering*, 4(1), pp. 87–88. doi: 10.1515/cdbme-2018-0022.

Graser, B. *et al.* (2013) 'Using a shape prior for robust modeling of the mitral annulus on 4D ultrasound data', *International Journal of Computer Assisted Radiology and Surgery*. Springer Berlin Heidelberg, 9(4), pp. 635–644. doi: 10.1007/s11548-013-0942-3.

Graser, B. *et al.* (2014) 'Computerunterstütztes „ring sizing" für die Anuloplastie', *Zeitschrift für Herz-,Thorax- und Gefäßchirurgie*. Springer Berlin Heidelberg, 28(5), pp. 347–351. doi: 10.1007/s00398-014-1103-x.

Gray, R. A. and Pathmanathan, P. (2018) 'Patient-Specific Cardiovascular Computational Modeling: Diversity of Personalization and Challenges', *Journal of Cardiovascular Translational Research*. Springer US, 11(2), pp. 80–88. doi: 10.1007/s12265-018-9792-2.

Health Canada (2011) 'Guidance for the Interpretation of Significant Change of a Medical Device'. Ottawa: Health Canada, pp. 14–22. Available at: https://www.canada.ca/en/health-canada/services/drugs-health-products/medical-devices/application-information/guidance-documents/guidance-document-interpretation-significant-change-medical-device.html (Accessed: 18 June 2018).

Heath, D. E. (2017) 'Promoting Endothelialization of Polymeric Cardiovascular Biomaterials', *Macromolecular Chemistry and Physics*. John Wiley & Sons, Ltd, 218(8), p. 1600574. doi: 10.1002/macp.201600574.

Hecker, J. F. and Edwards, R. O. (1981) 'Effects of roughness on the thrombogenicity of a plastic', *Journal of Biomedical Materials Research*. Wiley-Blackwell, 15(1), pp. 1–7. doi: 10.1002/jbm.820150104.

Hecker, J. F. and Scandrett, L. A. (1985) 'Roughness and thrombogenicity of the outer surfaces of intravascular catheters', *Journal of Biomedical Materials Research*. John Wiley & Sons, Inc., 19(4), pp. 381–395. doi: 10.1002/jbm.820190404.

Henry, S. *et al.* (2018) 'Rapid one-step biotinylation of biological and non-biological surfaces', *Scientific Reports*. Nature Publishing Group, 8(1), pp. 1–6. doi: 10.1038/s41598-018-21186-3.

Hollander, D. A. *et al.* (2006) 'Structural, mechanical and in vitro characterization of individually structured Ti–6Al–4V produced by direct laser forming', *Biomaterials*. Elsevier, 27(7), pp. 955–963. doi: 10.1016/J.BIOMATERIALS.2005.07.041.

Hong, J. *et al.* (1999) 'Titanium is a highly thrombogenic biomaterial: possible implications for osteogenesis.', *Thrombosis and haemostasis*, 82(1), pp. 58–64. Available at: http://www.ncbi.nlm.nih.gov/pubmed/10456455 (Accessed: 18 June 2018).

Ilina, A. *et al.* (2017) 'Patient-specific pediatric silicone heart valve models based on 3D ultrasound'. Edited by R. J. Webster and B. Fei. International Society for Optics and Photonics, (March), p. 1013516. doi: 10.1117/12.2255849.

ISO (2017) 'Biological evaluation of medical devices - Part 4: Selection of tests for interactions with blood (ISO 10993-4:2017) Évaluation', pp. 1–69. Available at: https://www.iso.org/standard/63448.html (Accessed: 16 July 2019).

Izzo, R. L. *et al.* (2016) '3D printed cardiac phantom for procedural planning of a transcatheter native mitral valve replacement'. Edited by J. Zhang and T. S. Cook. International Society for Optics and Photonics, 9789, p. 978908. doi: 10.1117/12.2216952.

Jacobs, S. *et al.* (2008) '3D-Imaging of cardiac structures using 3D heart models for planning in heart surgery: a preliminary study', *Interactive CardioVascular and Thoracic Surgery*. Narnia, 7(1), pp. 6–9. doi: 10.1510/icvts.2007.156588.

Jäger, M. *et al.* (2017) 'Antimicrobial and osseointegration properties of nanostructured titanium orthopaedic implans', *Materials*. MDPI AG. doi: 10.3390/ma10111302.

Jaidev, L. R. and Chatterjee, K. (2019) 'Surface functionalization of 3D printed polymer scaffolds to augment stem cell response', *Materials & Design*. Elsevier, 161, pp. 44–54. doi: 10.1016/J.MATDES.2018.11.018.

Jain, K. K. (2017) 'Personalized Management of Cardiovascular Disorders.', *Medical principles and practice : international journal of the Kuwait University, Health Science Centre*. Karger Publishers, 26(5), pp. 399–414. doi: 10.1159/000481403.

Jardini, A. L. *et al.* (2014) 'Cranial reconstruction: 3D biomodel and custom-built implant created using additive manufacturing', *Journal of Cranio-Maxillofacial Surgery*, 42(8), pp. 1877–1884. doi: 10.1016/j.jcms.2014.07.006.

Jensen, M. O. *et al.* (2008) 'Saddle-Shaped Mitral Valve Annuloplasty Rings Experience Lower Forces Compared With Flat Rings', *Circulation*, 118(14 suppl 1).

Jiang, Z. *et al.* (2019) 'Direct Ink Writing of Poly(tetrafluoroethylene) (PTFE) with Tunable Mechanical Properties', *ACS Applied Materials and Interfaces*. American Chemical Society, 11(31), pp. 28289–28295. doi: 10.1021/acsami.9b07279.

Kaur, M. and Singh, K. (2019) 'Review on titanium and titanium based alloys as biomaterials for orthopaedic applications', *Materials Science and Engineering: C*. Elsevier, 102, pp. 844–862. doi: 10.1016/J.MSEC.2019.04.064.

Kazaz, H. *et al.* (2005) 'Mitral annuloplasty with biodegradable ring for infective endocarditis: a new tool for the surgeon for valve repair in childhood', *Interactive CardioVascular and Thoracic Surgery*. Oxford University Press, 4(4), pp. 378–380. doi: 10.1510/icvts.2005.105833.

Kheradvar, A. *et al.* (2015) 'Emerging Trends in Heart Valve Engineering: Part III. Novel Technologies for Mitral Valve Repair and Replacement', *Annals of Biomedical Engineering*. Kluwer Academic Publishers, pp. 858–870. doi: 10.1007/s10439-014-1129-y.

Klingvall Ek, R. *et al.* (2017) 'Micro- to Macroroughness of Additively Manufactured Titanium Implants in Terms of Coagulation and Contact Activation', *The International Journal of Oral & Maxillofacial Implants*, 32(3), pp. 565–574. doi: 10.11607/jomi.5357.

Komoda, T. *et al.* (2009) 'Growth of mitral annulus in the pediatric patient after suture annuloplasty of the entire posterior mitral annulus.', *Interactive cardiovascular and thoracic surgery*, 9(2), pp. 354–6. doi: 10.1510/icvts.2009.206060.

Konerding, M. A. *et al.* (2013) 'Comparison of the novel Medtentia double helix mitral annuloplasty system with the Carpentier-Edwards Physio annuloplasty ring: morphological and functional long-term outcome in a mitral valve insufficiency sheep model.', *Journal of cardiothoracic surgery*. BioMed Central, 8, p. 70. doi: 10.1186/1749-8090-8-70.

Kotlarz, M. *et al.* (2018) 'One step 3D printing of surface functionalized composite scaffolds for tissue engineering applications', *Acta of Bioengineering and Biomechanics*, 20(2), pp. 35–45. doi: 10.5277/ABB-01131-2018-02.

Kwon, Y.-S. and Park, J.-W. (2018) 'Osteogenic differentiation of mesenchymal stem cells modulated by a chemically modified super-hydrophilic titanium implant surface.', *Journal of biomaterials applications*. SAGE Publications Ltd, 33(2), pp. 205–215. doi: 10.1177/0885328218786873.

Lazam, S. *et al.* (2017) 'Twenty-Year Outcome after Mitral Repair Versus Replacement for Severe Degenerative Mitral Regurgitation: Analysis of a Large, Prospective, Multicenter, International Registry', *Circulation*. Lippincott Williams and Wilkins, 135(5), pp. 410–422. doi: 10.1161/CIRCULATIONAHA.116.023340.

Lecuyer, L. *et al.* (2011) 'Height of the anterior leaflet (A2), measured by echocardiography predicts accurately the annuloplasty ring size used during mitral valve reconstruction using Carpentier's techniques', *Archives of Cardiovascular Diseases Supplements*, 3(1). doi: 10.1016/S1878-6480(11)70164-1.

Lerebours, A. *et al.* (2019) 'Additive manufacturing process creates local surface roughness

modifications leading to variation in cell adhesion on multifaceted TiAl6V4 samples', *Bioprinting*. Elsevier B.V., 16, p. e00054. doi: 10.1016/j.bprint.2019.e00054.

Lim, K. H. A. *et al.* (2016) 'Use of 3D printed models in medical education: A randomized control trial comparing 3D prints versus cadaveric materials for learning external cardiac anatomy', *Anatomical Sciences Education*. John Wiley & Sons, Ltd, 9(3), pp. 213–221. doi: 10.1002/ase.1573.

Lim, Y. A. and Kang, S. J. (2017) 'Evaluation of kodecytes using function-spacer-lipid constructs as a survey material for external proficiency testing for ABO subgrouping', *Journal of Clinical Laboratory Analysis*. John Wiley and Sons Inc., 31(6), p. e22116. doi: 10.1002/jcla.22116.

Linneweber, J. *et al.* (2007) 'The Effect of Surface Roughness on Activation of the Coagulation System and Platelet Adhesion in Rotary Blood Pumps', *Artificial Organs*. Blackwell Publishing Inc, 31(5), pp. 345–351. doi: 10.1111/j.1525-1594.2007.00391.x.

Liu, J. *et al.* (2019) 'Achieving Ti6Al4V alloys with both high strength and ductility via selective laser melting', *Materials Science and Engineering A*. Elsevier Ltd, 766, p. 138319. doi: 10.1016/j.msea.2019.138319.

Lowther, M. *et al.* (2019) 'Clinical, industrial, and research perspectives on powder bed fusion additively manufactured metal implants', *Additive Manufacturing*. Elsevier, 28, pp. 565–584. doi: 10.1016/J.ADDMA.2019.05.033.

Lu, M. *et al.* (2018) 'Uncemented three-dimensional-printed prosthetic reconstruction for massive bone defects of the proximal tibia', *World Journal of Surgical Oncology*. BioMed Central, 16(1), p. 47. doi: 10.1186/s12957-018-1333-6.

Madesis, A. *et al.* (2014) 'Review of mitral valve insufficiency: repair or replacement.', *Journal of thoracic disease*. AME Publications, 6 Suppl 1(Suppl 1), pp. S39-51. doi: 10.3978/j.issn.2072-1439.2013.10.20.

Magne, J. *et al.* (2008) 'Restrictive Annuloplasty for Ischemic Mitral Regurgitation May Induce Functional Mitral Stenosis', *Journal of the American College of Cardiology*, 51(17), pp. 1692–1701. doi: 10.1016/j.jacc.2007.11.082.

Mahmood, F. *et al.* (2013) 'Mitral Annulus: An Intraoperative Echocardiographic Perspective', *Journal of Cardiothoracic and Vascular Anesthesia*, 27(6), pp. 1355–1363. doi: 10.1053/j.jvca.2013.02.008.

Mahmood, F. *et al.* (2014) 'Echocardiography derived three-dimensional printing of normal and abnormal mitral annuli.', *Annals of cardiac anaesthesia*. Medknow Publications and Media Pvt. Ltd., 17(4), pp. 279–83. doi: 10.4103/0971-9784.142062.

Mahmood, F. *et al.* (2015) 'Three-Dimensional Printing of Mitral Valve Using Echocardiographic Data', *JACC: Cardiovascular Imaging*, pp. 227–229. doi: 10.1016/j.jcmg.2014.06.020.

Maitz, M. F. (2015) 'Applications of synthetic polymers in clinical medicine', *Biosurface and Biotribology*. Elsevier, 1(3), pp. 161–176. doi: 10.1016/J.BSBT.2015.08.002.

Mashari, A. *et al.* (2016) 'Hemodynamic Testing of Patient-Specific Mitral Valves Using a Pulse Duplicator: A Clinical Application of Three-Dimensional Printing', *Journal of Cardiothoracic and Vascular Anesthesia*, 30(5), pp. 1278–1285. doi: 10.1053/j.jvca.2016.01.013.

Matena, J. *et al.* (2015) 'SLM produced porous titanium implant improvements for enhanced vascularization and osteoblast seeding.', *International journal of molecular sciences*. Multidisciplinary Digital Publishing Institute (MDPI), 16(4), pp. 7478–92. doi: 10.3390/ijms16047478.

Matthews, A. M. (1998) 'The development of the Starr-Edwards heart valve.', *Texas Heart Institute journal*. Texas Heart Institute, 25(4), pp. 282–93. Available at: http://www.ncbi.nlm.nih.gov/pubmed/9885105 (Accessed: 6 October 2016).

De Mel, A., Cousins, B. G. and Seifalian, A. M. (2012) 'Surface Modification of Biomaterials: A Quest for Blood Compatibility', *International Journal of Biomaterials*. Hindawi Publishing Corporation, 2012. doi: 10.1155/2012/707863.

Mitchell-Smith, J. *et al.* (2018) 'Electrochemical jet processing for skeletal implant surfaces demonstrating enhanced stem cell differentia', in *International Symposium on ElectroChemical machining Technology*, pp. 205–212. Available at: https://www.researchgate.net/publication/329610624_Electrochemical_jet_processing_for_skeletal_implant_surfaces_demonstrating_enhanced_stem_cell_differentia (Accessed: 12 November 2019).

Mitchell-Smith, J. and Clare, A. T. (2016) 'ElectroChemical Jet Machining of Titanium: Overcoming Passivation Layers with Ultrasonic Assistance', *Procedia CIRP*. Elsevier, 42, pp. 379–383. doi: 10.1016/J.PROCIR.2016.02.215.

Müller, R. *et al.* (2005) 'Surface engineering of stainless steel materials by covalent collagen immobilization to improve implant biocompatibility', *Biomaterials*, 26(34), pp. 6962–6972. doi: 10.1016/j.biomaterials.2005.05.013.

Murphy, C. M. and O'Brien, F. J. (2011) 'Differences in Cell Size and Motility between Stem Cells and Osteoblasts Demonstrates the Importance of Designing Scaffolds for Tissue Engineering for Cell Specific Applications', *ORS 2011 Annual Meeting*, (308). Available at: https://www.ors.org/Transactions/57/0308.pdf (Accessed: 16 November 2017).

Murr, L. E. *et al.* (2010) 'Next-generation biomedical implants using additive manufacturing of complex, cellular and functional mesh arrays', *Philosophical Transactions of the Royal Society of London A: Mathematical, Physical and Engineering Sciences*, 368(1917).

Myers, P. O. and Kalangos, A. (2013) 'Valve repair using biodegradable ring annuloplasty: from bench to long-term clinical results.', *Heart, lung and vessels*. Edizioni Medico Scientifiche, 5(4), pp. 213–8. Available at: http://www.ncbi.nlm.nih.gov/pubmed/24364015 (Accessed: 21 October 2016).

NHS Digital (2019) *Hospital Episode Statistics (HES)*, *NHS HES publications*. Available at: https://digital.nhs.uk/data-and-information/data-tools-and-services/data-services/hospital-episode-statistics (Accessed: 23 May 2020).

Nuevo-Ordóñez, Y. *et al.* (2011) 'Titanium release in serum of patients with different bone fixation implants and its interaction with serum biomolecules at physiological levels', *Analytical and Bioanalytical Chemistry*. Springer-Verlag, 401(9), pp. 2747–2754. doi: 10.1007/s00216-011-5232-8.

Owais, K. *et al.* (2014) 'Three-Dimensional Printing of the Mitral Annulus Using Echocardiographic Data: Science Fiction or in the Operating Room Next Door?', *Journal of Cardiothoracic and Vascular Anesthesia*, 28(5), pp. 1393–1396. doi: 10.1053/j.jvca.2014.04.001.

Owida, A. *et al.* (2011) 'Artery vessel fabrication using the combined fused deposition modeling and electrospinning techniques', *Rapid Prototyping Journal*. Emerald Group Publishing Limited, 17(1), pp. 37–44. doi: 10.1108/13552541111098617.

Pagani, F. D. *et al.* (2009) 'Extended Mechanical Circulatory Support With a Continuous-Flow Rotary Left Ventricular Assist Device', *Journal of the American College of Cardiology*. Elsevier, 54(4), pp. 312–321. doi: 10.1016/J.JACC.2009.03.055.

Palta, S., Saroa, R. and Palta, A. (2014) 'Overview of the coagulation system.', *Indian journal of anaesthesia*. Wolters Kluwer -- Medknow Publications, 58(5), pp. 515–23. doi: 10.4103/0019-5049.144643.

Pan, X. *et al.* (2013) 'Bone–patellar tendon–bone autograft versus LARS artificial ligament for anterior cruciate ligament reconstruction', *European Journal of Orthopaedic Surgery & Traumatology*. Springer Paris, 23(7), pp. 819–823. doi: 10.1007/s00590-012-1073-1.

Parlak, Z. V. *et al.* (2019) 'High-strength ceramics as innovative candidates for cardiovascular implants', *Journal of Biomaterials Applications*. SAGE Publications Ltd, 34(4), pp. 585–596. doi: 10.1177/0885328219861602.

Petrus, A. H. J. *et al.* (2019) 'Impact of recurrent mitral regurgitation after mitral valve repair for functional mitral regurgitation: long-term analysis of competing outcomes.', *European heart journal*, 40(27), pp. 2206–2214. doi: 10.1093/eurheartj/ehz306.

Plummer, K. *et al.* (2012) 'Study into the recyclability of a thermoplastic polyurethane powder for use in laser sintering', *Proceedings of the Institution of Mechanical Engineers, Part B: Journal of Engineering Manufacture*. SAGE Publications, 226(7), pp. 1127–1135. doi: 10.1177/0954405412440066.

Polishetty, A. *et al.* (2017) 'Cutting Force and Surface Finish Analysis of Machining Additive Manufactured Titanium Alloy Ti-6Al-4V', *Procedia Manufacturing*. Elsevier B.V., 7, pp. 284–289. doi: 10.1016/j.promfg.2016.12.071.

Post, A., Wang, E. and Cosgriff-Hernandez, E. (2019) 'A Review of Integrin-Mediated Endothelial Cell Phenotype in the Design of Cardiovascular Devices', *Annals of Biomedical Engineering*. Springer US, 47(2), pp. 366–380. doi: 10.1007/s10439-018-02171-3.

Van Praet, K. M. *et al.* (2018) 'Minimally invasive surgical mitral valve repair: State of the art review', *Interventional Cardiology Review*. Radcliffe Cardiology, 13(1), pp. 14–19. doi: 10.15420/icr.2017:30:1.

Prinzing, A. *et al.* (2018) 'Initial Experience With a New Mitral Ring Designed to Simplify Length Determination of Neochords', *Annals of Thoracic Surgery*. Elsevier USA, 105(6), pp. 1784–1789. doi: 10.1016/j.athoracsur.2017.12.030.

Publications Office (1993) *Council Directive 93/42/EEC on Medical Devices (MDD) (1993)*. Brussels: European Union. Available at: https://eur-lex.europa.eu/legal-content/EN/TXT/?uri=CELEX:01993L0042-20071011 (Accessed: 1 April 2020).

Publications Office (2017) *Regulation (EU) 2017/745*. Brussels: European Union. Available at: https://eur-lex.europa.eu/legal-content/EN/TXT/?uri=CELEX:02017R0745-20170505 (Accessed: 1 April 2020).

Purser, M. F. *et al.* (2010) 'A Novel Shape Memory Alloy Annuloplasty Ring for Minimally Invasive Surgery: Design, Fabrication, and Evaluation', *Annals of Biomedical Engineering*, 39(1), pp. 367–377. doi: 10.1007/s10439-010-0126-z.

Raffoul, R. *et al.* (1998) 'Clinical Evaluation of the Physio Annuloplasty Ring', *Chest*, 113(5), pp. 1296–1301. doi: 10.1378/chest.113.5.1296.

Rafi, H. K. *et al.* (2013) 'Microstructures and Mechanical Properties of Ti6Al4V Parts Fabricated by Selective Laser Melting and Electron Beam Melting', *Journal of Materials Engineering and Performance*, 22(12), pp. 3872–3883. doi: 10.1007/s11665-013-0658-0.

Raisian, S. *et al.* (2017) 'Customized Titanium Mesh Based on the 3D Printed Model vs. Manual Intraoperative Bending of Titanium Mesh for Reconstructing of Orbital Bone Fracture: A Randomized Clinical Trial', *Reviews on Recent Clinical Trials*. Bentham Science Publishers Ltd., 12(3). doi: 10.2174/1574887112666170821165206.

Robinson, S. S. *et al.* (2018) 'Patient-specific design of a soft occluder for the left atrial appendage', *Nature Biomedical Engineering*. Nature Publishing Group, 2(1), pp. 8–16. doi: 10.1038/s41551-017-0180-z.

Rostagno, C., Carone, E. and Stefàno, P. L. (2017) 'Role of mitral valve repair in active infective endocarditis: Long term results', *Journal of Cardiothoracic Surgery*. BioMed Central Ltd., 12(1), p. 29. doi: 10.1186/s13019-017-0604-6.

Rotaru, H. *et al.* (2015) 'Selective laser melted titanium implants: a new technique for the reconstruction of extensive zygomatic complex defects', *Maxillofacial Plastic and Reconstructive Surgery*. Springer Berlin Heidelberg, 37(1), p. 1. doi: 10.1186/s40902-015-0001-9.

Sawazaki, M. *et al.* (2014) 'Controversy in mitral valve repair, resection or chordal replacement?', *General Thoracic and Cardiovascular Surgery*. Springer Japan, 62(10), pp. 581–585. doi: 10.1007/s11748-014-0459-x.

Scanlan, A. B. *et al.* (2018) 'Comparison of 3D Echocardiogram-Derived 3D Printed Valve Models to Molded Models for Simulated Repair of Pediatric Atrioventricular Valves', *Pediatric Cardiology*. Springer US, 39(3), pp. 538–547. doi: 10.1007/s00246-017-1785-4.

Shimokawa, T. *et al.* (2011) 'Mechanisms of recurrent regurgitation after valve repair for prolapsed mitral valve disease', *Annals of Thoracic Surgery*. Elsevier USA, 91(5), pp. 1433–1439. doi: 10.1016/j.athoracsur.2011.01.015.

Shunmugavel, M. *et al.* (2017) 'A comparative study of mechanical properties and machinability of wrought and additive manufactured (selective laser melting) titanium alloy - Ti-6Al-4V', *Rapid Prototyping Journal*. Emerald Group Publishing Ltd., 23(6), pp. 1051–1056. doi: 10.1108/RPJ-08-2015-0105.

Sidambe, A. T. (2014) 'Biocompatibility of advanced manufactured titanium implants-A review', *Materials*. MDPI AG, pp. 8168–8188. doi: 10.3390/ma7128168.

Silberman, S. *et al.* (2009) 'Repair of Ischemic Mitral Regurgitation: Comparison Between Flexible and Rigid Annuloplasty Rings', *The Annals of Thoracic Surgery*, 87(6), pp. 1721–1727. doi: 10.1016/j.athoracsur.2009.03.066.

SME (2018) *Medical Additive Manufacturing/ 3D Printing*. Southfield, MI. Available at: https://www.sme.org/globalassets/sme.org/media/white-papers-and-reports/2018-sme-medical-am3dp-annual-report.pdf (Accessed: 2 March 2020).

Smith, S. A., Travers, R. J. and Morrissey, J. H. (2015) 'How it all starts: Initiation of the clotting cascade.', *Critical reviews in biochemistry and molecular biology*. NIH Public Access, 50(4), pp. 326–36. doi: 10.3109/10409238.2015.1050550.

Speidel, A. *et al.* (2016) 'Electrolyte Jet Machining of Titanium Alloys Using Novel Electrolyte Solutions', *Procedia CIRP*. Elsevier, 42, pp. 367–372. doi: 10.1016/J.PROCIR.2016.02.200.

Stone, G. W. *et al.* (2012) 'Prospective, Randomized, Multicenter Evaluation of a Polyethylene Terephthalate Micronet Mesh–Covered Stent (MGuard) in ST-Segment Elevation Myocardial Infarction', *Journal of the American College of Cardiology*. Journal of the American College of Cardiology, 60(19), pp. 1975–1984. doi: 10.1016/j.jacc.2012.09.004.

Sud, K. *et al.* (2016) 'Degenerative Mitral Stenosis', *Circulation*, 133(16), pp. 1594–1604. doi: 10.1161/CIRCULATIONAHA.115.020185.

Sulaiman, A. *et al.* (2008) 'In vitro non-rigid life-size model of aortic arch aneurysm for endovascular prosthesis assessment', *European Journal of Cardio-Thoracic Surgery*. Elsevier, 33(1), pp. 53–57. doi: 10.1016/j.ejcts.2007.10.016.

Sündermann, S. H. *et al.* (2013) 'Implantation of personalized, biocompatible mitral annuloplasty rings: feasibility study in an animal model.', *Interactive cardiovascular and thoracic surgery*. Oxford University Press, 16(4), pp. 417–22. doi: 10.1093/icvts/ivs531.

Suri, R. M. *et al.* (2006) 'Recurrent mitral regurgitation after repair: should the mitral valve be re-repaired?', *The Journal of thoracic and cardiovascular surgery*, 132(6), pp. 1390–7. doi: 10.1016/j.jtcvs.2006.07.018.

Taheri Andani, M. *et al.* (2016) 'Achieving biocompatible stiffness in NiTi through additive manufacturing', *Journal of Intelligent Material Systems and Structures*. SAGE Publications, 27(19), pp. 2661–2671. doi: 10.1177/1045389X16641199.

Tatooles, A. J. *et al.* (2004) 'Minimally invasive mitral valve repair using the da Vinci robotic system', *The Annals of Thoracic Surgery*, 77(6), pp. 1978–1984. doi: 10.1016/j.athoracsur.2003.11.024.

Tejero, R., Anitua, E. and Orive, G. (2014) 'Toward the biomimetic implant surface: Biopolymers on titanium-based implants for bone regeneration', *Progress in Polymer Science*, 39(7), pp. 1406–1447. doi: 10.1016/j.progpolymsci.2014.01.001.

Thermo Scientific (2013) *X-ray Photoelectron Spectroscopy XPS*, *XPS Simplified*. Available at: https://xpssimplified.com/index.php (Accessed: 21 July 2019).

Timek, T. A. *et al.* (2014) 'Five-year real world outcomes of GeoForm ring implantation in patients with ischemic mitral regurgitation.', *The Journal of thoracic and cardiovascular surgery*, 148(5), pp. 1951–6. doi: 10.1016/j.jtcvs.2014.02.051.

Tomšič, A., Klautz, R. J. M. and Palmen, M. (2018) 'Respect versus resect: Two different repair techniques or two different tools in the toolbox?', *The Journal of thoracic and cardiovascular surgery*. Elsevier, 155(2), pp. 600–601. doi: 10.1016/j.jtcvs.2017.09.085.

Townsend, A. *et al.* (2016) 'Surface texture metrology for metal additive manufacturing: a review', *Precision Engineering*. Elsevier, 46, pp. 34–47. doi: 10.1016/J.PRECISIONENG.2016.06.001.

Vaezi, M. and Yang, S. (2015) 'Extrusion-based additive manufacturing of PEEK for biomedical applications', *Virtual and Physical Prototyping*, 10(3), pp. 123–135. doi: 10.1080/17452759.2015.1097053.

Vaithilingam, J. *et al.* (2015) 'Functionalisation of Ti6Al4V components fabricated using

selective laser melting with a bioactive compound', *Materials Science and Engineering C*. Elsevier Ltd, 46, pp. 52–61. doi: 10.1016/j.msec.2014.10.015.

Vaithilingam, J. *et al.* (2016) 'Surface chemistry of Ti6Al4V components fabricated using selective laser melting for biomedical applications', *Materials Science and Engineering: C*. Elsevier, 67, pp. 294–303. doi: 10.1016/J.MSEC.2016.05.054.

Vashistha, R. *et al.* (2019) 'Quest for cardiovascular interventions: precise modeling and 3D printing of heart valves', *Journal of Biological Engineering*. BioMed Central, 13(1), p. 12. doi: 10.1186/s13036-018-0132-5.

Votta, E. *et al.* (2007) 'The Geoform Disease-Specific Annuloplasty System: A Finite Element Study', *The Annals of Thoracic Surgery*, 84(1), pp. 92–101. doi: 10.1016/j.athoracsur.2007.03.040.

Vukicevic, M., Puperi, D. S., *et al.* (2017) '3D Printed Modeling of the Mitral Valve for Catheter-Based Structural Interventions', *Annals of Biomedical Engineering*, 45(2), pp. 508–519. doi: 10.1007/s10439-016-1676-5.

Vukicevic, M., Mosadegh, B., *et al.* (2017) 'Cardiac 3D Printing and its Future Directions', *JACC: Cardiovascular Imaging*. Elsevier, 10(2), pp. 171–184. doi: 10.1016/J.JCMG.2016.12.001.

Wache, H. M. *et al.* (2003) 'Development of a polymer stent with shape memory effect as a drug delivery system', in *Journal of Materials Science: Materials in Medicine*. Kluwer Academic Publishers, pp. 109–112. doi: 10.1023/A:1022007510352.

Wan, S. *et al.* (2015) 'The choice of mitral annuloplastic ring-beyond "surgeon's preference"', *Annals of cardiothoracic surgery*. AME Publications, 4(3), pp. 261–5. doi: 10.3978/j.issn.2225-319X.2015.01.05.

Wang, M. *et al.* (2016) 'Fabrication and characterization of selective laser melting printed Ti–6Al–4V alloys subjected to heat treatment for customized implants design', *Progress in Natural Science: Materials International*. Elsevier B.V., 26(6), pp. 671–677. doi: 10.1016/j.pnsc.2016.12.006.

Wei, Q. *et al.* (2015) 'Selective laser melting of stainless-steel/nano-hydroxyapatite composites for medical applications: Microstructure, element distribution, crack and mechanical properties', *Journal of Materials Processing Technology*, 222, pp. 444–453. doi: 10.1016/j.jmatprotec.2015.02.010.

Williams, E. *et al.* (2016) 'Ultra-Fast Glyco-Coating of Non-Biological Surfaces', *International Journal of Molecular Sciences*. MDPI AG, 17(1), p. 118. doi: 10.3390/ijms17010118.

Witschey, W. R. T. *et al.* (2014) 'Three-Dimensional Ultrasound-Derived Physical Mitral Valve Modeling', *The Annals of Thoracic Surgery*, 98(2), pp. 691–694. doi: 10.1016/j.athoracsur.2014.04.094.

Wong, K. C. *et al.* (2015) 'One-step reconstruction with a 3D-printed, biomechanically evaluated custom implant after complex pelvic tumor resection', *Computer Aided Surgery*. Taylor & Francis, 20(1), pp. 14–23. doi: 10.3109/10929088.2015.1076039.

Wood, A. E. *et al.* (2005) 'Mitral valve reconstruction in a pediatric population: Late clinical results and predictors of long-term outcome', *The Journal of Thoracic and Cardiovascular Surgery*, 130(1), pp. 66–73. doi: 10.1016/j.jtcvs.2005.03.025.

Wysocki, B. *et al.* (2016) 'Post Processing and Biological Evaluation of the Titanium

Scaffolds for Bone Tissue Engineering', *Materials*. Multidisciplinary Digital Publishing Institute, 9(3), p. 197. doi: 10.3390/ma9030197.

Xiong, Y. Z. *et al.* (2020) 'Rationally designed functionally graded porous Ti6Al4V scaffolds with high strength and toughness built via selective laser melting for load-bearing orthopedic applications', *Journal of the Mechanical Behavior of Biomedical Materials*. Elsevier Ltd, 104, p. 103673. doi: 10.1016/j.jmbbm.2020.103673.

Zareidoost, A. *et al.* (2012) 'The relationship of surface roughness and cell response of chemical surface modification of titanium.', *Journal of materials science. Materials in medicine*. NIH Public Access, 23(6), pp. 1479–88. doi: 10.1007/s10856-012-4611-9.

Zhang, S. *et al.* (2018) 'Cardiac implant registries 2006-2016: a systematic review and summary of global experiences.', *BMJ open*. British Medical Journal Publishing Group, 8(4), p. e019039. doi: 10.1136/bmjopen-2017-019039.

Zhang, X. *et al.* (2020) 'Preparation and bioactive response of super-hydrophilic surface on selective laser melting titanium', in *Procedia CIRP*. Elsevier B.V., pp. 222–227. doi: 10.1016/j.procir.2020.05.145.

Zhao, Y. and Kunieda, M. (2019) 'Investigation on electrolyte jet machining of three-dimensional freeform surfaces', *Precision Engineering*. Elsevier BV, 60, pp. 42–53. doi: 10.1016/j.precisioneng.2019.06.009.